WAVEGUIDING AND RADIATION CHARACTERISTICS OF A THIN WALL PARALLEL PLATE STRUCTURE

By
RAMESH GARG

DEPARTMENT OF PHYSICS
INDIAN INSTITUTE OF TECHNOLOGY KANPUR
MAY 1974

WAVEGUIDING AND RADIATION CHARACTERISTICS OF A THIN WALL PARALLEL PLATE STRUCTURE

A Thesis Submitted
In Partial Fulfilment of the Requirements
for the Degree of
DOCTOR OF PHILOSOPHY

By
RAMESH GARG

to the

DEPARTMENT OF PHYSICS
INDIAN INSTITUTE OF TECHNOLOGY KANPUR
MAY, 1974

TO THOSE WHO ARE DEDICATED TO WORK

CERTIFICATE

The work reported in this thesis entitled 'WAVEGUIDING AND RADIATION CHARACTERISTICS OF A THIN WALL PARALLEL PLATE STRUCTURE' by Mr. Ramesh Garg has been carried out under our supervision and this work has not been submitted elsewhere for a degree.

(Dr. R. Sharan)

(Dr. K.C. Gupta)

Assistant Professors
Department of Electrical Engineering
and
Advanced Centre for Electronic Systems
Indian Institute of Technology
Kanpur

ACKNOWLEDGEMENTS

It is with great pleasure that I acknowledge my deep gratitude to Dr K C Gupta and Dr R Sharan for initiating me into this field and providing excellent guidance throughout the course of this work

I am thankful to Prof P Venkateswarlu, then convener DPGC, for allowing me to choose thesis supervisors from outside the Physics Department

I have also gained by frequent discussions on related areas with Mr I J Bahl, the friend and fellow-research scholar

Sincere thanks go to Mr B M Bahl for providing cheerful association during the course of this work

I appreciate the care and interest taken by Mr S V Sirbhai in typing this thesis

Lastly, but not the least, I am thankful to numerous others, especially Mr P Lal, for providing the research facilities here

TABLE OF CONTENTS

ERRATA

Page No.	Line, Eqn. or Fig.No.	Correction
30	Eqn.(2.13) and line before it	Read 'ξ' for 'θ_m'.
31	Line before (2.21)	Add '(See Appendix D)' at the end of sentence.
37	Second line from top	+x and -x are interchanged.
64 and onwards		Read (4.6), (4.7) ... etc. for (4.16), (4.17). . etc.
66	Fig 4.2	Add to the caption '$f = 9$ GHz, $b = 0.95$ in. $\sigma = 1.08 \times 10^{5}$ mho/m and $t = 1300$ AU'.
67	After (4.25)	Add 'where $x = \sin\theta - \gamma/k_o$'
70	Last sentence in first para	'It is shown that multiple... ...single beam' should read 'It is shown that <u>three</u>... ... single beam for $\lambda/2b = 0.2$.
72	Eqn. (4.32)	Delete $(k_o L/2)^2$
73, 72	Eqn.(4.34), (4.35)	Delete $k_o L/2$
84	Eqn.(4.58)	R.H.S. is inverted.
88	Fig.4.9	For $\varepsilon_r = 2.6$ $b = 0.42$ in.
100	Fig. 5.5(b)	Ordinate should read <u>Relative</u> power (dB).
103	End of first para	Add The value of propagation constant used is obtained theoretically, (2.9a), for the set of parameters indicated.

LIST OF TABLES

LIST OF FIGURES

LIST OF SYMBOLS

The more important symbols used in this thesis are shown below.

b : separation between the parallel plates

c : velocity of light in free space

E_y : y-component of electric field vector

$F(\theta), F_1(\theta), F_2(\theta)$: Radiation pattern functions

f : frequency of operation

$G(x,z)$: Green's function solution

H_y : y-component of magnetic field vector

h_1, h_2, h_3 : transverse propagation constants in the dielectric, imperfect wall, and free space respectively

K : complex dielectric constant of the metal of imperfect wall $(1+j\sigma/\omega\varepsilon_0)$

k_0 : free space wavenumber

L : length of antenna

N : an integer giving the number of beams in the radiation pattern

n : an integer denoting the mode number

R_s : sheet resistivity of metal of imperfect wall $(1/\sigma\delta)$

r : radius vector for field point

m : thickness of the support for thin wall

t : thickness of the imperfect wall

v : phase velocity of the wave

Z_m : characteristic impedance of metal of imperfect wall

Z_0 : characteristic impedance of free space

Z_T : transverse wave impedance of free space for the leaky wave

Z_1, Z_{in} : impedances used in transverse resonance technique

α : attenuation constant in the direction of propagation

α_d : attenuation constant due to losses in the dielectric

β : phase constant in the direction of propagation

δ : skin depth at a frequency f and conductivity σ

$\delta(x), \delta(z)$: Dirac's delta function

$\delta\beta$: change in phase constant

$\delta\gamma$: change in propagation constant

ε_0 : permittivity of free space (8.85×10^{-12} F/m)

ε_r : relative dielectric constant of the dielectric filling the space between the parallel plates

ε_{r3} : relative dielectric constant of the medium used as a support for the thin film (imperfect wall)

ε' : loss tangent of lossy dielectric

η : efficiency of antenna

γ : perturbed value of propagation constant in the direction of propagation

γ_0 : unperturbed value of propagation constant in the direction of propagation

λ : wavelength in free space

λ_g : guide wavelength

μ_0 : permeability of free space ($4\pi x10^{-7}$H/m)

ω : radian frequency

σ : conductivity of metal of the imperfect wall

θ : angle of radiation measured from the transverse direction

θ_m : position of main beam measured from the transverse direction

$\theta_{m,n}$: position of main beam contributed by TE_{no} mode

SYNOPSIS

RAMESH GARG Ph.D.
Department of Physics,
Indian Institute of Technology, Kanpur
May 1974

WAVEGUIDING AND RADIATION CHARACTERISTICS OF A THIN WALL PARALLEL PLATE STRUCTURE

Propagation in a parallel plate waveguide with perfectly conducting plates ($\sigma=\infty$) has been treated by many authors. The effect of finite conductivity of plates on attenuation has also been taken into account. But the effect of finite thickness t of imperfectly conducting ($\sigma\neq\infty$) plates on the propagation constant has not been investigated.

The radiation and waveguiding properties of a parallel plate waveguide with an imperfect plate has been studied in this thesis. When the imperfect plate is thin ($t < \delta$, where δ is skin depth) there is a leakage of power. This leakage of power gives rise to radiation. Based on the results of the radiation properties of the structure, a leaky wave antenna called TLA, has been tested successfully at X-band frequencies.

The major conclusions of this study are as follows: (1) there is an optimum thickness of the imperfect plate at which attenuation is minimum. This optimum thickness is given by $t/\delta=\pi/2$.

(ii) for $t/\delta < 10^{-4}$, a new type of leaky wave has been observed. For this type of wave, the phase velocity is less than the velocity of light and growth in transverse direction is same as that for leaky waves. This wave has been called a slow leaky wave, and
(iii) TLA can be designed to give narrow beams in a direction away from endfire also.

In order to investigate the waveguiding and radiation properties of the structure it is necessary to know the propagation constant of the structure for various possible modes. Propagation constant is obtained by solving the dispersion relation. Hence, dispersion relations have been obtained for TEM-like, TM and TE modes. These dispersion relations have been solved numerically for the propagation constants. Analytical approximate closed form expressions for propagation constant have also been obtained. It has been found that for $t/\delta < \pi/2$, the attenuation constant and the phase constant for all the above modes increase with decrease in either or both σ and t. These constants also increase with increase in the dielectric constant of the medium separating the plates . For $t/\delta < 10^{-4}$, slow-leaky waves ($c/v > 1$) are obtained. These waves have not been reported earlier.

Attenuation constant α/k_0, has been obtained in terms of surface resistance of imperfect plate by using the transverse resonance technique also. Here, the effect of

(0.9" x 0.4") has been used for fabricating TLA and a thin film of bismuth has been chosen for the imperfect wall. Thickness and conductivity of bismuth film used are 1300 AU and 1.08 x 10^5 mho/m respectively. Measurements have been carried out at 9, 10 and 11 GHz. The agreement between the experimental and theoretical values is fairly good.

TLA has been compared with other leaky wave antennas. It has been observed that designing a TLA would be easier as compared with other leaky wave antennas. This is so since c/v variation of TLA is essentially that of a simple parallel plate waveguide and α/k_0 also is given by a simple expression. TLA can be designed to give narrow beams in a direction ether than endfire also. To obtain narrow beams the attenuation should be correspondingly low. Low values of attenuatmon can be easily obtained by increasing the thickness of imperfect wall. Thus, a long TLA can be used with a narrow beam pointing away from endfire. TLA has been found to have better sidelobe characteristics than slotted waveguide antenna. In the radiation pattern of slotted waveguide antenna there is another sidelobe due to slot mode. This mode is not present in TLA.

CHAPTER 1

INTRODUCTION

CHAPTER 1

INTRODUCTION

The study of propagation of electromagnetic energy in waveguiding structures has been of considerable interest. One of the simple waveguiding structures can be obtained by a set of parallel plates. The propagation characteristics in this type of structure has been extensively studied for different cases.

Propagation in a parallel plate waveguide with perfectly conducting plates has been treated by many authors [1-3]. The effect of finite conductivity of plates on the attenuation has been taken into account by Ramo et al. [1], Jordan and Balmain [2], and Adler et al.[3]. However, in [1-3] the thickness of the imperfect plate has been taken to be much greater than the skin depth. Therefore, the effect of finite conductivity on the phase constant is negligible. In the present work the effect of finite thickness and finite conductivity on propagation constant in a parallel plate structure has been studied. In order to put the study in proper perspective some of the relevant literature is briefly reviewed.

Ramo et al.[1] and Jordan et al.[2] have obtained the expressions for the attenuation constant by the usual

technique of calculating the power lost in the imperfect wall and the power transmitted in the longitudinal direction. Adler et al. [3] have derived the expressions for the TEM-mode and TM-modes by solving the transverse resonance equation. Their investigation is based on the perturbation treatment of the unperturbed mode.

Rectangular waveguide structure with a narrow wall replaced by a slab ($t >> \delta$) of semiconductor has been reported in the literature [4,5]. The dominant mode of propagation in such a structure has been investigated by Larrabee [4] and Gunn and Sheikh [5]. These investigations are aimed at the measurement of the dielectric constants of the semiconductors.

Karbowiak [9] has obtained the propagation constants for TE-modes and TM-modes in a rectangular waveguide by using the surface impedance Z_s, of the imperfect plate. The method used is based on the perturbation of the unperturbed mode. The only assumption underlying this treatment is that the surface impedance Z_s is very small compared to free space impedance Z_0 (377 ohms). This assumption leads to a lower limit on the values of conductivity (σ) and thickness (t) of the imperfect plate. As a result of the approximation $|Z_s| << Z_0$, Karbowiak's method [9] holds good for only those values of t at which change

in phase constant is negligible.

As mentioned earlier the present work concerns itself with the effect of conductivity and thickness of the imperfect plate on the phase constant and attenuation constant of a parallel plate waveguide structure. The analysis holds good even for very small thicknesses of imperfect wall. For these small thicknesses a fraction of the power flowing inside the guide leaks out. This property of the structure has been utilized to construct a leaky wave antenna. In the specific antenna configuration discussed, one of the narrow walls of a rectangular waveguide is replaced by a thin film ($t < \delta$) of a metal. Hereafter, this antenna is abbreviated as 'TLA' (Thin wall Leaky waveguide Antenna).

The waveguiding properties of a parallel plate structure with a thin wall are discussed in Chapter 2. The dispersion relations for TEM-like, TM and TE-modes are obtained and they are solved for the propagation constant using the perturbation approach. The effect of various parameters on phase constant and attenuation constant is discussed. It is seen that the values of phase constant and attenuation constant increases with the decrease in thickness t of imperfect plate. Very low values of t give rise to slow leaky waves ($\beta > k_0$). These slow leaky waves are also discussed.

Simplified expressions for the attenuation constants for various modes, which take into account the effect of various parameters, is included in Chapter 3. Variation of attenuation with thickness (obtained in Chapter 2) is explained here by calculating the surface resistance of imperfect plate. The method of transverse resonance is used. It is shown that the attenuation is minimum when the thickness of imperfect plate is such that $t/\delta = \pi/2$. Propagation near cut-off is also discussed in this chapter.

In Chapter 4, the radiation properties of the structure are included. First, the steepest-descent method is used to evaluate the radiation pattern of an infinitely long antenna when the structure is excited by a distribution of line sources. Finite length antenna is analysed by means of the Kirchhoff-Huygens integration method. The antenna efficiency η and the beamwidth of infinitely long TLA is also included. A simple expression giving the position of minimum beamwidth is obtained.

Experimental measurements on TLA constitutes Chapter 5. A thin film of bismuth is used for imperfect wall. Experimental results for guide wavelength and attenuation are compared with theoretical results. Radiation patterns at X-band frequencies are seen to be in fair agreement with theoretically computed patterns.

TLA is compared with the slotted waveguide antenna and channel guide antenna in Chapter 6. It is pointed out that designing a TLA is easier compared with other leaky wave antennas. c/v variation of TLA is essentially that of a simple rectangular waveguide. Very low values of attenuation can be obtained so that a long antenna can be used even with the beam directed away from endfire.

The last chapter summarises the major conclusions and the suggestion for further work is also included here.

CHAPTER 2

WAVEGUIDING CHARACTERISTICS

CHAPTER 2

WAVEGUIDING CHARACTERISTICS

Waveguiding properties of a parallel plate waveguide with a thin imperfect wall are discussed in this chapter. In order to investigate these characteristics of the structure, it is necessary to know the propagation constants of various modes possible. The propagation constants for TEM, TM and TE modes are obtained in the following sections.

2.1 PROPAGATION CONSTANT OF THE STRUCTURE

Here we are interested in finding the deviations in the propagation constant of a parallel plate waveguide with an imperfect wall as compared to that with perfect walls.

In a parallel plate waveguide with perfectly conducting walls the dominant mode of propagation is TEM mode. However, when the conductivity of one of the parallel plates is reduced to a finite value, it gives rise to a tangential component of the electric field. This component of the electric field is required to drive the linear current density against the non-zero surface impedance of the metal wall [3]. This mode has been termed as TEM-like mode by Adler et al.[2].

TE and TM modes will also propagate when the separation between the plates is greater than half the

wavelength in the dielectric medium separating the plates. Unlike TEM mode finite values of conductivity and thickness of imperfect plate do not give rise to an additional component of electromagnetic field in TE and TM modes.

Due to the finite conductivity of the metal wall the electromagnetic field penetrates into the metal. This may cause coupling between different modes and the purity of the mode may be spoiled. The coefficient of coupling is proportional to the resistive part of the surface impedance of the imperfect plate [9]. This coupling is absent only when TE_{10}-mode is propagating [9]. In all other cases, the coupling to other modes is neglected in the following analysis.

The propagation constant for the structure is obtained by using the perturbation approach [2]. In the perturbation method, an approximate expression for the propagation constant is obtained by solving the dispersion relation by assuming a perturbed mode in the structure.

2.1.1 Dispersion relation for the structure

The dispersion relation for the structure is obtained by utilizing the Maxwell's equations and the boundary conditions. Since the transverse components of electric and magnetic fields for TEM-like and TM_{no} modes

differ only in the number of half wave variations, they belong to the same class of TM_{no} modes (n=0 represents TEM-like mode). Thus, the dispersion relation is the same for all these modes.

Configuration of the structure and the coordinate system is shown in Figure 2.1. Here b is the thickness of the dielectric separating the parallel plates. The dielectric has been assumed to be lossless and its relative dielectric constant has been taken to be ε_r. The case of lossy dielectric is treated in Sec.3.2. The conductivity of the imperfect plate is σ and its thickness is t. Alternatively, the imperfect plate may be characterised by skin depth δ and the dimensionless quantity t/δ. Skin depth δ is given by $(\pi f \mu_0 \sigma)^{-\frac{1}{2}}$.

The field components for TE_{n0} modes are E_y, H_x and H_z. The expression for E_y in the different regions of the structure may be written as

$$E_{y1} = e^{jh_1 x} + Re^{-jh_1 x} \quad (-b < x < 0) \qquad (2.1a)$$

$$E_{y2} = Pe^{jh_2 x} + Qe^{-jh_2 x} \quad (0 < x < t) \qquad (2.1b)$$

and $$E_{y3} = Te^{jh_3 x} \quad (x > t) \qquad (2.1c)$$

The expression for H_y for TM_{no} modes may be written as

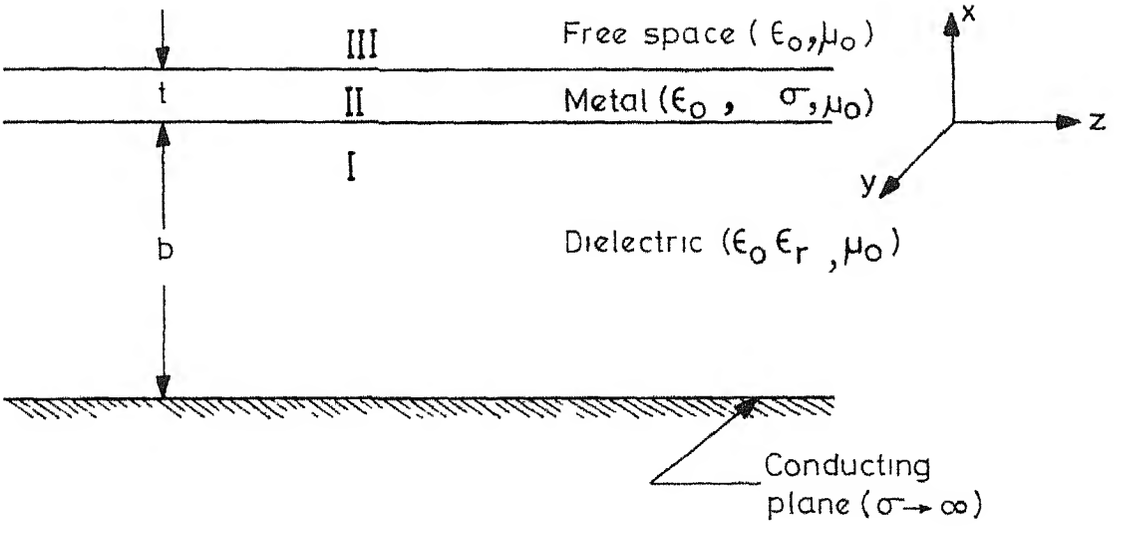

Fig.2.1 Configuration of the structure

$$H_{y1} = e^{jp_1 x} + R' e^{-jp_1 x} \qquad (-b < x < 0) \qquad (2.2a)$$

$$H_{y2} = P' e^{jp_2 x} + Q' e^{-jp_2 x} \qquad (0 < x < t) \qquad (2.2b)$$

$$H_{y3} = T' e^{jp_3 x} \qquad (x > t) \qquad (2.2c)$$

The field variation along Z has been assumed to be exp $(j\gamma Z)$. The time variation has been taken to be exp $(-j\omega t)$. Expressions for the other two field components are obtained by using the Maxwell's equations and expressions for E_y or H_y given in eqns. (2.1) and (2.2) respectively.

h_1, h_2, h_3 and p_1, p_2, p_3 are the transverse propagation constants in the different regions of the structure for TE and TM modes respectively. They are related to the propagation constant along the z-direction, $\gamma = \beta + j\alpha$, through the expressions:

$$h_1 = k_0 [\varepsilon_r - (\gamma/k_0)^2]^{\frac{1}{2}} \qquad (2.3a)$$

$$h_2 = k_0 [K - (\gamma/k_0)^2]^{\frac{1}{2}} \qquad (2.3b)$$

$$h_3 = k_0 [1 - (\gamma/k_0)^2]^{\frac{1}{2}} \qquad (2.3c)$$

$$p_1 = k_0 [\varepsilon_r - (\gamma/k_0)^2]^{\frac{1}{2}} \qquad (2.3d)$$

$$p_2 = k_0 [K - (\gamma/k_0)^2]^{\frac{1}{2}} \qquad (2.3e)$$

and $$p_3 = k_0 [1 - (\gamma/k_0)^2]^{\frac{1}{2}} \qquad (2.3f)$$

where γ in eqns. (2.3a-2.3c), and in eqns.(2.3d-2.3f) corresponds to TE and TM modes respectively

Also,

$$k_0^2 = \omega^2 \mu_0 \varepsilon_0$$

and $$K = 1+j\sigma/\omega\varepsilon_0 \qquad (2.4)$$

In the case of parallel plate structure with the perfectly conducting plates $p_1 b=0$ for TEM-like mode. For TE and TM modes respectively, one gets $h_1 b=n\pi$ and $p_1 b=n\pi$.

The dispersion relation is obtained by applying boundary and continuity conditions on the appropriate components of electric and magnetic fields. The boundary condition for TE mode is:

(1) $E_{y1} = 0$ at $x=-b$

The continuity conditions for TE mode are:

(2) (a) $E_{y1} = E_{y2}$ at $x=0$

(b) $H_{z1} = H_{z2}$ at $x=0$

(3) (a) $E_{y2} = E_{y3}$ at $x=t$

(b) $H_{z2} = H_{z3}$ at $x=t$

Using eqns. (2.1) and above mentioned conditions the following dispersion relation is obtained for TE mode:

$$h_1[jh_3 \tan h_2 t - h_2] + h_2 \tan h_1 b\,[jh_3 + h_2 \tan h_2 t] = 0 \qquad (2.5a)$$

Similarly, the dispersion relation for TEM-like and TM_{no}

modes is obtained as:

$$Kp_1 \tan p_1 b[jKp_3 \tan p_2 t - p_2] - \varepsilon_r p_2[jKp_3 + p_2 \tan p_2 t] = 0 \qquad (2.5b)$$

Note that, the above equations should give rise to the dispersion relations for grounded dielectric slab when t=0. Under this condition eqns. (2.5) become.

$$h_1 \cot h_1 b = jh_3 \qquad (2.6a)$$

$$p_1 \tan p_1 b = -j\varepsilon_r p_3 \qquad (2.6b)$$

Equations (2.6a) and (2.6b) are the dispersion relations for odd-mode TE-waves and even-mode TM-waves respectively on a grounded dielectric slab [10].

Roots of the dispersion relations (2.5) are the propagation constants for the structure. These may be obtained from numerical solution of eqns.(2.5). However, an approximate closed form solution will be obtained first using perturbation methods.

2.1.2 Evaluation of the propagation constants

The propagation constants are obtained by considering the perturbation of modes in the corresponding structure with perfect walls. The normalised propagation constant may be written as

$$\gamma/k_0 = \gamma_0/k_0 + \delta\gamma/k_0 \qquad (2.7)$$

where γ_0/k_0 is the propagation constant for the unperturbed mode and is given by

$$\gamma_0/k_0 = [\varepsilon_r-(n\pi/k_0b)^2]^{\frac{1}{2}} \qquad (2.8)$$

(n=0 for TEM-mode)

The procedure for obtaining the expressions for $\delta\gamma/k_0$ is as follows:

(i) substitute eqn. (2.7) in eqns (2.3) and neglect higher order terms in $\delta\gamma/k_0$,

(ii) use h_1,h_2,h_3; p_1,p_2,p_3, thus obtained, in eqns (2.5),

(iii)further approximate

$$\tan(p_1b) = p_1b \quad \text{for TEM-like mode}$$

$$\tan(p_1b) = p_1b-n\pi \quad \text{for TM modes}$$

$$\tan(h_1b) = h_1b-n\pi \quad \text{for TE modes}$$

A discussion of the approximations made in (i) and (iii) is given in Appendix A. The implications of these approximations in limiting the range of values of various parameters (b,f,t and σ) is also included in Appendix A.

(iv) neglect, the higher order terms in $\delta\gamma/k_0$ arising again due to product terms in eqns (2.5).

Following the above procedure the expressions for $\delta\gamma/k_0$ for various modes, are obtained as;

Case I $\quad \varepsilon_r = 1$

(a) TE modes:

$$\frac{\delta\gamma}{k_0} = -\frac{h_2 t - j \tan(h_2 t)\, n\pi k_0 t/k_0 b}{jk_0 t\, k_0 b \tan(h_2 t)\left[\frac{2}{n\pi} - jK(k_0 b/n\pi)^2\right] - h_2 t (k_0 b/n\pi)^2 [1 - jn\pi]} \frac{1}{\gamma_0/k_0} \tag{2.9a}$$

(b) TM-modes

$$\frac{\delta\gamma}{k_0} = -\frac{1}{K} \frac{h_2 b[j\,Ky + h_2 t \tan(h_2 t)]}{(k_0 b)^2[j\,K\,y \tan(h_2 t) - h_2 t] - jh_2 b(k_0 t)^2/y} \frac{1}{\gamma_0/k_0} \tag{2.9b}$$

where $y = n\pi k_0 t/k_0 b$

(c) TEM-like mode:

$$\frac{\delta\gamma}{k_0} = \frac{X^2}{2} \tag{2.9c}$$

where $X = \dfrac{-1 + [1 - 4\sqrt{K} \tan(h_2 t)/k_0 b\,]^{\frac{1}{2}}}{2\sqrt{K} \tan(h_2 t)}$

Case II $\quad \varepsilon_r > 1$. Here, the expressions used for h_3 are different than that for $\varepsilon_r = 1$ (Appendix A). These expressions for h_3 do not reduce to the corresponding expressions for h_3 for $\varepsilon_r = 1$. Therefore expressions for $\delta\gamma/k_0$ given below also do not reduce to the corresponding relations for $\delta\gamma/k_0$ for $\varepsilon_r = 1$.

(a) TE-modes.

$$\frac{\delta\gamma}{k_0} = -\frac{(n\pi)^2}{(k_0 b)^3} \frac{h_2 t - jk_0 t\, A \tan(h_2 t)}{h_2 t(jA + h_2 t \tan(h_2 t)/k_0 t - 1/k_0 b} \frac{1}{\gamma_0/k_0} \tag{2.10a}$$

(b) TM-modes.

$$\frac{\delta\gamma}{k_0} = -\frac{\varepsilon_r}{K} \frac{h_2}{k_0} \frac{jK\, k_0 t\, A + h_2 t \tan(h_2 t)}{k_0 b[jK\, k_0 t \tan(h_2 t) A - h_2 t] - j\varepsilon_r h_2 t} \frac{1}{\gamma_0/k_0} \tag{2.10b}$$

where $A = 1 - \frac{1}{2}(\gamma_0/k_0)^2$

(c) TEM-like mode.

$$\frac{\delta\gamma}{k_0} = \frac{1}{2}\left(\frac{\Delta}{k_0 b}\right)^2 \frac{1}{\gamma_0/k_0} \tag{2.10c}$$

where $\Delta = j\left[\frac{\varepsilon_r h_2 b}{K} \frac{-K\, k_0 t \sqrt{\varepsilon_r - 1} + h_2 t \tan(h_2 t)}{-K\, k_0 t \tan(h_2 t)\sqrt{\varepsilon_r - 1} - h_2 t}\right]^{1/2}$

The expressions for the propagation constants are obtained by using the approximate expressions from eqns.(2.9) or eqns. (2.10) in eqn. (2.7). Phase constant and attenuation constant, thus obtained, are plotted (dotted curves) in Figures 2.2 and 2.3 using some typical values of parameters indicated in these figures. The other curves (solid lines) shown in Figures 2.2 and 2.3 are the numerical solutions of

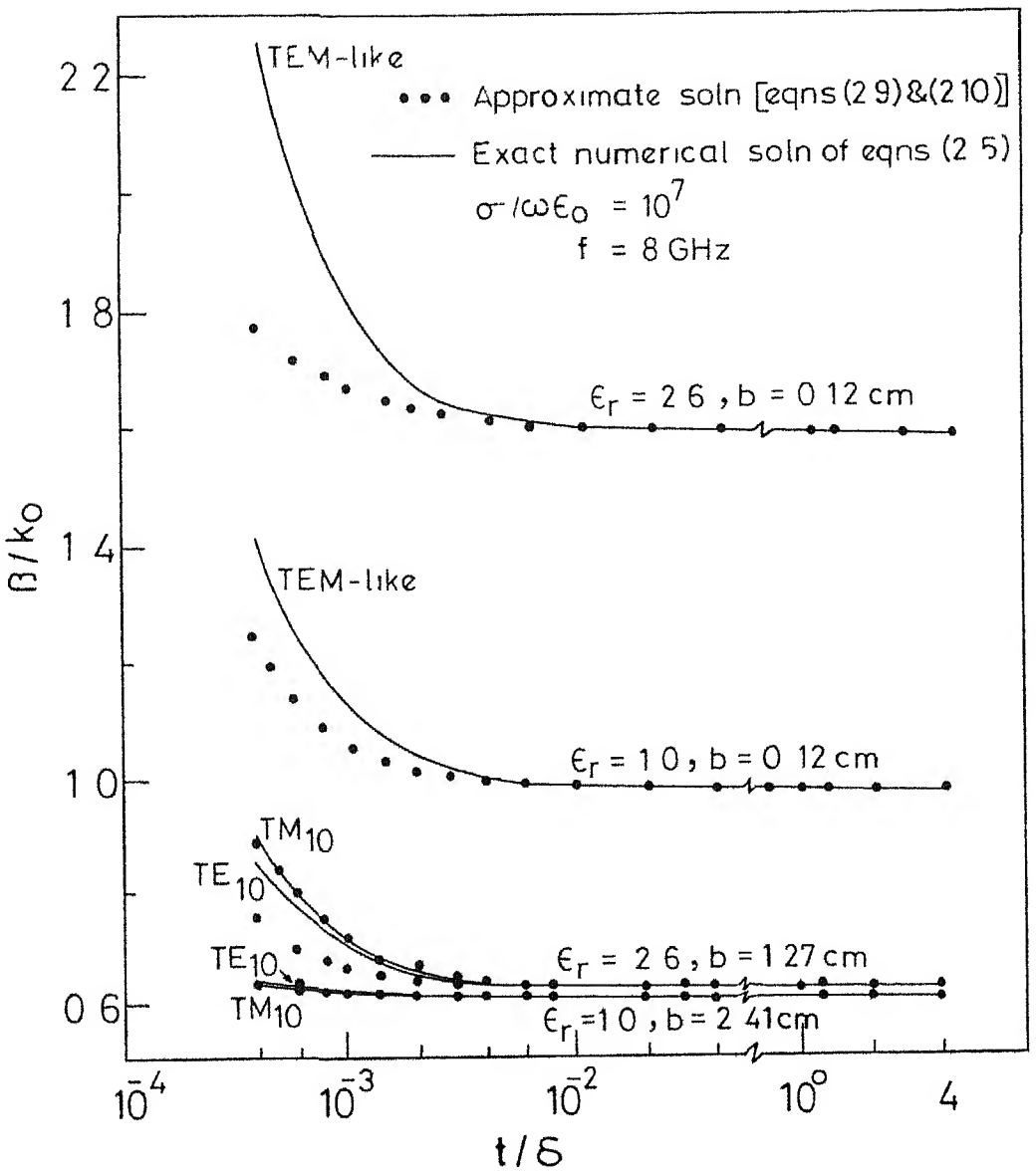

Fig.2.2 Comparison of β/k_0 obtained from approximate solution and exact numerical solution for TE_{10}-mode, TM_{10}-mode and TEM-like mode

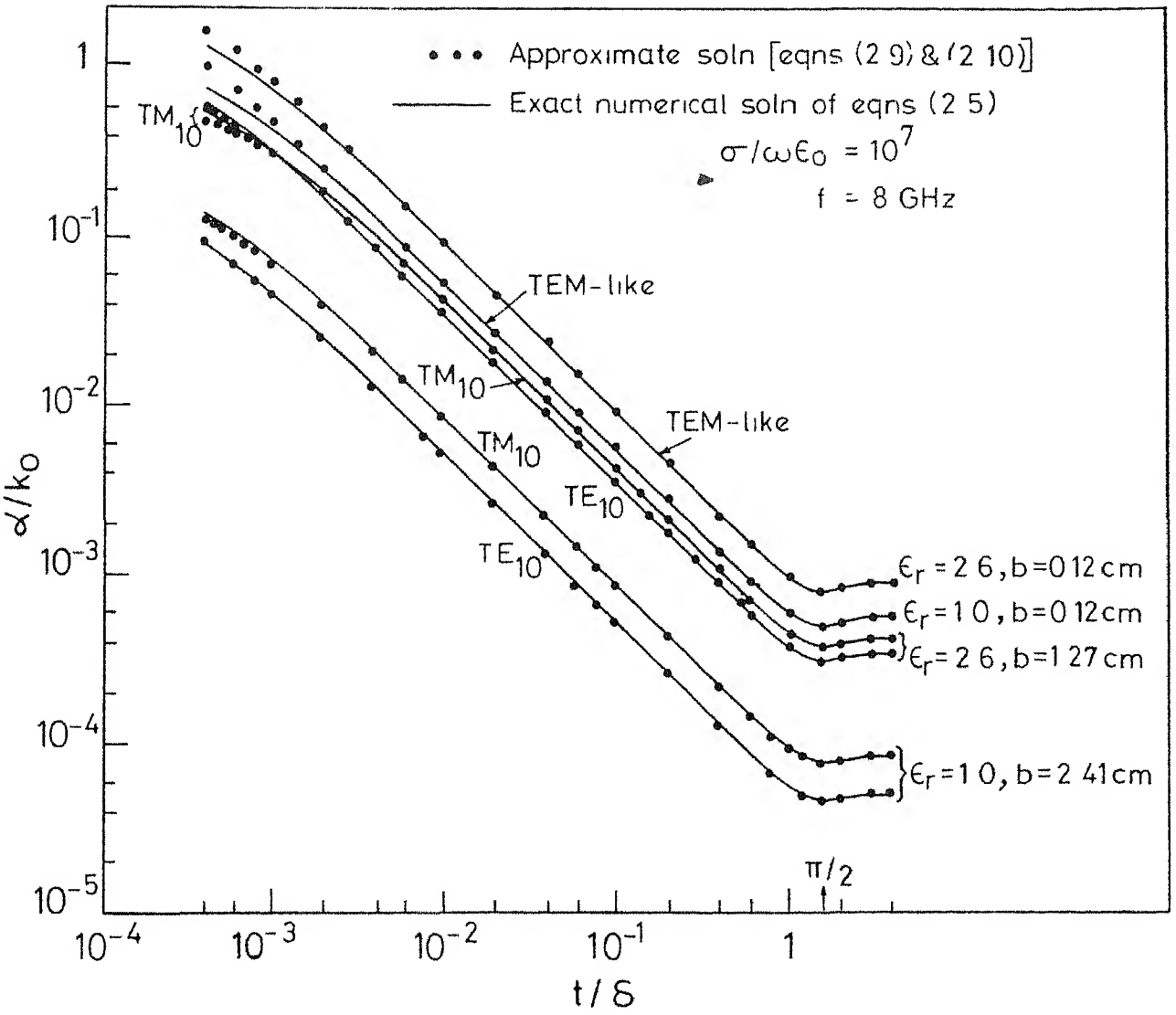

Fig.2.3 Comparison of α/k_0 obtained from approximate solution and exact numerical solution for TE_{10}-mode, TM_{10}-mode and TEM-like mode

eqns. (2.5). The numerical values are obtained by taking the analytical results (eqns.(2.7) and (2.8)) as the initial root of the dispersion relation and calculating the exact root numerically on a computer. For all the cases (excepting some phase constants at low values of t/δ) shown in Figures 2.2 and 2.3, the agreement between the analytical results and the numerically computed values is good. Limitations on the values of parameters for eqns.(2.9) and (2.10) to hold good are given in Appendix A.

The results reported here are for the case when only one plate is imperfect. If both plates of the structure are taken to be the same (same t and σ) the attenuation should be multiplied by a factor of 2. The change in phase constant $\delta\beta$, will also become double.

The attenuation constant obtained here consists of two parts. Part of it is due to dissipation in the imperfectly conducting wall and the rest is due to leakage of power through the thin wall. This leakage of power gives rise to radiation. Radiation characteristics of the structure are discussed in Chapter 4.

Effect of thickness t and ε_r

In the variation of normalised phase constant β/k_0, and normalised attenuation constant α/k_0, with t/δ, shown

In Figures 2.2 and 2.3, the following features are worth noting:

(1) In Figure 2.2, β/k_0 for all the cases is almost equal to the corresponding unperturbed values for t/δ above a certain limit. Below this limit (on t/δ), β/k_0 increases in all the cases. The rate of increase with decreasing t/δ is different for approximate (analytical) and numerical solutions. However, it has been noted that this discrepancy decreases with the increase in value of conductivity σ.

(2) It is seen in Figure 2.3 that α/k_0 varies inversely with t for $0.004 \leq t/\delta \leq 0.4$ in all the cases. For $t/\delta < 0.004$, α/k_0 varies slowly than 1/t variation. This is due to the increase in the value of β/k_0. It is to be noted from Figure 2.3 that the attenuation is minimum for a thickness t such that t/δ is equal to $\pi/2$. The shape of the attenuation curve can be explained by considering the imperfect wall as a transmission line of thickness t with propagation in the transverse direction. This treatment is carried out in Section 3.1.

Effect of conductivity σ

Figures 2.4 and 2.5 show the effect of variation of conductivity of imperfect plate on the phase constant and the attenuation constant respectively for TE_{10} mode.

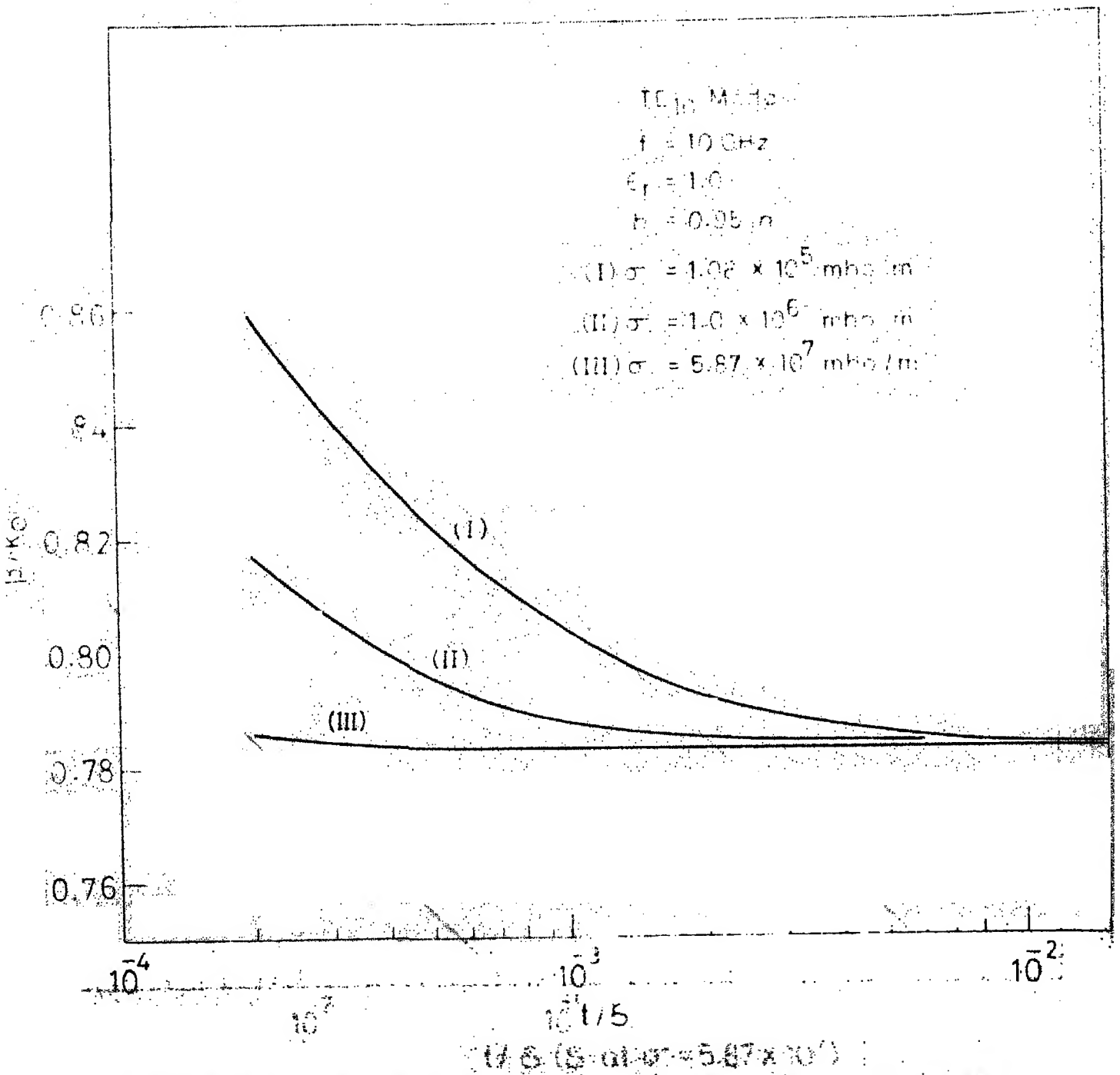

Fig.2.4 Variation of λ/λ_0 with t/λ for various values of conductivity of imperfect plate walls

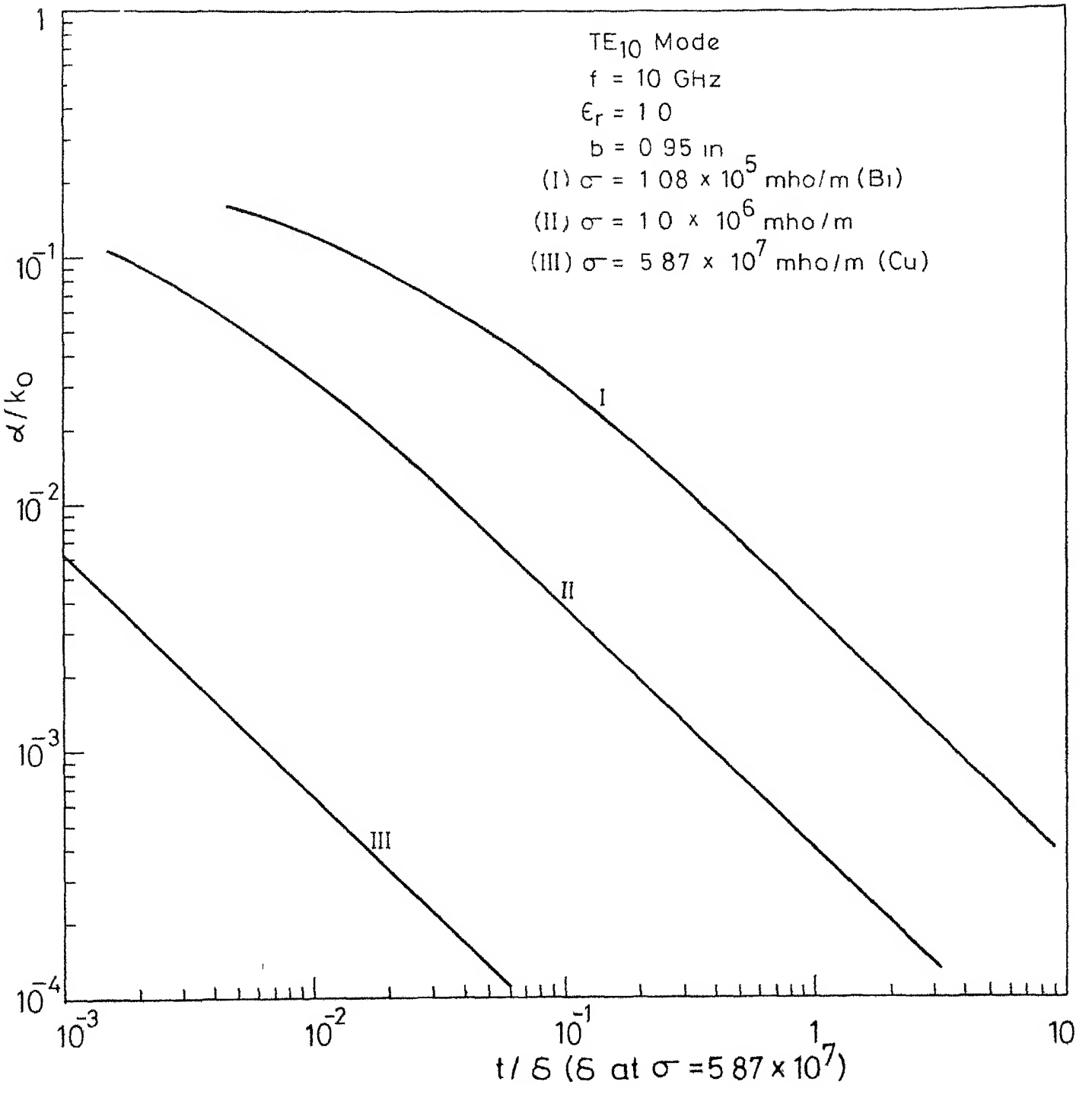

Fig.2.5 Variation of α/k_0 with t for various values of conductivity of imperfect plate

The values of σ chosen are shown in the graph. In Figure 2.5 t has been normalised with respect to skin depth at $\sigma=5.87\times10^7$ mho/m.

Figure 2.4 shows that β/k_0 versus t/δ graph is constant for $t/\delta >> R_s/Z_0$ (irrespective of the value of σ in the range considered). This fact is useful in establishing the range over which the approximate expression for the attenuation constant (given in Section 3.1) can be used. Figure 2.5 shows that α/k_0 increases with the decrease in value of σ. The effect of decreasing σ is the same as that of decreasing t. In fact, for some range of values of σ and t (shown in Figure 3.2) α/k_0 is proportional to $1/\sigma t$.

Effect of frequency f

The variation of β/k_0 and α/k_0 with t/δ and frequency as a parameter for TE_{10} mode is included in Figures 2.6 and 2.7 respectively. Here, t has been normalised with respect to skin depth at f=9 GHz. The rate of variation of phase constant with frequency determines the rate of scanning of main beam for TLA. The change in attenuation with frequency will give the change in beamwidth of main beam. We note from Figure 2.7 that for a given value of t attenuation increases with decrease in the value of frequency.

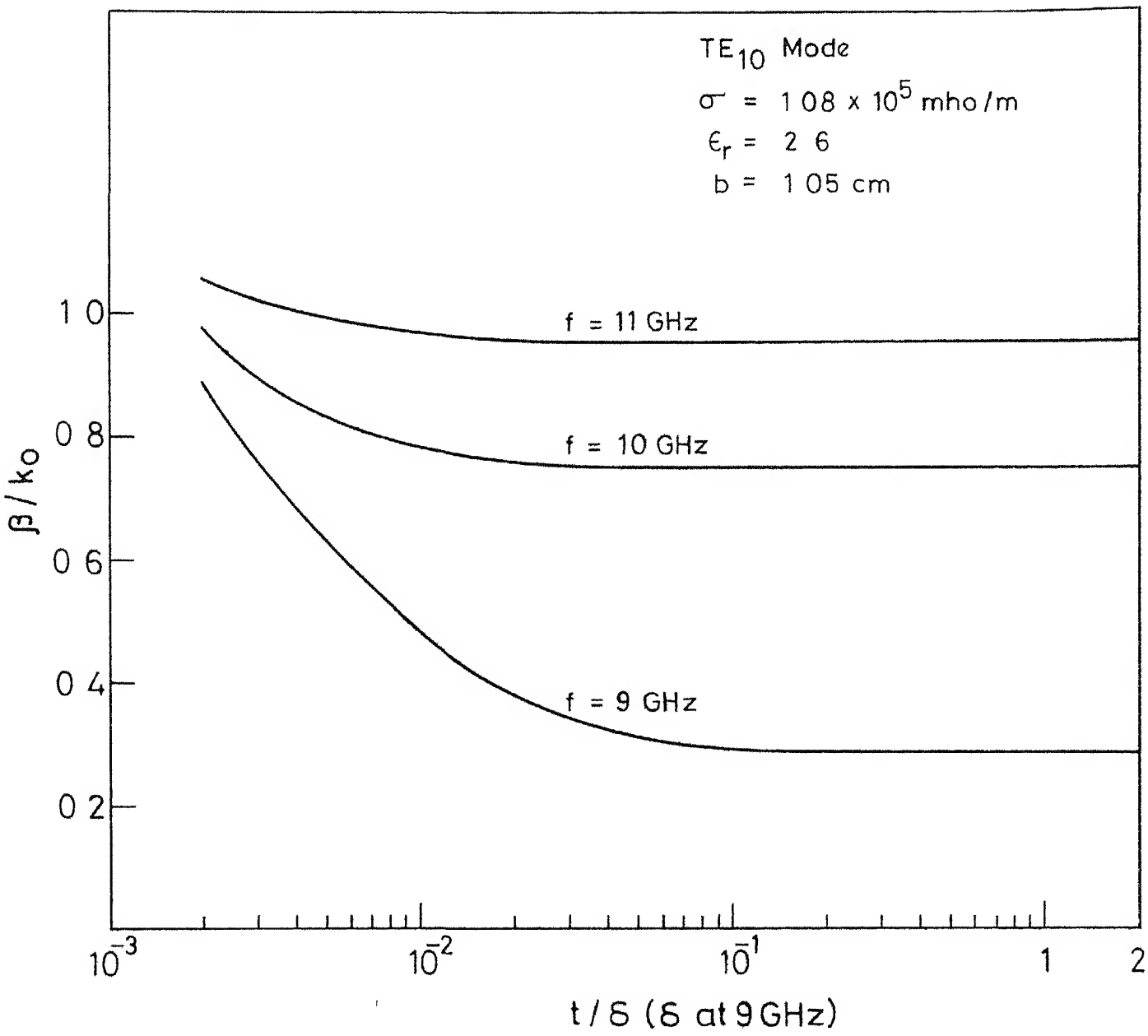

Fig.2.6 Variation of β/k_0 with t/δ and frequency as a parameter

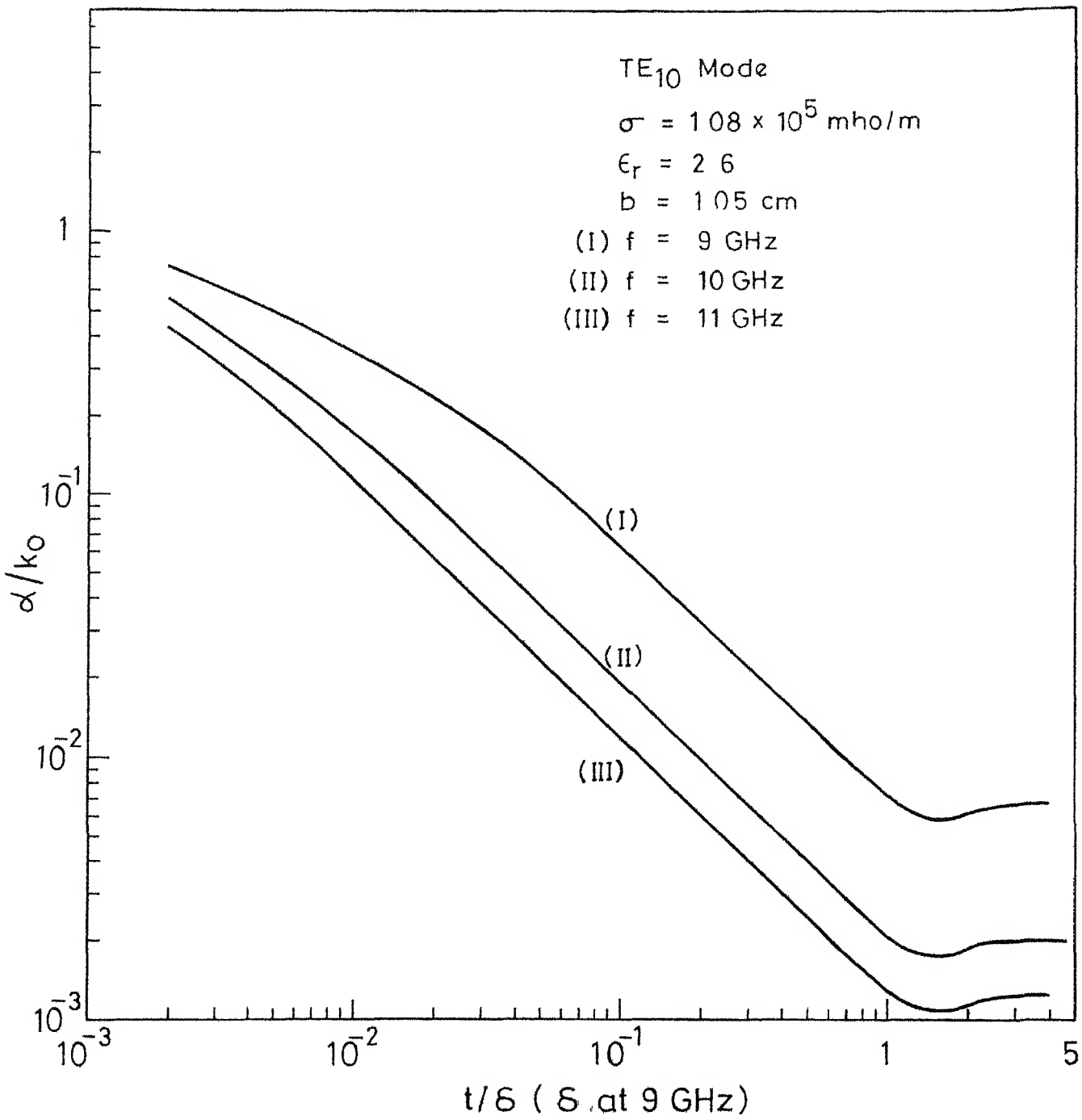

Fig.2.7 Variation of attenuation constant with t and frequency as a parameter

2.2 NATURE OF WAVES GUIDED ALONG THE SURFACE OF STRUCTURE

Till now our effort has been directed towards studying and interpreting propagation constant. Now we will use this knowledge for studying the nature of waves guided along the surface of the structure. The important parameters in this study are γ and h_3 or p_3. From a knowledge of γ c/v ratio can be easily obtained, which is an important parameter in the study of waves guided along the structure.

The guiding surface of the structure is metal-air interface defined by the plane x=t (Figure 2.1). Waves supported by this interface can be classified into two categories: fast waves and slow waves. Fast waves are characterised by the fact that their phase velocity along the longitudinal direction is greater than the velocity of light (c) in free space. These waves are associated with the radiation pattern of a leaky wave antenna. For slow waves, the phase velocity along the longitudinal direction is less than or equal to c, i.e. β is greater than or equal to k_0. Antennas which utilize slow waves and radiate in endfire direction are called surface wave antennas. It is shown in the next section that there is another class of waves called slow leaky waves which utilize slow waves

($c/v > 1$) and radiate away from endfire.

In the remaining portion of this section we want to study the effect of variation of thickness of the imperfect plate (with conductivity held constant) on the nature of TEM-like, TM and TE waves supported by this structure.

Case I TEM-like mode: Here it is shown that in this case, leaky waves cannot be supported.

The phase velocity for the TEM-mode is equal to $c/\sqrt{\epsilon_r}$. For finite values of t TEM-like mode starts propagating and as seen from Figure 2.2 the value of β increases with decrease in t (for $t/\delta > \pi/2$). Therefore, the wave becomes slower with the decrease in t. Consideration of expressions for γ and p_3 for TEM-like mode (eqn.(2.3f)), shows that the wave attenuates along the direction of propagation z and in the transverse direction x. This is similar to the surface wave on a lossy interface [11].

Case II TM, TE modes: Here it is shown that both the fast leaky wave and slow leaky waves are possible.

When the unperturbed structure propagates TM_{n0} or TE_{n0} mode, the corresponding wave is a fast wave. It has been shown in Figure 2.2 that for TM_{10} and TE_{10} modes, the value of β increases with the decrease in t. But,

β remains less than k_0. Consideration of expressions for γ and p_3 or h_3 for these modes given by eqn. (2.3f) or (2.3c) shows that for all values of t the wave is growing along the transverse direction and attenuating along the direction of propagation. Thus, the TM_{10} or TE_{10} waves propagating along the structure are leaky waves. If the conductivity and/or thickness of the imperfect plate is decreased to very low values slow leaky waves are obtained. Nature and characteristics of this type of waves is discussed in the next section.

2.3 SLOW LEAKY WAVES

A slow leaky wave is defined to be characterised by phase velocity less than the velocity of light and the wave grows along the transverse direction. In the knowledge of the author** this type of wave has not been reported earlier. Table 2.1 gives some typical sets of parameters for which slow leaky waves are obtained.

** However, Oliner has reported slow leaky space charge waves [22]. These are space charge waves present on a modulated electron beam. In contrast to slow leaky waves reported here slow leaky space charge waves grow in the longitudinal direction.

TABLE 2.1

Sets of parameters for which slow leaky waves are obtained

Mode	f	ε_r	b(cm)	K	t/δ	γ/k_0	θ_m
TE	8 GHz	2.6	1.27	$1+j10^7$	2×10^{-4}	1.006 + j0.89	36°
	9 GHz				2×10^{-4}	1.088 + j0.50	51°
	9 GHz				4×10^{-4}	1.015 + j0.33	54°
TM	8 GHz	1	2.41	16+j16	6×10^{-4}	1.09 + j0.62	33°

Table 2.1 shows that slow leaky waves are associated with relatively large values of attenuation. This large attenuation is responsible for radiation away from endfire although the phase velocity is less than c. The direction of maximum radiation (θ_m) is given by [8]

$$\sin\theta_m = \sin\xi/\cosh\eta \qquad (2.11)$$

where ξ and η are related to β/k_0 and α/k_0 through the relation

$$\sin\xi\cosh\eta + j\cos\xi\sinh\eta = \beta/k_0 + j\alpha/k_0 \qquad (2.12)$$

Equations (2.11) and (2.12) give for θ_m

$$2\sin^2\theta_m = 1+\left(\frac{\alpha}{k_0}\right)^2+\left(\frac{\beta}{k_0}\right)^2-\left[\left\{1+\left(\frac{\alpha}{k_0}\right)^2+\left(\frac{\beta}{k_0}\right)^2\right\}^2-4\left(\frac{\beta}{k_0}\right)^2\right]^{\frac{1}{2}} \qquad (2.13)$$

Equation (2.13) has been used in calculating θ_m given in Table 2.1. A relation between β/k_0 and α/k_0 for slow leaky waves may be obtained as follows.

Let the variation of the field along the structure be of the form

$$E = e^{jhx+j\gamma z} \tag{2.14}$$

where $$\gamma = \beta + j\alpha \tag{2.15}$$

and $$h/k_0 = [\varepsilon_r' - (\gamma/k_0)^2]^{\frac{1}{2}} \tag{2.16}$$

Substitution of eqn. (2.15) for γ in eqn. (2.16) gives

$$h/k_0 = [X-jY]^{\frac{1}{2}} \tag{2.17}$$

where $$X = \varepsilon_r' - (\beta/k_0)^2 + (\alpha/k_0)^2 \tag{2.18}$$

and $$Y = 2\,\alpha/k_0\,\beta/k_0 \tag{2.19}$$

From the behaviour of Re (h/k_0) and Im (h/k_0) the conditions on β/k_0 and α/k_0, which give surface waves, leaky waves and slow leaky waves; are obtained.

(i) Leaky waves: For leaky waves the condition on 'h' is

$$\text{Re } (h) > 0 \tag{2.20a}$$

$$\text{Im } (h) < 0 \tag{2.20b}$$

The conditions (2.20) are satisfied for $X \geq 0$, i.e.

$$\varepsilon_r' - (\beta/k_0)^2 + (\alpha/k_0)^2 \geq 0 \tag{2.21}$$

(ii) Surface Waves: The conditions on 'h' are

$$\text{Re}\,(h) < 0 \tag{2.22a}$$

$$\text{Im}\,(h) > 0 \tag{2.22b}$$

The conditions for surface waves are satisfied for $X < 0$, i.e.

$$\varepsilon_r - (\beta/k_0)^2 + (\alpha/k_0)^2 < 0 \tag{2.23}$$

For radiation in free space ε_r is unity. Therefore, the conditions for leaky waves and surface waves become

$$1 + (\alpha/k_0)^2 \geq (\beta/k_0)^2 \text{ (Leaky wave)} \tag{2.24a}$$

$$1 + (\alpha/k_0)^2 < (\beta/k_0)^2 \text{ (Surface wave)} \tag{2.24b}$$

Equations (2.24) show that the curve defined by

$$(\beta/k_0)^2 = 1+(\alpha/k_0)^2 \tag{2.25}$$

separates the leaky wave region from the surface wave region. Eqn. (2.25) is the equation of a hyperbola. It has been plotted in Figure 2.8. Surface wave and leaky wave regions have been marked in it. The portion of the leaky wave region with $\beta/k_0 > 1$, where the phase velocity is less than the velocity of light, is the region for slow leaky waves.

Radiation characteristics of slow leaky waves is different from fast leaky waves. It is discussed in Chapter 4.

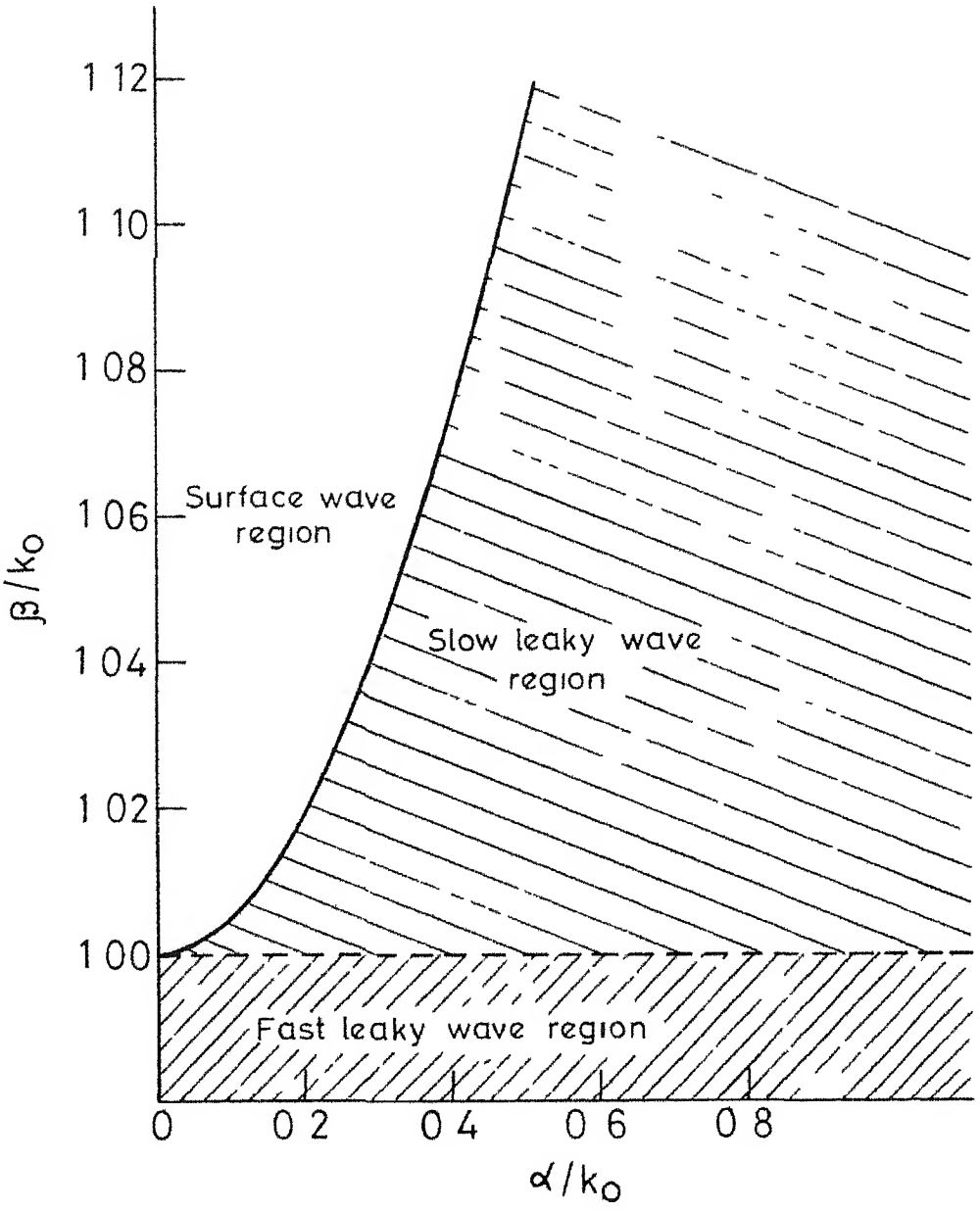

Fig. 2.8 Graph showing the relation between β/k_0 and α/k_0 for surface waves, leaky waves and slow leaky waves

CHAPTER 3

ATTENUATION CHARACTERISTICS

CHAPTER 3

ATTENUATION CHARACTERISTICS

In the last chapter the expression for the propagation constant was obtained by finding the roots of the dispersion relation. However, in some cases it may not be necessary to solve the dispersion relation. Instead, the effect of thickness and conductivity on attenuation may be taken into account by considering the input impedance Z_{in} of the imperfect plate. This is achieved by using transverse resonance technique. The results for attenuation obtained in this chapter are valid when the phase constant is almost equal to the unperturbed value. This condition is satisfied when sheet resistance $1/\sigma t$ is much less than free space impedance i.e. $\sigma t >> 1/120\pi$. It will be shown that the attenuation is minimum for a thickness t such that $t/\delta=\pi/2$. Propagation near cut-off has also been discussed.

3.1 PROPAGATION CONSTANT USING TRANSVERSE RESONANCE TECHNIQUE

In this method analysis is carried out in terms of the propagation in the transverse direction. Matching the impedances transverse to the interface (x=0) yields the dispersion relation which is solved for the propagation constant. The effect of the thickness t of the imperfect plate is taken into account by considering it as a

transmission line of length t. For the range of values of σ and t, which are useful in the design of a leaky wave antenna, the attenuation given by eqns. (2.9) and (2.10) may be replaced by a very simple expression. This simplification will permit us to analytically predict the beamwidth of antenna. The complete analysis will be carried out for TE_{no}-mode only

Figure 3.1 shows the transmission line representation of the waveguide structure shown in Fig.2.1.

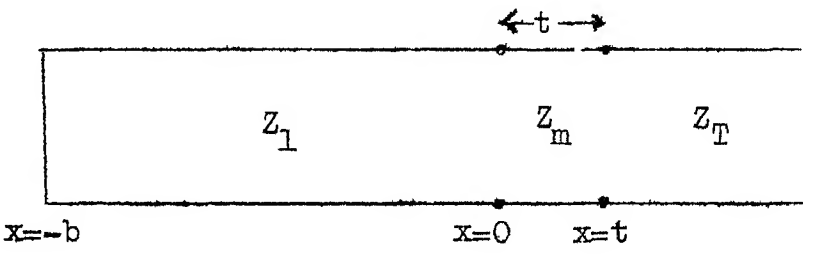

Fig.3.1 Transmission line representation of the structure in Fig.2.1

Here Z_1 is the x-directed wave impedance for the incident wave, Z_m is the intrinsic impedance of metal and Z_T is the wave impedance for the transmitted wave. Equating the impedances at the interface defined by x=0 the following relation is obtained

$$Z + Z_{in} = 0 \qquad (3.1)$$

where Z is the impedance of the wave as seen in the +x direction and Z_{in} is the impedance in -x direction. Both Z and Z_{in} are evaluated at the interface x=0. From the transmission line theory Z_{in} is obtained as

$$Z_{in} = Z_m \frac{Z_T - jZ_m \tan(h_2 t)}{Z_m - jZ_T \tan(h_2 t)} \tag{3.2}$$

with $h_2 = (1+j)/\delta$ (3.3)

and $Z_m = (1-j)\, R_s$ (3.4)

R_s is the sheet resistance or skin depth resistance of metal plate. It is given by $1/\sigma\delta$. Also, impedance Z is given by

$$Z = -jZ_1 \tan(h_1 b) \tag{3.5}$$

Using eqn. (3.5) for Z, eqn. (3.1) becomes

$$jZ_1 \tan(h_1 b) = Z_{in} \tag{3.6}$$

When the wave impedances are substituted in terms of transverse propagation constants for TEM-like, TM or TE-mode, eqn. (3.6) gives the corresponding dispersion relation. For TE_{no}-mode

$$Z_1 = \omega\mu_0/h_1 \tag{3.7a}$$

$$Z_m = \omega\mu_0/h_2 \tag{3.7b}$$

and $$Z_T = \omega\mu_0/h_3 \tag{3.7c}$$

Using eqns.(3.7) and substituting eqn. (3.2) for Z_{in} in

eqn.(3.6) yields the dispersion relation (2.5a). This dispersion relation will be solved in the next section for the case when change in phase constant $\delta\beta$ is negligible.

3.1.1 Simplified expression for attenuation constant

Substituting the expression for Z_1 (eqn.(3.7a)), eqn.(3.6) becomes

$$j\,\omega\mu_0 \tan(h_1 b) = h_1 Z_{in} \qquad (3.8)$$

Using eqn. (1A) for h_1 and eqn. (2A) for $\tan(h_1 b)$ (from Appendix A), the expression for $\delta\gamma/k_0$ for TE-mode is obtained as

$$\frac{\delta\gamma}{k_0} = j\,\frac{Z_{in}}{Z_0 n\pi}\left(\frac{n\pi}{k_0 b}\right)^3 \frac{1}{\gamma_0/k_0} \qquad (3.9)$$

where Z_0 is the free space impedance. Similarly expressions for $\delta\gamma/k_0$ for TM-mode and TEM-like mode are obtained as

$$\frac{\delta\gamma}{k_0} = j\frac{Z_{in}}{Z_0}\,\frac{\epsilon_r}{k_0 b}\,\frac{1}{\gamma_0/k_0} \quad \text{(TM-mode)} \qquad (3.10)$$

$$\frac{\delta\gamma}{k_0} = j\frac{Z_{in}}{2Z_0}\,\frac{\epsilon_r}{k_0 b}\,\frac{1}{\gamma_0/k_0} \quad \text{(TEM-like mode)} \qquad (3.11)$$

Note that the value of $\delta\gamma/k_0$ for TEM-like mode is not half of $\delta\gamma/k_0$ for TM-mode because the value of b is different in the two cases. Also,

$$\frac{\delta\gamma}{k_0} = \frac{\delta\beta}{k_0} + j\,\frac{\alpha}{k_0} \qquad (3.12)$$

Therefore, expressions for attenuation constant are obtained as

$$\frac{\alpha}{k_0} = \frac{\mathrm{Re}(Z_{in})}{Z_0}\frac{1}{n\pi}\left(\frac{n\pi}{k_0 b}\right)^3 \frac{1}{\gamma_0/k_0} \quad \text{(TE-mode)} \qquad (3.13)$$

$$\frac{\alpha}{k_0} = \frac{\mathrm{Re}(Z_{in})}{Z_0}\frac{\varepsilon_r}{k_0 b}\frac{1}{\gamma_0/k_0} \quad \text{(TM-mode)} \qquad (3.14)$$

$$\text{and } \frac{\alpha}{k_0} = \frac{\mathrm{Re}(Z_{in})}{2Z_0}\frac{\varepsilon_r}{k_0 b}\frac{1}{\gamma_0/k_0} \quad \text{(TEM-like mode)} \qquad (3.15)$$

The above expressions for attenuation agree with those given in [1] except that the quantity Z_{in} takes into account the effect of thickness also. The above expressions indicate that the attenuation is proportional to Re (Z_{in}). In order to see the effect of thickness on attenuation the behaviour of Z_{in} with respect to t is discussed next.

Equation (3.2) for Z_{in} shows that Z_{in} is a function of thickness t, impedances Z_m and Z_T, and transverse wave number h_2 in metal. If under certain conditions Z_{in} becomes independent of the mode propagating in the waveguide the same expression for Z_{in} can be used in all the three expressions for α/k_0. The only quantity in Z_{in} which depends on the mode propagating in the waveguide is Z_T. Z_m and h_2 are almost independent of the modes as can be seen from eqns. (3.4) and (3.3).

For good conductors $|Z_m| << |Z_T|$. For example, the value of $|Z_m|$ for copper ($\sigma=5.87\times10^7$ mho/m) at 8 GHz is 0.023 ohm while the value of Z_T may be greater than 100 ohms. Assuming t is large so that $|Z_T \tan(h_2 t)| >> |Z_m|$, eqn. (3.2) for Z_{in} may be simplified as

$$Z_{in} = j Z_m \cot(h_2 t) \qquad (3.16)$$

This expression for Z_{in} is independent of the mode propagating in the structure.

When t approaches infinity $\tan(h_2 t)$ approaches j. Therefore Z_{in} tends to Z_m and Re (Z_{in}) tends to R_s. In this limit eqns.(3.13) to (3.15) for the attenuation constant become

$$\frac{\alpha}{k_0} = \frac{R_s}{Z_0 n\pi} \left(\frac{n\pi}{k_0 b}\right)^3 \frac{1}{\gamma_0/k_0} \quad \text{(TE-mode)} \qquad (3.17)$$

$$\frac{\alpha}{k_0} = \frac{R_s}{Z_0} \frac{\varepsilon_r}{k_0 b} \frac{1}{\gamma_0/k_0} \quad \text{(TM-mode)} \qquad (3.16)$$

and $$\frac{\alpha}{k_0} = \frac{R_s}{2Z_0} \frac{\varepsilon_r}{k_0 b} \frac{1}{\gamma_0/k_0} \quad \text{(TEM-like mode)} \qquad (3.19)$$

These expressions agree with those in [1]. Now that the expressions for attenuation as a function of thickness have been obtained, the behaviour of attenuation curve (Fig.2.3) is discussed in the following section.

3.1.2 Optimum thickness of the imperfect plate

In Section 3.1.1 simplified expressions for the attenuation constant were obtained. In this section optimum thickness of the conductor, which gives rise to minimum attenuation is obtained. Moreover, the shape of the attenuation curve (Fig.2.3) is also explained.

It has been observed in the last section that attenuation is directly proportional to R, the resistive part of Z_{in}. Hence, optimisation of R with respect to t will give the optimum thickness of the conductor.

The optimum thickness occurs for a value of t such that eqn. (3.16) may be used for Z_{in}. This approximation is consistent with the end results as can be seen later (eqn. 3.21). Optimisation of real part of eqn. (3.16) shows that it is minimum for t given by

$$\text{Re}\ (h_2 t) = \pi/2 \qquad (3.20)$$

$$\text{or}\quad t/\delta = \pi/2 \qquad (3.21)$$

The imperfect plate with a thickness t specified by eqn. (3.21) corresponds to a quarter wave line. Hence, minimum attenuation due to metal takes place when it is quarter wave in thickness. This result is verified from Figs. 2.3, 2.5 and 2.7. A similar behaviour has also been reported for microstrip lines. Horton et al. [23] have

shown that for microstrip minimum attenuation is obtained when the thickness of the strip is such that it is about twice the skin depth.

The percentage decrease in losses for thickness given by eqn. (3.21) may be obtained by calculating R for t equal to $\pi/2$ times the skin depth and for infinite thickness. The values of R are obtained as

$$R \approx 0.91\ R_s \qquad (\text{at } t/\delta=\pi/2) \qquad (3.22)$$

$$\text{and} \quad R \longrightarrow R_s \qquad (\text{as } t/\delta \longrightarrow \infty) \qquad (3.23)$$

It is obvious from above equations that the maximum decrease in R obtained is about 9 percent. The corresponding decrease in attenuation will also be about 9 percent. This compares very well with a decrease of about 10 percent obtained by Horton et al.,[23] for microstrip. The decrease in the value of R or Z_{in} for $t/\delta=\pi/2$ will give rise to an increase in the value of reflection coefficient R'. R' may be obtained from

$$R' = \frac{Z_{in} - Z_1}{Z_{in} + Z_1}$$

where Z_1 is the wave impedance for the incident wave at the interface.

The above analysis for the optimum thickness of metals shows that the reflectivity is maximum and conductor

losses is minimum for a thickness t such that $t/\delta=\pi/2$. These results can be utilized in increasing the reflectivity of metal sheets. Also, the Q of a metal cavity can be increased by about 9 percent. It is seen that increasing the number of layers of metal separated by layers of dielectric do not improve the reflectivity or decrease the conductor losses by more than 9 percent as reported here.

3.1.3 Effect of variation of thickness t on attenuation

Since attenuation is proportional to the resistive part of Z_{in} ($Re(Z_{in})$), the behaviour of attenuation curves with t, obtained earlier and shown in Figs. 2.3, 2.5 and 2.7 can be explained on the basis of behaviour of Re (Z_{in}). Figure 3.2 shows the plot of $Re(Z_{in})$ as a function of t. Consider eqn. (3.2) for Z_{in}. When the thickness is very large tan (h_2t) approaches j and the attenuation becomes constant with the increase in t. This region extends for $t/\delta > 3$. When the value of t is decreased, R passes through the optimum thickness region. For $t/\delta \leq 0.4$, tan (h_2t) may be approximated by h_2t and R becomes equal to $1/\sigma t$ which is equal to the d.c resistance of the metal sheet. The curve deviates from this inverse law behaviour when t is so small that the assumption $|Z_m| \ll |Z_T \tan(h_2t)|$ is no longer valid. For very small values of t

such that $|Z_T \tan(h_2 t)| << |Z_m|$, R is equal to $|Z_T|$. This defines the upper limit on the value of R. All these regions are shown in Fig.3.2. The attenuation curves for all the modes show this type of behaviour.

It is shown later in Chapter 4 that for TLA the region of interest of Re (Z_{in}) curve is that given by Re $(Z_{in}) = 1/\sigma t$. The expression for attenuation for TE_{10}-mode, eqn. (3.13), in this region may be written as

$$\frac{\alpha}{k_0} = \frac{1}{Z_0} \quad \frac{1}{\sigma t} \quad \frac{\pi^2}{(k_0 b)} \quad \frac{1}{\gamma_0/k_0} \qquad (3.24)$$

The value of attenuation given by above expression has been compared in Fig.3.3 with the exact numerical value. The set of parameters selected is $\varepsilon_r=2.6$, f=9GHz, $\sigma=10^6$ mho/m and $t/\delta=0.038$ and b varies from 1.05 cm to 1.3 cm. The agreement is seen to be very good. Therefore, eqn. (3.24) for the attenuation constant may be used to calculate the beamwidth of TLA.

Next, the effect of losses in dielectric on the attenuation is considered.

3.2 ATTENUATION DUE TO IMPERFECT DIELECTRIC

Losses in the dielectric may be taken into account by substituting $\varepsilon_r + j\varepsilon'$ for ε_r in the analyses for perfect

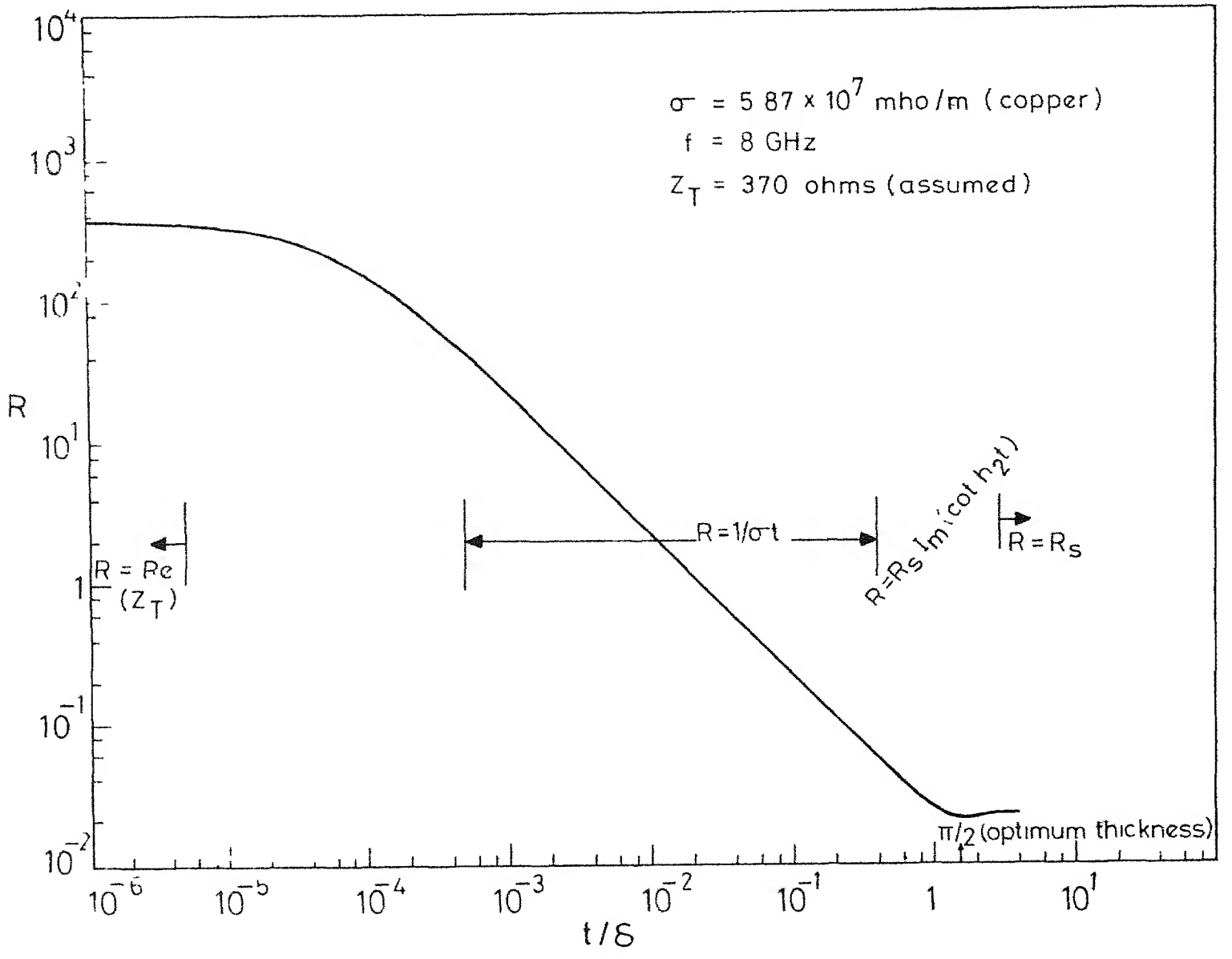

Fig.3.? Variation of surface resistance R with t/δ

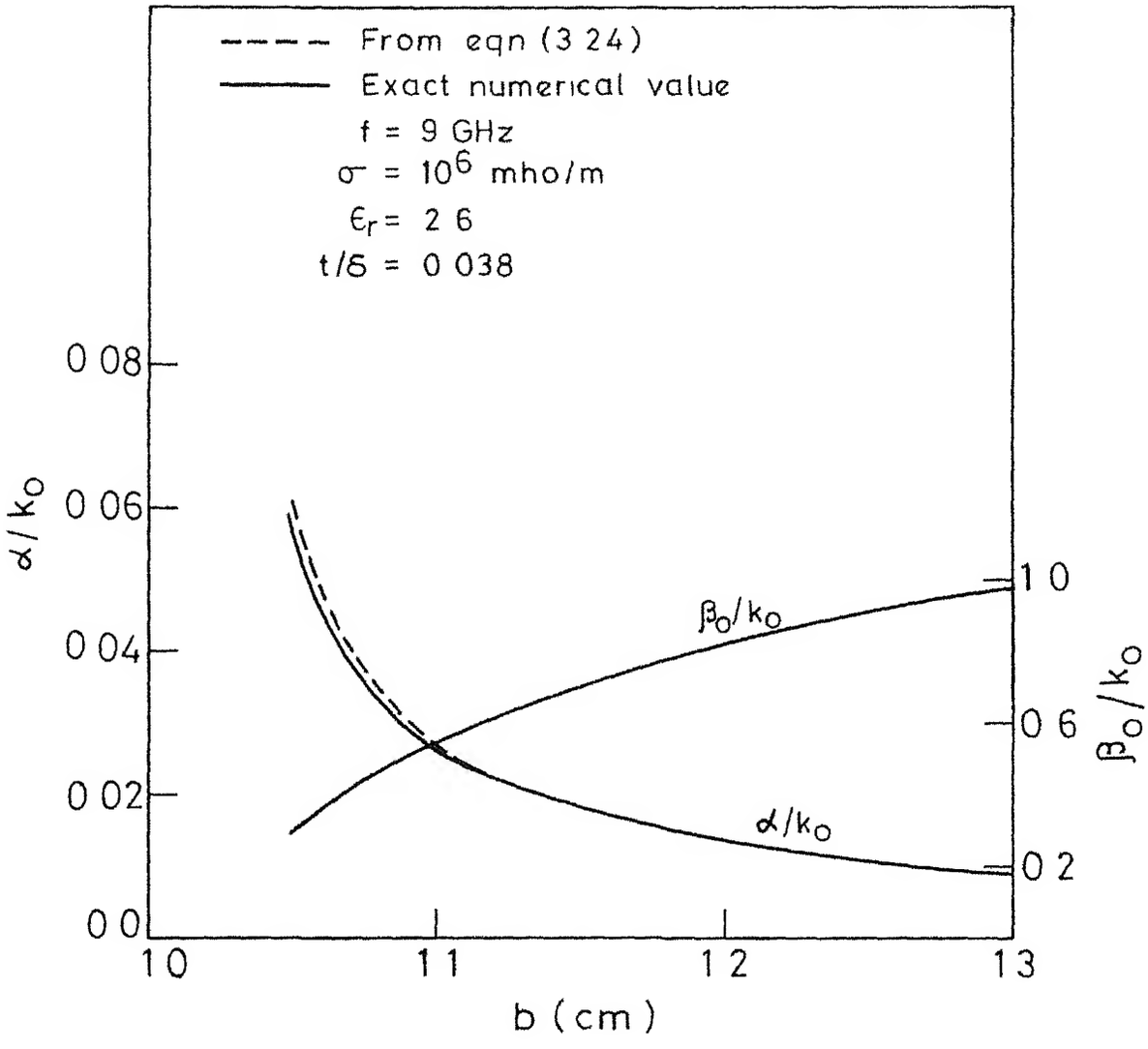

Fig.3.3 Comparison of α/k_0 obtained from the simplified expression and the exact numerical value

dielectric. Here, ε' is the loss tangent of the dielectric. The first order effect of losses in the dielectric may be obtained by expanding the expression for the propagation constant in a binomial series. This treatment has been carried out in [1]. Attenuation due to imperfect dielectric has been obtained as [ ].

$$\frac{\alpha_d}{k_0} = \frac{1}{2} \frac{\varepsilon'}{\gamma_0/k_0} \tag{3.25}$$

Since this analysis [ ] assumes a perfect conductor the coupling term between the dielectric loss α_d and the conductor loss α does not exist. It is shown below that the coupling term produces a second order effect in attenuation.

Due to losses in the dielectric the expression for h_1/k_0, eqn. (1A), is modified to

for TE_{no} and TM_{no} modes·

$$\frac{h_1}{k_0} = \frac{n\pi}{k_0 b} - \frac{k_0 b}{n\pi} \left[\frac{\gamma_0}{k_0} \frac{\delta_\gamma}{k_0} - \frac{1}{2} j\varepsilon'\right] \tag{3.26}$$

for TEM-like mode:

$$\frac{h_1}{k_0} = \left[-2 \frac{\gamma_0}{k_0} \frac{\delta_\gamma}{k_0} + j\varepsilon'\right]^{\frac{1}{2}} \tag{3.27}$$

Carrying out the analysis for attenuation in the same way as has been done in Section 3.1.1, expressions for the attenuation constant for the modes discussed are obtained as,

$$\frac{\alpha}{k_0} = \frac{R_s}{Z_0} \frac{(n\pi)^2}{(k_0 b)^2} \frac{1}{\gamma_0/k_0} + \frac{1}{2} \frac{\varepsilon'}{\gamma_0/k_0} - \frac{R_s}{2Z_0 k_0 b} \frac{\varepsilon'}{\gamma_0/k_0}$$

(TE-mode) (3.28)

$$\frac{\alpha}{k_0} = \frac{R_s}{Z_0} \frac{\varepsilon_r}{k_0 b} \frac{1}{\gamma_0/k_0} + \frac{1}{2} \frac{\varepsilon'}{\gamma_0/k_0} - \frac{R_s}{2Z_0} \frac{k_0 b \varepsilon_r}{(n\pi)^2} \frac{\varepsilon'}{\gamma_0/k_0}$$

(TM-mode) (3.29)

$$\frac{\alpha}{k_0} = \frac{R_s}{2Z_0} \frac{\varepsilon_r}{k_0 b} \frac{1}{\gamma_0/k_0} + \frac{1}{2} \frac{\varepsilon'}{\gamma_0/k_0} - \frac{R_s}{2Z_0} \frac{1}{k_0 b} \frac{\varepsilon'}{\gamma_0/k_0}$$

(TEM-like mode) (3.30)

It is seen from above expressions that total attenuation consists of three terms. These are due to conductor loss, dielectric loss and the coupling term between the conductor loss and the dielectric loss. The loss term due to the dielectric is the same for all the modes and is equal to that given in eqn. (3.25). The coupling term is different in the three cases. Also, it is proportional to the sheet resistance R_s and the loss tangent ε'. Since the coupling term is proportional to the product of two small quantitites R_s and ε', it gives rise to only a second order effect in attenuation.

3.3 ATTENUATION NEAR CUT-OFF

For a waveguide with perfectly conducting plates the cut-off point is determined by the relation $\gamma_0/k_0=0$. Consequently, the attenuation at cut-off, given by eqns. (3.17) to (3.19), should reach infinity. But, in practice the attenuation does not reach infinity at cut-off due to finite conductivity of the waveguide material [24]. Southworth [24] has shown that for frequencies immediately near cut-off the attenuation increases first rapidly (with decrease in frequency) but later more slowly approaching π/b nepers per meter for TE_{10} mode in a parallel plate waveguide. Moreover, a kind of 'cut-off' occurs at which phase constant and attenuation constant have the same value [24]. The critical frequency f_{cr}, at which this 'cut-off' occurs is lower than the cut-off frequency f_c for a perfectly conducting waveguide. These results were obtained for copper waveguide with infinite thickness. The effect of finite thickness of imperfect conductor on the propagation near cut-off is discussed here.

Equations (2.9) and (2.10) obtained earlier do not hold near cut-off. Moreover, it is not possible to predict even qualitatively the propagation near cut-off using these equations. Therefore, simple expressions for phase constant and attenuation constant in terms of surface

resistance and surface reactance of imperfect plate are derived here. These are then used to obtain qualitative information about the behaviour of β/k_0 and α/k_0 near cut-off.

Consider eqn. (2.3a) for h_1. It gives

$$\gamma/k_0 = [\varepsilon_r - (h_1/k_0)^2]^{\frac{1}{2}} \qquad (3.31)$$

For a perfect conductor $h_1=\pi/b$. For an imperfect conductor, let $h_1=\pi/b + \Delta h$. Substituting this expression for h_1 in eqn.(3.31) and neglecting the term containing $(\Delta h)^2$ gives

$$\frac{\gamma}{k_0} = [\varepsilon_r - (\frac{\pi}{k_0 b})^2 - 2 \frac{\pi}{k_0 b} \frac{\Delta h}{k_0}]^{\frac{1}{2}} \qquad (3.32)$$

The expression for Δh is obtained by comparing the ralation $h_1 = \pi/b + \Delta h$ and eqn. (1a A) (Appendix A) for h_1/k_0. It gives

$$\frac{\Delta h}{k_0} = - \frac{k_0 b}{\pi} \frac{\gamma_0}{k_0} \frac{\delta\gamma}{k_0} \qquad (3.33)$$

Using eqn. (3.9) for $\delta\gamma/k_0$ in above equation yields

$$\frac{\Delta h}{k_0} = - j \frac{Z_{in}}{\pi Z_0} (\frac{\pi}{k_0 b})^2 \qquad (3.34)$$

Substitute the above expression for $\Delta h/k_0$ in eqn.(3.32). It gives

$$\frac{\gamma}{k_0} = [\varepsilon_r - (\frac{\pi}{k_0 b})^2 + 2j \frac{Z_{in}}{\pi Z_0} (\frac{\pi}{k_0 b})^3]^{\frac{1}{2}} \qquad (3.35)$$

Writing $Z_{in} = R - jX$, eqn. (3.35) may be put in the form

$$\frac{\gamma}{k_0} = [\varepsilon_r - (\frac{\pi}{k_0 b})^2 + 2\frac{X}{\pi Z_0} (\frac{\pi}{k_0 b})^3 + 2j \frac{R}{\pi Z_0} (\frac{\pi}{k_0 b})^3]^{\frac{1}{2}} \tag{3.36}$$

Separating the real and imaginary parts of eqn.(3.36) yields,

$$\frac{\beta}{k_0} = \frac{1}{\sqrt{2}} [(A^2 + B^2)^{\frac{1}{2}} + A]^{\frac{1}{2}} \tag{3.37}$$

and $$\frac{\alpha}{k_0} = \frac{B}{2\beta/k_0} \tag{3.38}$$

where $$A = \varepsilon_r - (\frac{\pi}{k_0 b})^2 + 2 \frac{X}{\pi Z_0} (\frac{\pi}{k_0 b})^3 \tag{3.39}$$

and $$B = 2 \frac{R}{\pi Z_0} (\frac{\pi}{k_0 b})^3 \tag{3.40}$$

Note that the above expression for α/k_0 is the same as given in eqn. (3.13). For large thicknesses ($t > 4\delta$), $R = X = 1/\sigma\delta$ and the expressions for β/k_0 and α/k_0, eqns. (3.38) and (3.37), reduce to the corresponding expressions given in [24-25]. Behaviour of β/k_0 and α/k_0 near cut-off is discussed next and is verified for TE_{10} mode by using the numerical solution of eqn. (2.5a).

Position of cut-off

From eqns.(3.37) and (3.38) we see that 'cut-off', the position at which β/k_0 and α/k_0 have equal values, occurs.

when A is equal to zero, i.e.

$$\varepsilon_r - \left(\frac{\pi}{k_0 b}\right)^2 = -2\,\frac{X}{\pi Z_0}\left(\frac{\pi}{k_0 b}\right)^3 \qquad (3.41)$$

Since the surface reactance X is positive for TE_{10} mode R.H.S. of eqn. (3.41) is negative. For L.H.S. of above relation also to be negative the value of $k_0 b$ should be less than $\pi/\sqrt{\varepsilon_r}$. It means that either critical frequency f_{cr} is less than cut-off frequency f_c or critical thickness b_{cr} is less than cut-off thickness $b_c = \lambda_c/2$. This point is verified from Figures 3.4 and 3.5 where β/k_0 and α/k_0 have been plotted as a function of frequency near cut-off for TE_{10} mode. The values of β/k_0 and α/k_0 have been obtained by solving eqn. (2.5a) numerically. The values of parameters chosen are also listed in these figures. It is noted from these figures that the frequency f_{cr}, at which α/k_0 and β/k_0 are equal, is less than the cut off frequency f_c for infinite conductivity. The value of f_{cr} has been obtained by extrapolating the curves near f_c. The value of f_{cr} is lower than f_c by about 7.5 MHz at both the frequencies considered.

Since eqns. (3.37) and (3.38) are approximate this value of α/k_0 $(=\beta/k_0)$ is only approximate. However, it can be seen that this value of α/k_0 or β/k_0 is independent

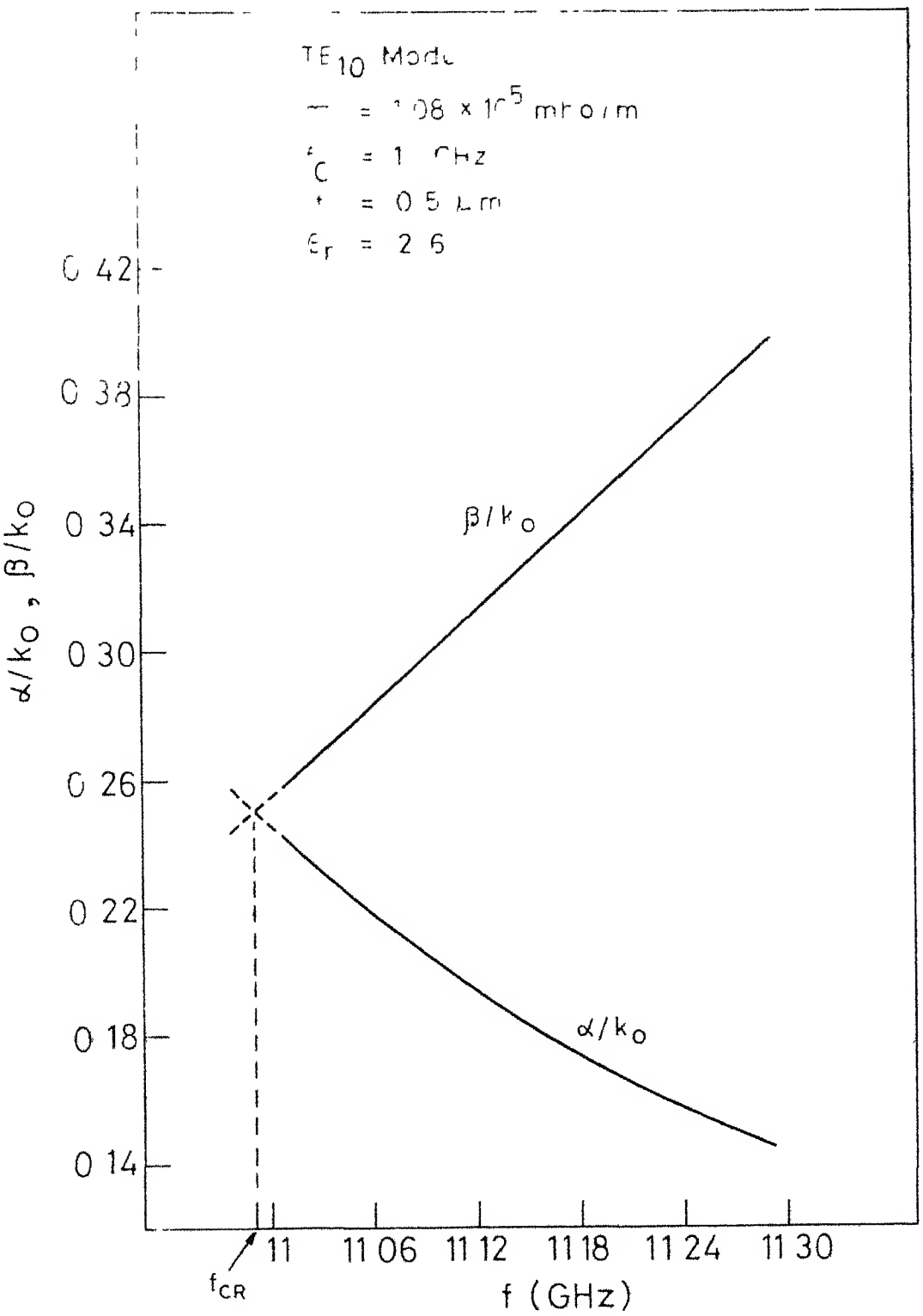

Fig.3.5 Variation of β/k_0 and α/k_0 with frequency near cutoff (f_c=11 GHz, σ=1.08x10^5 mho/m, t=0.5 μm, ε_r=2.6)

of frequency. This is also verified in Figures 3.4 and 3.5 which are based on exact numerical results.

The value of β/k_0 and α/k_0 at f_{cr} is $(B/2)^{\frac{1}{2}}$. The value of B decreases with the increase in value of σ because $R = 1/\sigma t$. For two different conductivities σ_1 and σ_2, the relationship between phase constants β_1 and β_2 at f_{cr} given by eqn. (3.40) is $\beta_1/\beta_2 = \sqrt{\sigma_2}/\sqrt{\sigma_1}$. Therefore, crossover should occur at lower values of β/k_0 or α/k_0 when σ is increased. This point is verified from Figures 3.4 and 3.6. Figure 3.4 (σ=1.08x10^5 mho/m) shows that the value of β/k_0 at cross over is 0.25. For σ = 1.08x10^6 mho/m the value of β/k_0 at cross over given by $\beta_1/\beta_2 = \sqrt{\sigma_2}/\sqrt{\sigma_1}$ is obtained as 0.079. Figure 3.6 shows that for this value of conductivity the value of β/k_0 at cross over point is 0.08.

Thus, we see that near cut-off phase constant is non-zero and the attenuation constant has a finite but not very large value. Exact values of attenuation constant can be obtained numerically.

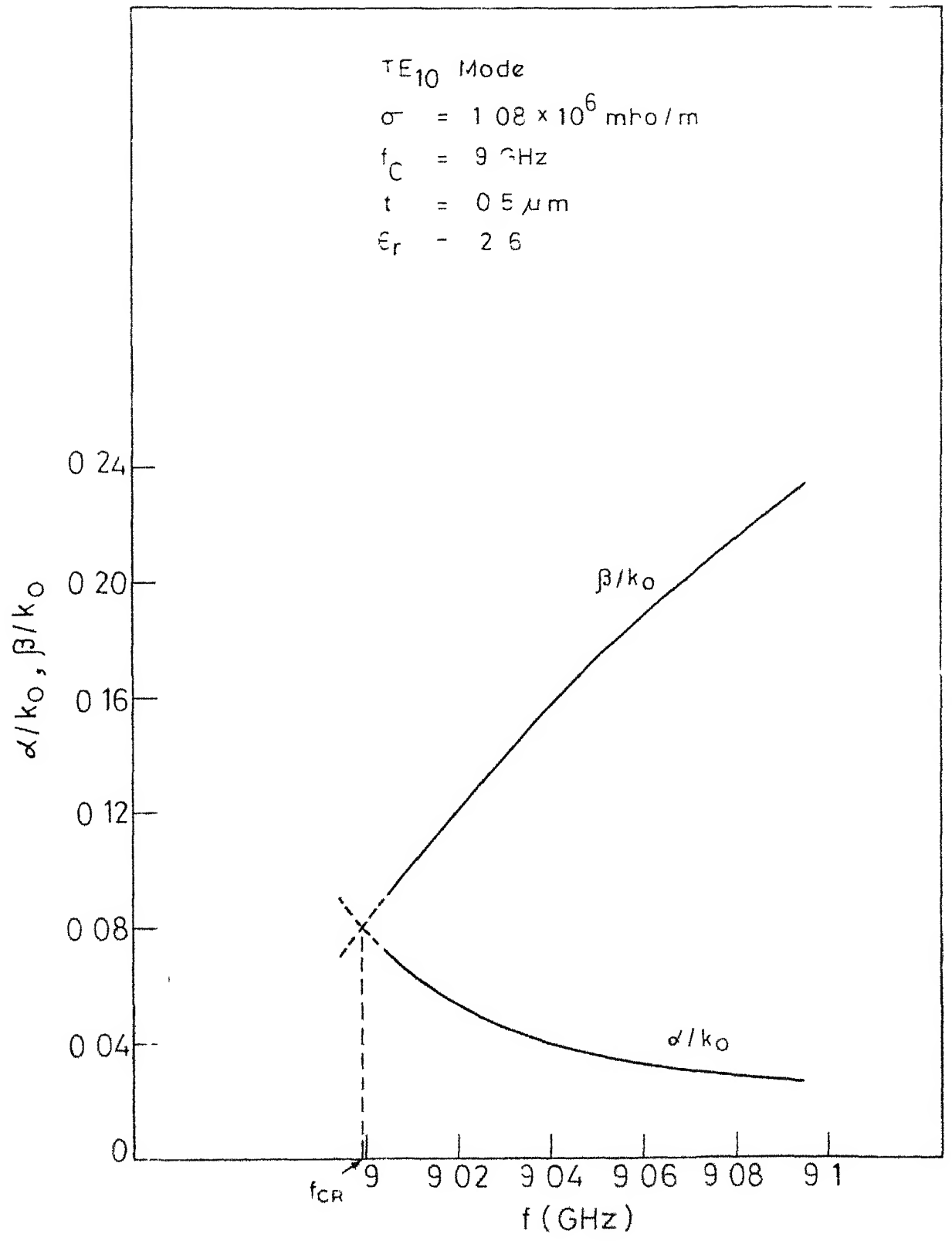

Fig.3.6 Variation of β and α/k_0 with frequency near cut-off

CHAPTER 4
RADIATION ~~ATTENUATION~~ CHARACTERISTICS

CHAPTER 4

RADIATION CHARACTERISTICS

In the last two chapters the waveguiding properties of the structure were discussed. The propagation constants obtained there will now be utilized to investigate the radiation characteristics of the structure. Radiation patterns will be obtained by using the method of steepest-descent and the Kirchhoff-Huygens method. Beamwidth and efficiency of TLA are also discussed. It is shown that there is a position of main beam θ_m at which beamwidth is minimum. A very simple expression for calculating this position θ_m is given. For large values of attenuation the main beam is not symmetrical about the half-power points. Also, antenna efficiency increases with the decrease in thickness and conductivity of imperfect wall. Increase in the value of ε_r gives rise to an increase in antenna efficiency.

4.1 LEAKY WAVE RADIATION USING TE MODE

In a parallel plate waveguide with perfectly conducting walls, all the energy is confined within the waveguide. There is no power flow outside the structure. But, when one of the plates is imperfectly conducting and sufficiently thin ($t << \delta$) a part of the power flowing inside the guide leaks out. This leakage of power gives rise to the

radiation pattern.

It was observed in Section 2.2 that the structure supports leaky waves when it is operated in TM_{no} or TE_{no} modes. This characteristic of the structure may be utilized to construct a leaky wave antenna using a TM_{no} or TE_{no} mode. However, it is difficult to construct a leaky wave antenna by exciting TM_{10} mode in a parallel plate structure since the dominant mode in a parallel plate waveguide is the TEM mode. This difficulty does not arise for TE_{10} mode in a rectangular waveguide with one of the narrow walls replaced by a thin film of metal. The above simplification will not change the radiation pattern in H-plane. However, radiation pattern in E-plane will be affected.

For a leaky wave antenna the radiation properties of the antenna depends on its propagation constant and length [8]. For small attenuations the position of maximum radiation is governed by the phase constant. Attenuation constant controls the beamwidth and the efficiency of antenna.

The radiation pattern of the structure utilizing TE_{10} mode is discussed next.

4.2 RADIATION PATTERN OF THE STRUCTURE

There are two different methods to obtain the theoretical radiation pattern of a leaky wave antenna. These are the method of steepest-descent [11] and the Kirchhoff-Huygens method. Steepest-descent method is useful for the radiation pattern of an infinitely long antenna. This method involves the solution of inhomogeneous wave equation using Fourier transform and contour integration. The integration is carried out by using the method of steepest-descent. This method has been discussed in detail by Tamir and Oliner [12]. This technique has been used by Gupta et al. [13] also.

In practice, it is not possible to construct an antenna with infinite length. However, because of the continuous leakage of power, as the wave propagates towards the other end of the antenna, the power left in the wave after a certain length of antenna becomes negligible and the effect of reflected wave may be neglected. Therefore, an infinite length antenna may be approximated in practice by an antenna of suitable finite length. The main advantage of the steepest descent method is that the radiation pattern may be obtained without solving the dispersion relation. Thus, it is of considerable help in the initial study of the leaky wave antennas.

4.2.1 Radiation pattern by steepest-descent method

In order to excite the TE_{10} mode in the waveguide, a distribution of electric line sources having the amplitude variation sin $(\pi x/b)$ and directed along the y-axis is assumed to be located at $z=0$, $-b \leq x \leq 0$. It is shown in Figure 4.1. These line sources are assumed to be uniform in the y direction so that the field produced by them is invariant with respect to y. Since, the structure is infinite in the y direction the field excited by this line source distribution has only the components E_y, H_x and H_z.

The solution for the radiation field is found by solving the following inhomogeneous wave equation for E_y

$$(\nabla^2 + k_o^2 \varepsilon_r) E_y(x,z) = j\omega \mu_0 \sin(\pi x/b)\delta(z) \qquad (4.1)$$

First, the solution for the Green's function $G(x,x',z)$ will be obtained. Green's function G is defined as the solution of eqn. (4.1) with a single line source of unit amplitude $\delta(x-x')\delta(z)$. Fourier transform of eqn. (4.1) with a single line source of unit amplitude gives

$$\left(\frac{\partial^2}{\partial x^2} - p^2 + k_0^2 \varepsilon_r\right) \Psi = j\omega \mu_0 \delta(x-x') \qquad (4.2)$$

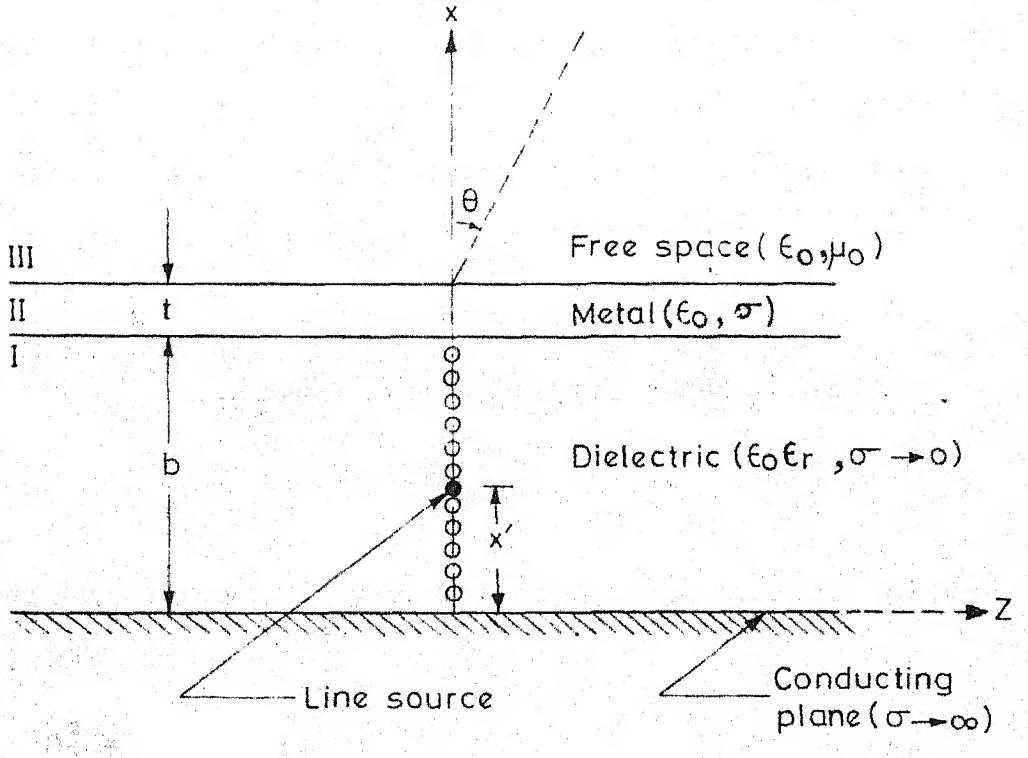

Fig. 4.1 Parallel plate configuration with line source distribution

where

$$\psi(x',x,p) = \int_{-\infty}^{\infty} G(x',x,z)e^{-jpz}\,dz \qquad (4.3)$$

Choosing a suitable form for $\psi(x',x,p)$ in the different regions of the structure, and matching the fields at the boundaries, an expression for ψ is obtained. Taking the inverse Fourier transform, it is found that, in the region defined by $x > t$, G is given by [10]

$$G = \frac{\omega\mu_0}{2\pi}\int_{-\infty}^{\infty} \frac{m_2 \sin(m_1 x')e^{jm_3(x-c)}}{\cos(m_1 b)\cos(m_2 t)[m_1(jm_3 \tan(m_2 t)-m_2)} e^{jpz}\,dp \qquad (4.4)$$

$$+ m_2 \tan(m_1 b)(jm_3+m_2 \tan(m_2 t))]$$

where m_1, m_2 and m_3, in the different regions, are given as follows:

$$m_1^2 = -p^2+k_0^2\,\varepsilon_r \qquad (4.5a)$$

$$m_2^2 = -p^2+k_0^2\,K \qquad (4.5b)$$

and $$m_3^2 = -p^2+k_0^2 \qquad (4.5c)$$

The steepest-descent method is customarily employed to solve the integrals of the type occuring in eqn.(4.4). In the present context, this method yields an asymptotic solution for the far-field. Following the usual method of evaluation [12], and using the transformation $x-t = r\cos\theta, z=r\sin\theta$, one obtains

$$G(r,\theta,x') \sim \frac{\omega\mu_0 F_1(\theta) e^{jk_0 r - j\pi/4}}{(2\pi k_0 r)^{\frac{1}{2}}} \tag{4.16}$$

where $F_1(\theta) = m_2' \sin(m_1' x') \frac{k_0 \cos\theta}{f(\theta)}$ (4.17)

and $f(\theta) = \cos(m_1' x')\cos(m_2' t)[m_1'(jm_3' \tan(m_2' t) - m_2')$

$$+ m'_2 \tan(m_1' x')(jm_3' + m_2' \tan(m_2' t))] \tag{4.18}$$

In eqns. (4.17) and (4.18) the expressions for m_1', m_2' and m_3' are

$$m_1' = k_0 (\epsilon_r - \sin^2\theta)^{\frac{1}{2}} \tag{4.19a}$$

$$m_2' = k_0 (K - \sin^2\theta)^{\frac{1}{2}} \tag{4.18b}$$

and $$m_3' = k_0 (1 - \sin^2\theta)^{\frac{1}{2}} \tag{4.19c}$$

The power radiation pattern given by $|F_1(\theta)|^2$, for a line source located at $x'=b/2$, is shown in Figure 4.2.

To determine the radiation pattern due to the distribution of line sources given by $\sin(\pi x/b)$, the principle of superposition is used and yields

$$E_y(r,\theta) = \int_0^b G(r,\theta,x') \sin(\pi x'/b) dx' \tag{4.20}$$

Substituting G from eqn. (4.16) and carrying out the integration gives,

$$E_y(r,\theta) = -\omega\mu_0 k_0 b\left(\frac{\pi}{2k_0 r}\right)^{\frac{1}{2}} F_2(\theta) e^{jk_0 r - j\pi/4} \qquad (4.21)$$

where the pattern function $F_2(\theta)$ is given by

$$F_2(\theta) = \frac{\sin(m_1' b) m_2'}{\pi^2 - (m_1' b)^2} \frac{\cos\theta}{f(\theta)} \qquad (4.22)$$

It is found that the factor $[\sin(m_1' b)/(\pi^2-(m_1' b)^2)]$ is a slowly varying function of θ. Therefore, the radiation pattern is governed principally by the other term $\cos\theta/f(\theta)$. The power radiation pattern obtained numerically by plotting $|F_2(\theta)|^2$ is shown in Figure 4.2. The third curve in this figure is from the Kirchhoff-Huygens method which is discussed in the next section. It is observed from this figure that the radiation pattern for a single line source and that due to a distribution of line sources, agree except for the amplitude near the broadside position. In both the cases the half power beamwidth is 6°.

Position of the peak in the radiation pattern

The maxima in the radiation pattern will occur for those values of θ for which $f(\theta)$ in eqns. (4.17) or (4.22) is minimum. This minimum can be found numerically. However, an expression for the position of the peak may also be derived for a special case when the metal film is several skin depths thick. Under this condition, $\tan(m_2' t)$ approaches j and $f(\theta)$ is minimum for

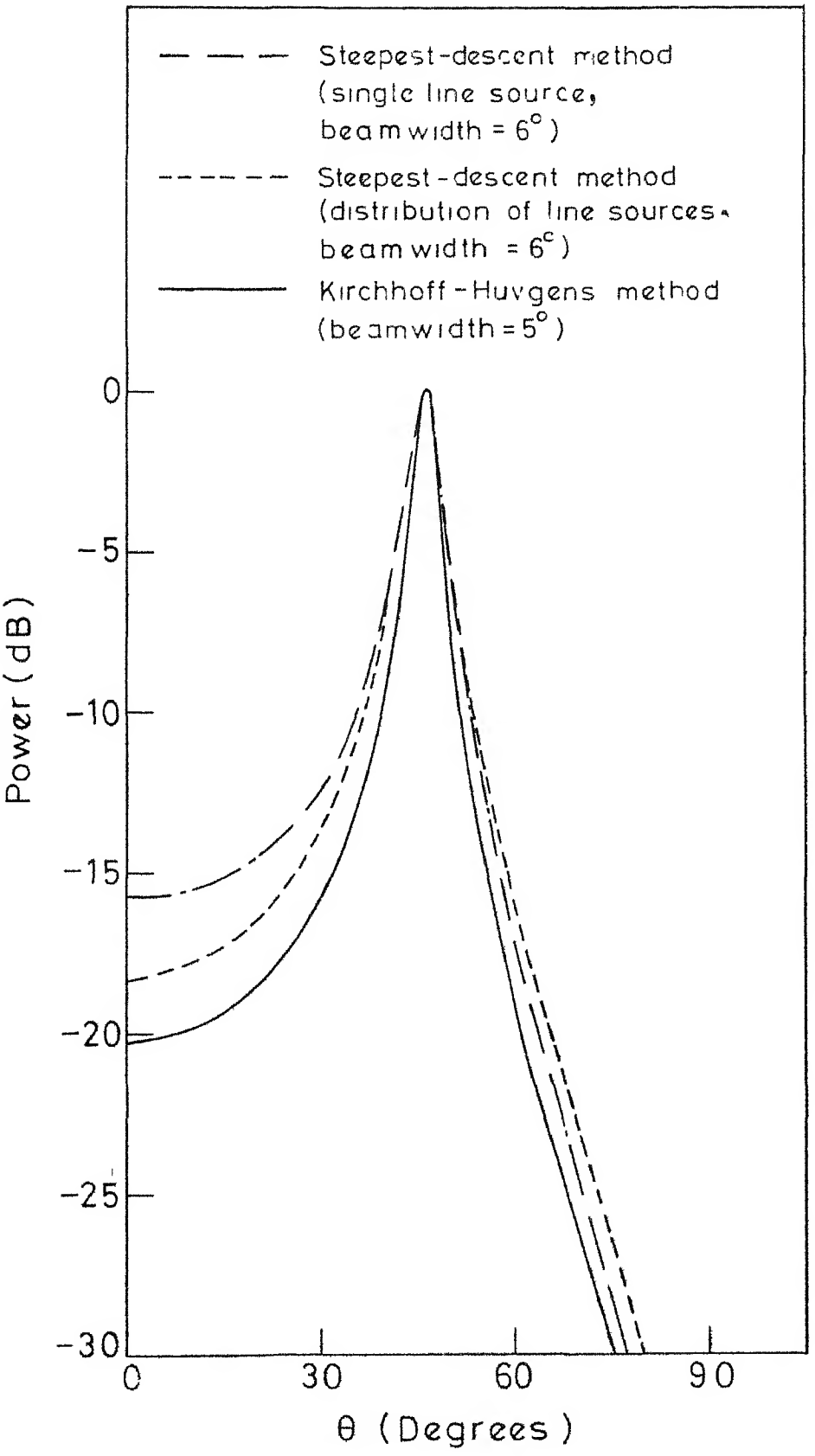

Fig.4.2 Comparison of radiation patterns obtained from the steepest-descent method and the Kirchhoff-Huygens method

$$\sin \theta_m = [\varepsilon_r - (\lambda/2b)^2]^{\frac{1}{2}} \qquad (4.23)$$

Therefore, the position of the peak is given by

$$\theta_m = \sin^{-1} [\varepsilon_r - (\lambda/2b)^2]^{\frac{1}{2}} \qquad (4.24)$$

The steepest-descent method discussed above cannot be used when the antenna has a finite length. The Kirchhoff-Huygens approach, on the other hand, allows one to study the effect of the antenna length also. It is discussed in the following section.

4.2.2 Radiation field using Kirchhoff-Huygens method

In this method the actual source of power is disregarded and a leaky wave distribution over the entire antenna aperture is assumed. The far field is found by a Kirchhoff-Huygens integration over the aperture [8]. The expression for the radiation pattern for an antenna of infinite length is given by [8]

$$F(\theta) = \frac{\cos^2 \theta}{|x|^2} \qquad (4.25)$$

and the radiation pattern for an antenna of finite length is obtained as [8]

$$F(\theta) = \cos^2(\theta) \left| \frac{\sin x}{x} \right|^2 \qquad (4.26)$$

where $x = (\sin \theta - \gamma/k_0) \cdot k_0 L/2$

$\underline{L}$ is the length of the antenna along z-direction and

θ is the angle of radiation measured from x-axis.

The radiation pattern obtained by using eqn. (4.25) is compared with the radiation pattern given by steepest-descent method. It is shown in Figure 4.2. It is to be noted that the agreement is quite good near the peak and on the end fire side of the peak. The beamwidth, obtained by using Kirchhoff-Huygens technique, is 5°. Steepest-descent method gives a beamwidth of 6°.

4.2.3 Radiation characteristics of slow leaky waves

It has been pointed out in section 2.3 that slow leaky waves are obtained when the thickness of imperfect plate is very small. This section deals with the radiation characteristics of these waves.

Slow leaky waves are associated with large values of attenuation α/k_0. This large value of α/k_0 is responsible for radiation away from end fire although the value of β is greater than k_0. Figure 4.3 shows the radiation pattern due to a slow leaky wave. Equation (4.26) has been used in calculating the radiation pattern. Note that the peak is obtained at an angle of 33°. Moreover, there are no sidelobes in the radiation pattern for the finite length of antenna. It is also due to large values of α/k_0.

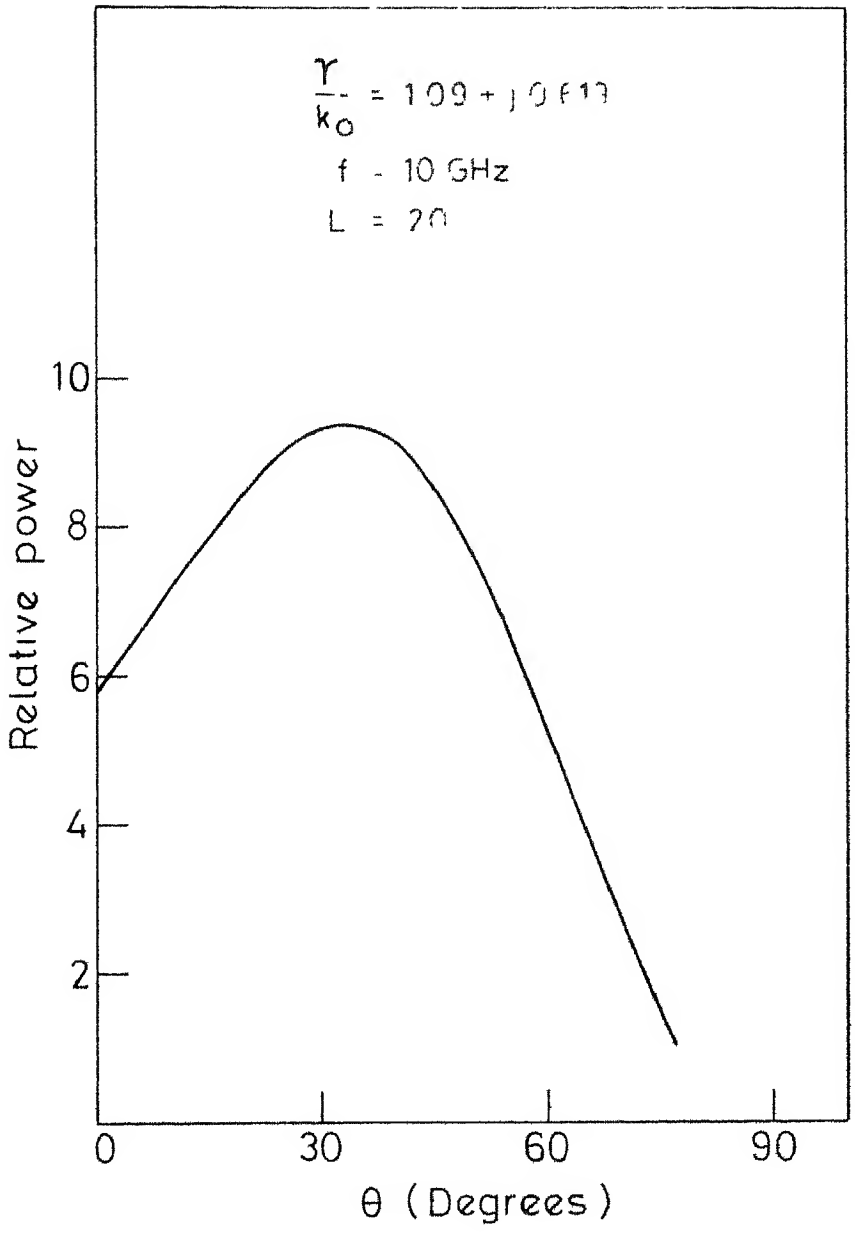

Fig. 4.3 Radiation pattern for a slow leaky wave antenna

4.2.4 Multiple beams

Multiple beams will be obtained in the radiation pattern whenever more than one mode of propagation contribute to the radiation pattern. It is shown that multiple beams are obtained for air dielectric ($\varepsilon_r=1$) while $\varepsilon_r=2.6$ gives rise to only a single beam.

When attenuation is not large the position of main beam θ_m is given by

$$\sin \theta_m = \beta/k_0 \qquad (4.27)$$

It is further assumed here that the change in phase constant $\delta\beta$ due to non-zero surface impedance is negligible. Under the above assumptions the position of beam $\theta_{m,n}$ for TLA is given by

$$\sin \theta_{m,n} = [\varepsilon_r-(n\lambda/2b)^2]^{\frac{1}{2}} \qquad (4.28)$$

Here, $\theta_{m,n}$ corresponds to the position of beam contributed by the $TE_{n,0}$ mode propagating in the structure. Large values of n give rise to beams located towards the broadside of the main beam. The number of beams N in the radiation region defined by θ_1 and θ_2 ($>\theta_1$) can be obtained by using eqn. (4.28). It is given by

$$N = \text{Integer}\left[\frac{2b}{\lambda}\sqrt{\varepsilon_r-\sin^2\theta_1}\right]-\text{Integer}\left[\frac{2b}{\lambda}\sqrt{\varepsilon_r-\sin^2\theta_2}\right] \qquad (4.29)$$

where Integer [x] stands for the highest integer $M \leq x$. Relation (4.29) is valid for values of $\lambda/2b$ such that $\theta_{m,1} \leq \theta_2$

For $\theta_1=0^\circ$ and $\theta_2=90^\circ$ the number of beams, given by eqn. (4.29), is

$$N = \text{Integer } [\frac{2b}{\lambda}\sqrt{\varepsilon_r}]-\text{Integer } [\frac{2b}{\lambda}\sqrt{\varepsilon_r-1}] \qquad (4.30)$$

Above relation shows that N increases with the increase in the value of $2b/\lambda$ and decrease in the value of (ε_r-1). The range of values of $\lambda/2b$ for leaky waves is given by

$$\sqrt{\varepsilon_r-1} < \lambda/2b < \sqrt{\varepsilon_r} \qquad (4.31)$$

For $\varepsilon_r=1$, N=Integer $(2b/\lambda)$ and the value of $2b/\lambda$ can be made as large as possible and still satisfying eqn. (4.28) for leaky waves. Therefore, the number of beams for air dielectric is very large. For $\varepsilon_r > 1$, second term in eqn. (4.30) is non-zero and the maximum value of $2b/\lambda$ is equal to $1/\sqrt{\varepsilon_r-1}$ which is not a large quantity. Therefore, the number of beams for $\varepsilon_r > 1$ is not very large.

Let us calculate the number of beams in the range $\theta_1 = 10^\circ$ and $\theta_2=70^\circ$. Further, let $\lambda/2b=0.2$. For $\varepsilon_r=1$, eqn. (4.29) gives the value of N equal to 3. These beams are located at 66°, 53° and 37°. For $\varepsilon_r=2.6$, only a single beam is obtained.

4.3 BEAMWIDTH OF TLA

Half-power beamwidth (HPBW) of an antenna is given in degrees by the difference between the half-power points located on either side of the main beam. Beamwidth of an antenna can be calculated from the radiation pattern. Alternatively, one can obtain an expression for the beamwidth from the expression giving the radiation pattern. It will be shown in Chapter 6 that one of the advantages of TLA is that it has low attenuation constant so that a long antenna can be used. Therefore, the beamwidth for an infinitely long antenna will be discussed. Equation (4.25) for the radiation pattern is used here to obtain the expression for HPBW.

The amplitude of power in the direction of maximum radiation θ_m (θ_m is specified by $\sin(\theta_m)=\beta/k_0$) is given by

$$F(\theta_m) = \cos^2(\theta_m)/(\alpha/k_0)^2\left(k_0L/2\right)^2 \qquad (4.32)$$

At the half-power point, let $\theta=\theta_1$. Equation (4.25) at the half-power point becomes

$$F(\theta_1) = \cos^2(\theta_1)/\,|x|^2 \qquad (4.33)$$

$$\text{where } x = (\sin\theta_1-\sin\theta_m - j\alpha/k_0)\,k_0L/2 \qquad (4.34)$$

Also,

$$F(\theta_1) = \tfrac{1}{2}F(\theta_m)$$

Therefore,

$$\cos^2\theta_1 / |x|^2 = \tfrac{1}{2} \cos^2\theta_m / (\alpha/k_0)^2 (b_0 L/2)^2 \qquad (4.35)$$

$$\text{or} \quad \frac{\cos^2\theta_1}{|\sin\theta_1 - \sin\theta_m - j\alpha/k_0|^2} = \tfrac{1}{2} \frac{\cos^2\theta_m}{(\alpha/k_0)^2} \qquad (4.36)$$

Expand $\sin\theta_1$ and $\cos\theta_1$ in a Taylor's series about θ_m and retain only the first two terms. The higher order terms $(\theta_1-\theta_m)^2$, $\sin^2\theta_m$ and $\cos^2\theta_m$ have been neglected because $(\theta_1-\theta_m)$, $\sin\theta_m$ and $\cos\theta_m$ are fractions. Under the above assumption, the expansion gives

$$\sin\theta_1 = \sin\theta_m + (\theta_1-\theta_m)\cos\theta_m \qquad (4.37)$$

$$\cos\theta_1 = \cos\theta_m - (\theta_1-\theta_m)\sin\theta_m \qquad (4.38)$$

Because of the approximation used in above equations the expression for beamwidth will also be an approximate one. The expression for beamwidth is obtained for two different degrees of approximations.

Case I Very sharp peak ($\theta_1 \simeq \theta_m$)

When the peak is very sharp and $\theta_m \neq \pi/2$, θ_1 approaches θ_m and $\cos\theta_1$ may be approximated by $\cos\theta_m$. This approximation in eqn. (4.36) gives

$$(\sin\theta_1 - \sin\theta_m)^2 + (\alpha/k_0)^2 = 2(\alpha/k_0)^2 \qquad (4.39)$$

Replacing $\sin\theta_1$ by the expression given in eqn. (4.37) one obtains,

$$\theta_1-\theta_m = \pm \frac{\alpha/k_\theta}{\cos(\theta_m)} \qquad (4.40)$$

Therefore,

$$BW(\text{degrees})=2\ |\theta_1-\theta_m| = 2\,\frac{\alpha/k_0}{\cos(\theta_m)}\cdot\frac{180}{\pi} \qquad (4.41)$$

Equation (4.41) shows that for very sharp peaks BW increases linearly with increase in α/k_0. The above expression for BW is valid for infinitely long antenna with low attenuation so that $\theta_1-\theta_m$ is small and the expansions, eqns (4.37) and (4.38), are justified. Relation (4.41) does not hold for θ_m near $\pi/2$.

4.3.1 Shape of the peak near half-power points

Equation (4.40) may be written in the form

$$\theta_1 = \theta_m \pm \frac{\alpha/k_\theta}{\cos(\theta_m)} \qquad (4.42)$$

The above equation shows that the two half-power points are situated equally spaced on either side of the main peak. This means that the shape of the peak, near half-power points, is symmetrical about its position. It is shown later in this section that for larger BW, when the assumption for very sharp peaks is not valid, the peak is not symmetrical about its position.

Case II When the peak is not very sharp or near broadside so that $\cos\theta_1=\cos\theta_m$ is not valid

Using eqns. (4.37) and (4.38) for $\sin\theta_1$ and $\cos\theta_1$

respectively in eqn. (4.36) gives

$$\theta_1-\theta_m = \frac{-B\pm(B^2-4AC)^{\frac{1}{2}}}{2A} \qquad (4.43)$$

where $A = 2\sin^2\theta_m\,(\alpha/k_0)^2 - \cos^4\theta_m$

$B = -2\sin(2\theta_m)\,(\alpha/k_0)^2$

and $C = \cos^2\theta_m\,(\alpha/k_0)^2$

Equation (4.43) is valid for $A<0$, i.e.

$$\alpha/k_0 < \frac{1}{\sqrt{2}}\,\frac{\cos^2\theta_m}{\sin\theta_m}$$

Note that when α/k_0 is very small such that $2\sin^2\theta_m(\alpha/k_0)^2 \ll \cos^4\theta_m$ and $B=0$, eqn. (4.43) reduces to eqn. (4.40) for sharp peaks.

Equation (4.43) may be written in the form

$$\theta_1 = \theta_m + \frac{-B\pm(B^2-4AC)^{\frac{1}{2}}}{2A} \qquad (4.44)$$

Denoting the two half-power points by θ_1' and θ_2' eqn.(4.44) gives for θ_1' and θ_2'

$$\theta_1' = \theta_m+\theta' \qquad (4.45)$$

$$\theta_2' = \theta_m-\theta'' \qquad (4.46)$$

where $$\theta' = \frac{-B+(B^2-4AC)^{\frac{1}{2}}}{2A} \qquad (4.47)$$

and $$\theta'' = \frac{B+(B^2-4AC)^{\frac{1}{2}}}{2A} \qquad (4.48)$$

Since θ' is not equal to θ'' the half-power points are not equidistant from θ_m and the peak is not symmetrical

near the half-power points. This is shown in Figure 4.4. However, when B approaches zero, θ' approaches θ'' and the peak becomes symmetrical.

Beamwidth is obtained by evaluating $|\theta'_1-\theta'_2|$. It is given by

$$BW(\text{degrees}) = \frac{\sqrt{B^2-4AC}}{A} \quad \frac{180}{\pi} \tag{4.49}$$

The effect of antenna parameters on the beamwidth of an infinitely long TLA has been considered in the following section.

4.3.2 Effect of variation of antenna parameters on BW of TLA

BW of an infinitely long antenna with sharp peaks is given by eqn. (4.42). This relation will be used here to calculate the BW of TLA. The value of α/k_0 for TLA operated in TE_{10} mode can be obtained from eqn. (3.13). The value of θ_m is given by the corresponding value of β/k_0. For TLA to radiate sufficient power the value of t/δ should be much less than unity. This can be seen from antenna efficiency curves plotted in Figures 4.7 to 4.9. For these values of t/δ, $Re(z_{in}) = 1/\sigma t$ and the expression for α/k_0 for TE_{10} mode (eqn. (3.13)) becomes

$$\frac{\alpha}{k_0} = \frac{1}{Z_0} \frac{\pi^2}{(k_0 b)^3} \frac{1}{\sigma t} \quad \frac{1}{\eta_0/k_0} \tag{4.50}$$

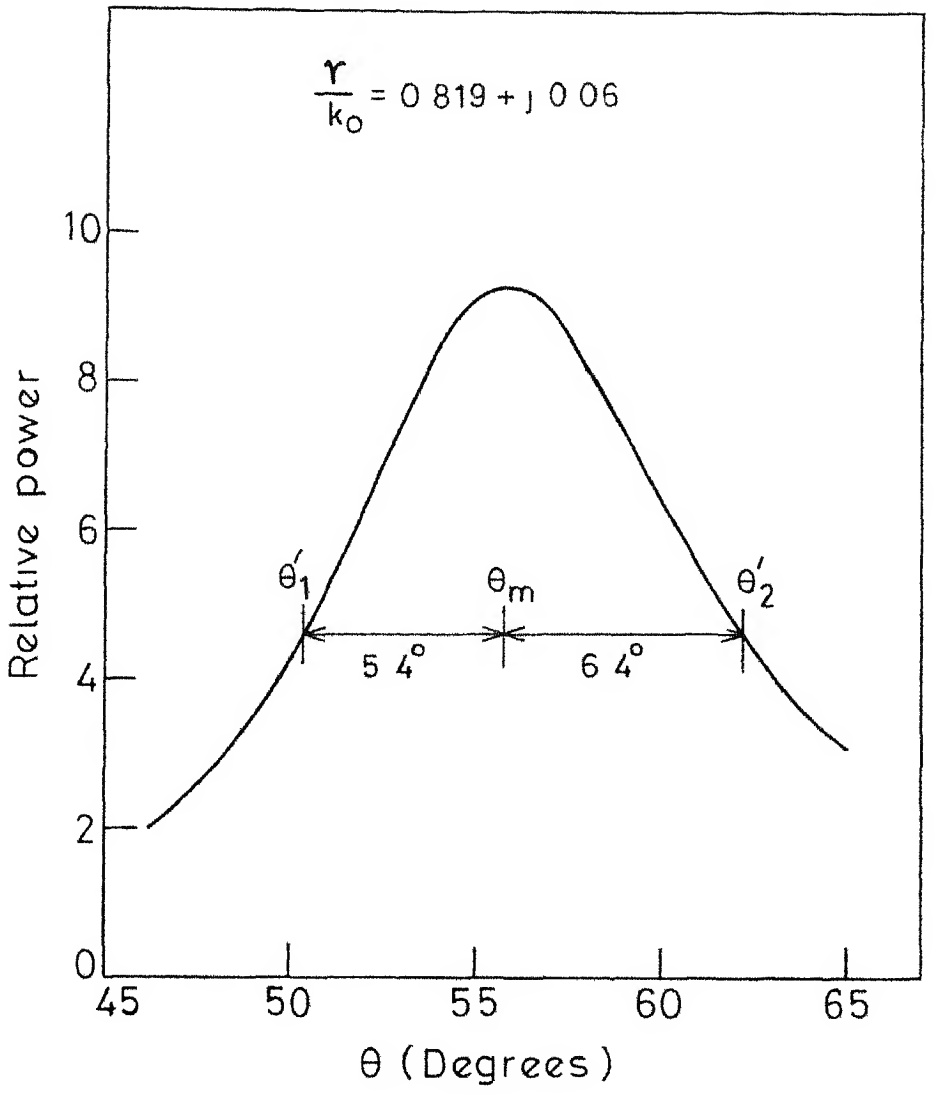

Fig.4.4 Shape of the main beam near half-power points

Substituting eqn. (4.50) for α/k_0 in eqn. (4.42), one obtains

$$BW = \frac{2}{Z_0} \frac{\pi^2}{(k_0 b)^3} \frac{1}{\sigma t} \frac{1}{\gamma_0/k_0} \frac{1}{\cos \theta_m} \qquad (4.51)$$

Equation (4.51) may be written in terms of $k_0 b$ by using eqn. (2.8). It gives

$$BW = \frac{2}{Z_0} \frac{\pi^2}{(k_0 b)^3} \frac{1}{\sigma t} \frac{1}{\sqrt{\varepsilon_r - (\pi/k_0 b)^2}} \frac{1}{\sqrt{1-\varepsilon_r + (\pi/k_0 b)^2}} \qquad (4.52)$$

Alternatively, one may write eqn. (4.51) in terms of θ_m by using $\gamma_0/k_0 = \sin \theta_m$. One obtains

$$BW = \frac{4}{Z_0} \frac{1}{\pi \sigma t} \frac{(\varepsilon_r - \sin^2 \theta_m)^{3/2}}{\sin (2\theta_m)} \qquad (4.53)$$

For $\varepsilon_r = 1$, the expression for BW becomes

$$BW = \frac{2}{Z_0} \frac{1}{\pi \sigma t} \frac{\cos^2 \theta_m}{\sin \theta_m} \qquad (4.54)$$

BW given by this expression has been compared in Figure 4.5 with the BW obtained from radiation patterns for $\sigma = 10^5$ mho/m and $t = 0.46$ μm. The agreement between the two values is seen to be very good.

4.3.3 Position of peak (θ_m) for optimum BW

To evaluate the effect of θ_m and ε_r on BW, eqn.(4.53) should be plotted as a function of θ_m with ε_r as a parameter.

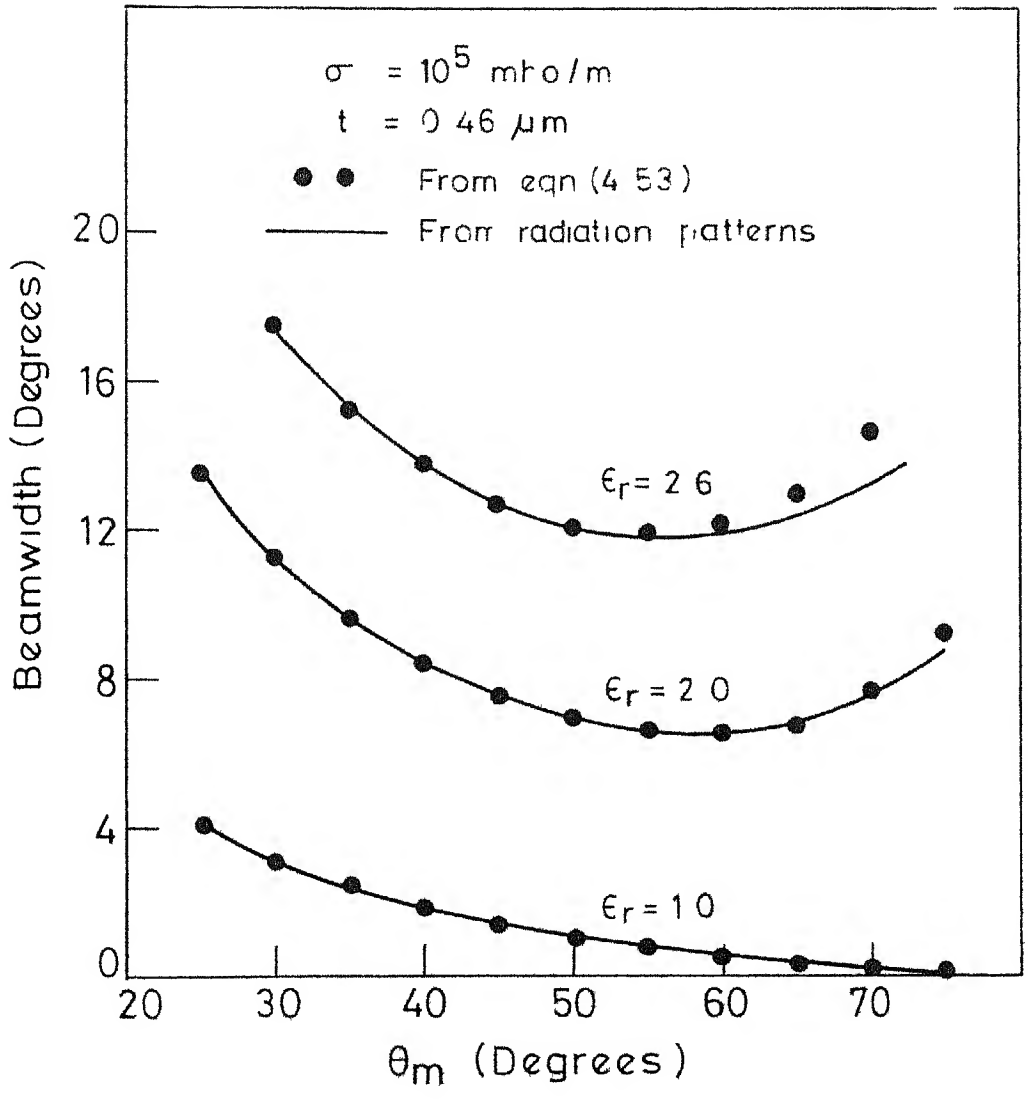

Fig.4.5 Variation of beamwidth with beam position θ_m

The effect of λ and b is also included here since θ_m depends on these quantities through $\sin\theta_m = \sqrt{\varepsilon_r-(\lambda/2b)^2}$. It is seen that when eqn. (4.53) is plotted as a function of θ_m a minimum occurs in BW. The position θ_m at which BW is minimum can be obtained by differentiating eqn. (4.53) with respect to θ_m and equating the differential to zero. This gives

$$\sin\theta_m \text{ (for min.BW)} = \sqrt{1-\varepsilon_r+\sqrt{\varepsilon_r^2-\varepsilon_r+1}} \qquad (4.55)$$

For $\varepsilon_r=2.6$, the above relation gives $\theta_m=52^\circ$ for minimum BW. For $\varepsilon_r=1.0$, minimum BW occurs near $\theta_m=90^\circ$. It is verified from Figure 4.5 where BW obtained by using eqn. (4.53) is compared with BW obtained from the radiation patterns. The figure shows that the position of minimum beamwidth shifts towards broad-on side as the value of dielectric constant ε_r is increased. Moreover, the range of θ_m within which BW is nearly constant decreases with the increase in the value of ε_r. For example, for $\varepsilon_r=2.6$ the position of minimum BW is 55° and the maximum range of θ_m within which BW does not vary by more than 1° is 22°. The corresponding values for $\varepsilon_r=2.0$ are 60° and 30° respectively. Once the values of ε_r and θ_m for minimum BW are known the value of k_0b required to obtain this value of θ_m can be obtained from $\sin\theta_m = \sqrt{\varepsilon_r-(\pi/k_0b)^2}$.

This analysis shows that it is very easy to predict the position of minimum BW for TLA. For other leaky wave antennas it is difficult to write the BW in a simplified form and therefore it is not possible to obtain the position of minimum BW analytically.

Effect of σ and t on BW

Equation (4.53) shows that BW is inversely proportional to σ t or directly proportional to sheet resistance of metal film. It has been plotted in Figure 4.6 for three different values of σ and for t/δ varying from 0.001 to 0.1. The shape of BW curve is identical to attenuation curve of Figure 2.5.

It is to be noted from eqn. (4.51) that BW is inversely proportional to $(k_0 b)^3$. Therefore, any change in the value of $k_0 b$ will have a relatively larger change in BW. This point can be verified from Figure 4.5.

For TLA with finite length the effect of length on BW can be taken into account by using eqn. (4.26) in place of eqn. (4.25). This treatment has been carried out by Bahl and Gupta [15].

4.4 ANTENNA EFFICIENCY η

One of the important parameters of an antenna is its radiation efficiency. It is defined as the ratio of the total power radiated by it to the power fed into it.

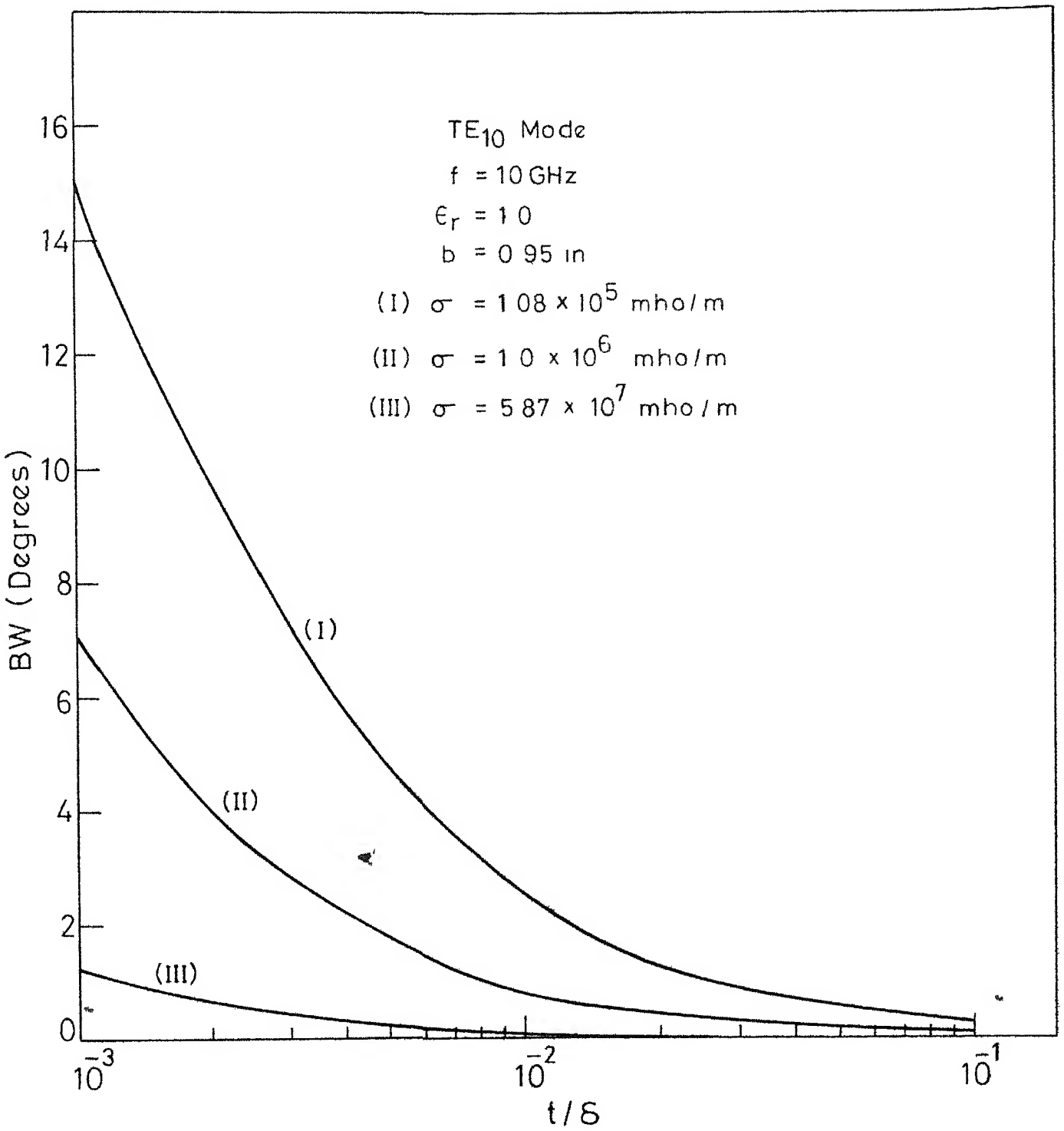

Fig.4.6 Variation of beamwidth of TLA with conductivity and thickness of imperfect plate.

Let it be denoted by η. The antenna efficiency of TLA is determined in this section.

The calculation of antenna efficiency, as defined above, involves the calculation of power fed into the antenna and the power radiated by it. These can be evaluated by considering the appropriate components of Poynting vector. The antenna efficiency will be calculated for TE_{10} mode only.

For a waveguide with perfectly conducting walls operated in TE_{10} mode there is only one non-zero component of Poynting vector, P_z. But, for TLA there is propagation in the transverse direction also. It gives rise to the transverse component of Poynting vector, P_x. This component of Poynting vector contributes to the radiation field.

For calculating the antenna efficiency of TLA the configuration used is shown in Figure 2.1. It is assumed in the analysis that all the power fed to TLA is either radiated in free space or dissipated in the imperfect plate. The power delivered at the other end is negligible. Therefore, power fed to TLA is equal to the power available at the plane $x = 0$. It is given by

$$P_{x=0} = \tfrac{1}{2} \text{ Re } (E_y H_z^*)_{x=0} \qquad (4.56)$$

The power radiated out of the structure is given by

$$P_{x=t} = \tfrac{1}{2} \text{Re} \, (E_y H_z^*)_{x=t} \tag{4.57}$$

and antenna efficiency η is defined as

$$\eta = \frac{P_{x=0}}{P_{x=t}} \tag{4.58}$$

The expressions for E_y at x=0 and at x=t are given by eqns (2.1a) and (2.1c) respectively. The expression for H_z can be obtained by using the corresponding expression for E_y and the Maxwell's equations. Using eqn. (2.1 a) for E_y in eqn. (4.56), the relation for $P_{x=0}$ becomes

$$P_{x=0} = \tfrac{1}{2} \text{Re} \left[\frac{h_1^*}{\omega \mu_0} (1+R)(1-R^*) \right] \tag{4.59}$$

similarly, expression for $P_{x=t}$ is obtained as

$$P_{x=t} = \tfrac{1}{2} \text{Re} \left[\frac{h_3^*}{\omega \mu_0} TT^* e^{jh_3 t} e^{-j\overset{*}{h}_3 t} \right] \tag{4.60}$$

The reflection coefficient R and the transmission coefficient T are obtained by applying the boundary conditions and continuity conditions. These are obtained as

$$R = -e^{-2jh_1 b} \tag{4.61}$$

and

$$T = \frac{4e^{-jh_3 t}}{(1-\frac{h_2}{h_1})(1-\frac{h_3}{h_2})e^{jh_2 t} + (1+\frac{h_2}{h_1})(1+\frac{h_3}{h_2})e^{-jh_2 t}} \tag{4.62}$$

Note that the expression for T, eqn. (4.62), is similar to the one obtained by Ramey et al. [19] for the transmission of power through thin metal films at microwave frequencies. Expression for R, eqn. (4.61), reduces to that given by Ramey et al [19] if the dispersion relation, (2.5a), is used to evaluate $e^{-2jh_1 b}$ in terms of h_1, h_2, h_3 and t. The above relation for T takes into account the multiple reflections in the thin film. The mechanism of multiple reflections is discussed in Appendix B.

The antenna efficiency η, is obtained by substituting eqns (4.61) and (4.62) in eqns. (4.59) and (4.60) respectively. Figure 4.7 shows the effect of thickness t and frequency f on the antenna efficiency. The effect of variation of conductivity σ on η is included in Figure 4.8. These figures show that antenna efficiency increases with decrease in conductivity and thickness of imperfect plate. Figure 4.9 shows the effect of variation of ε_r on η (for fixed β/k_0). It is to be noted that efficiency is more for higher values of ε_r. The effect of dielectric thickness b or beam position θ_m is included in Figure 4.10. Antenna efficiency decreases as the main beam scans towards end-fire side.

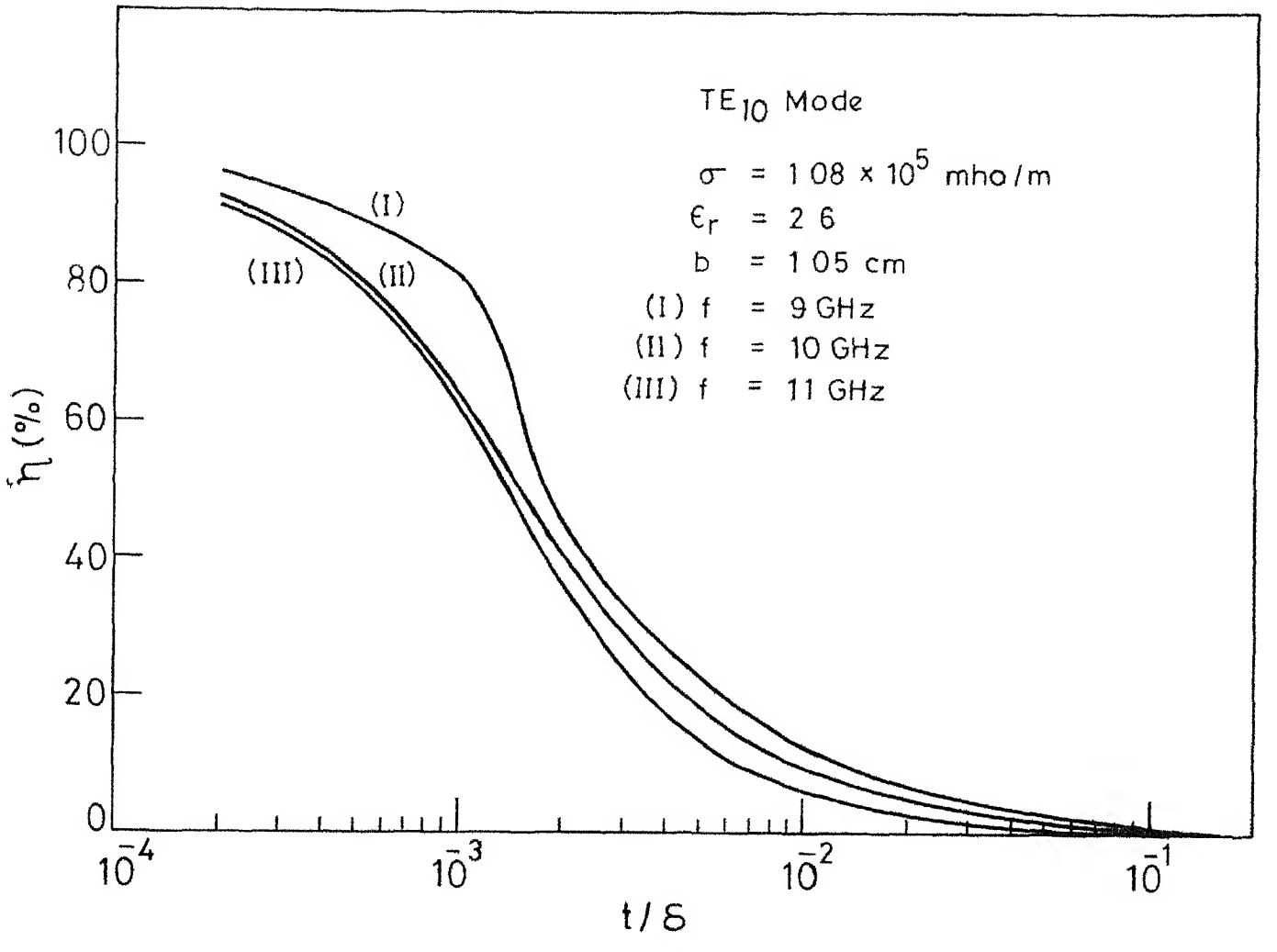

Fig.4.7 Variation of antenna efficiency with frequency and thickness

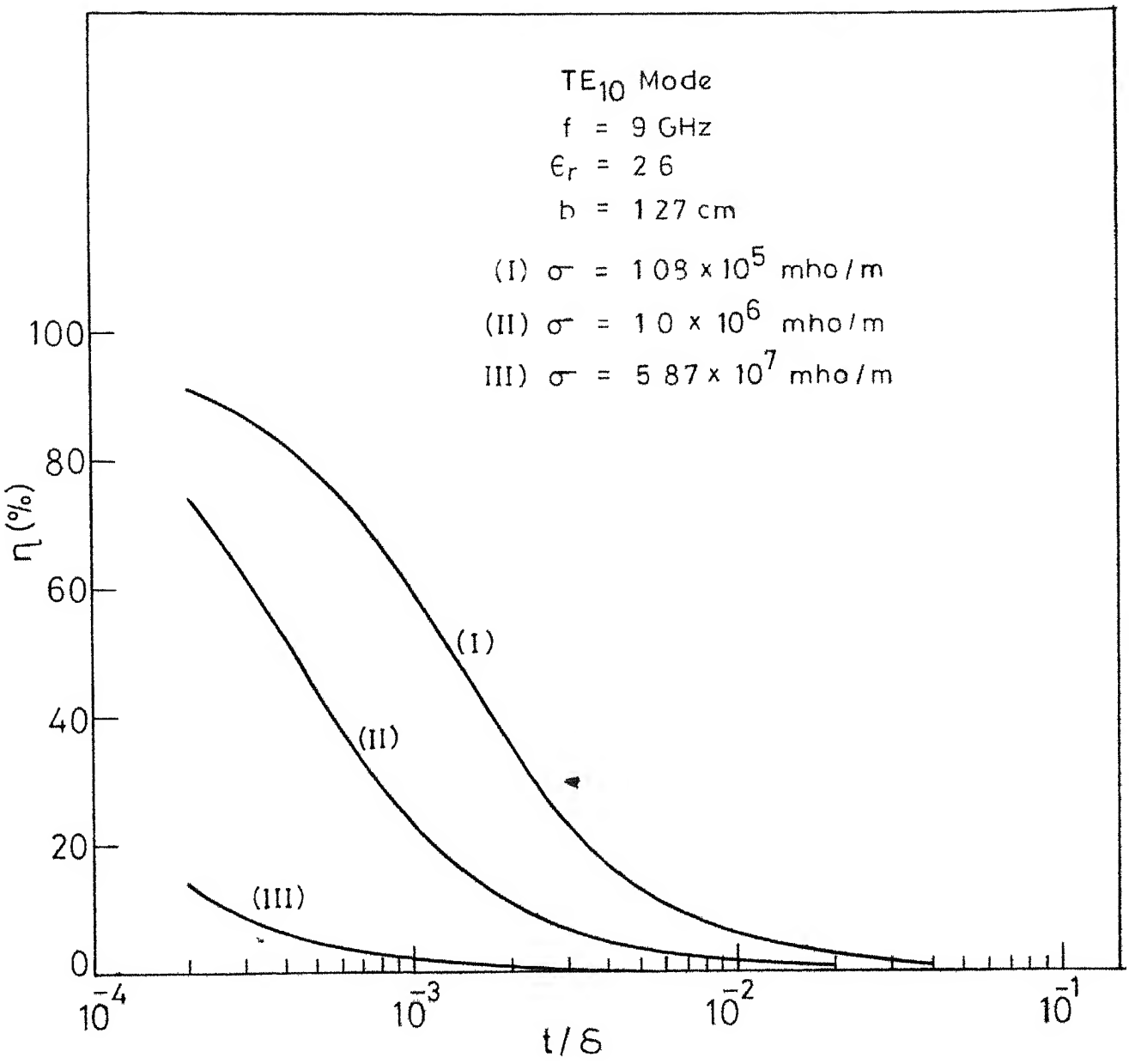

Fig. 4.8 Variation of antenna efficiency with conductivity and thickness

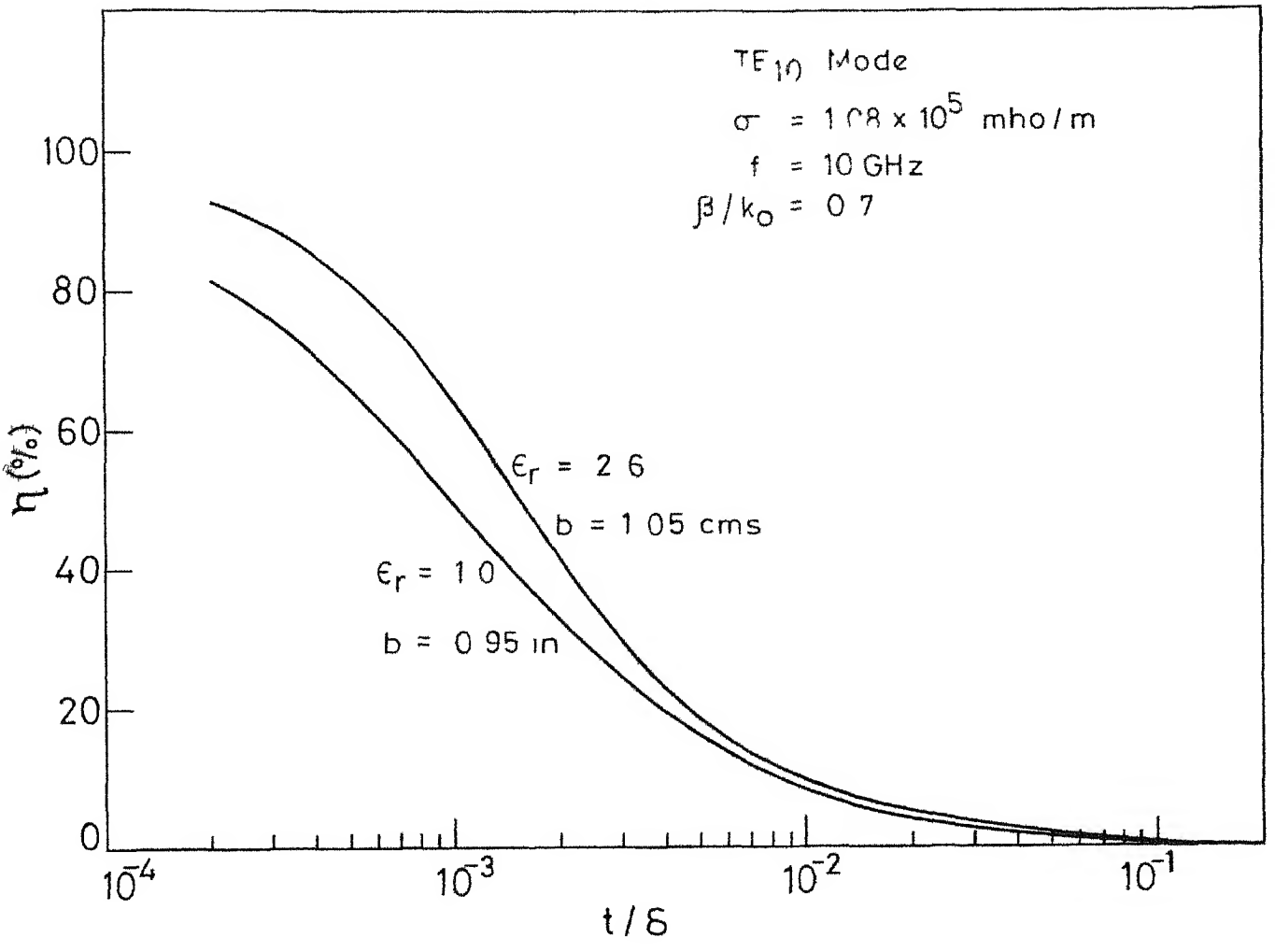

Fig.4.9 Variation of antenna efficiency with dielectric constant ε_r and t/δ

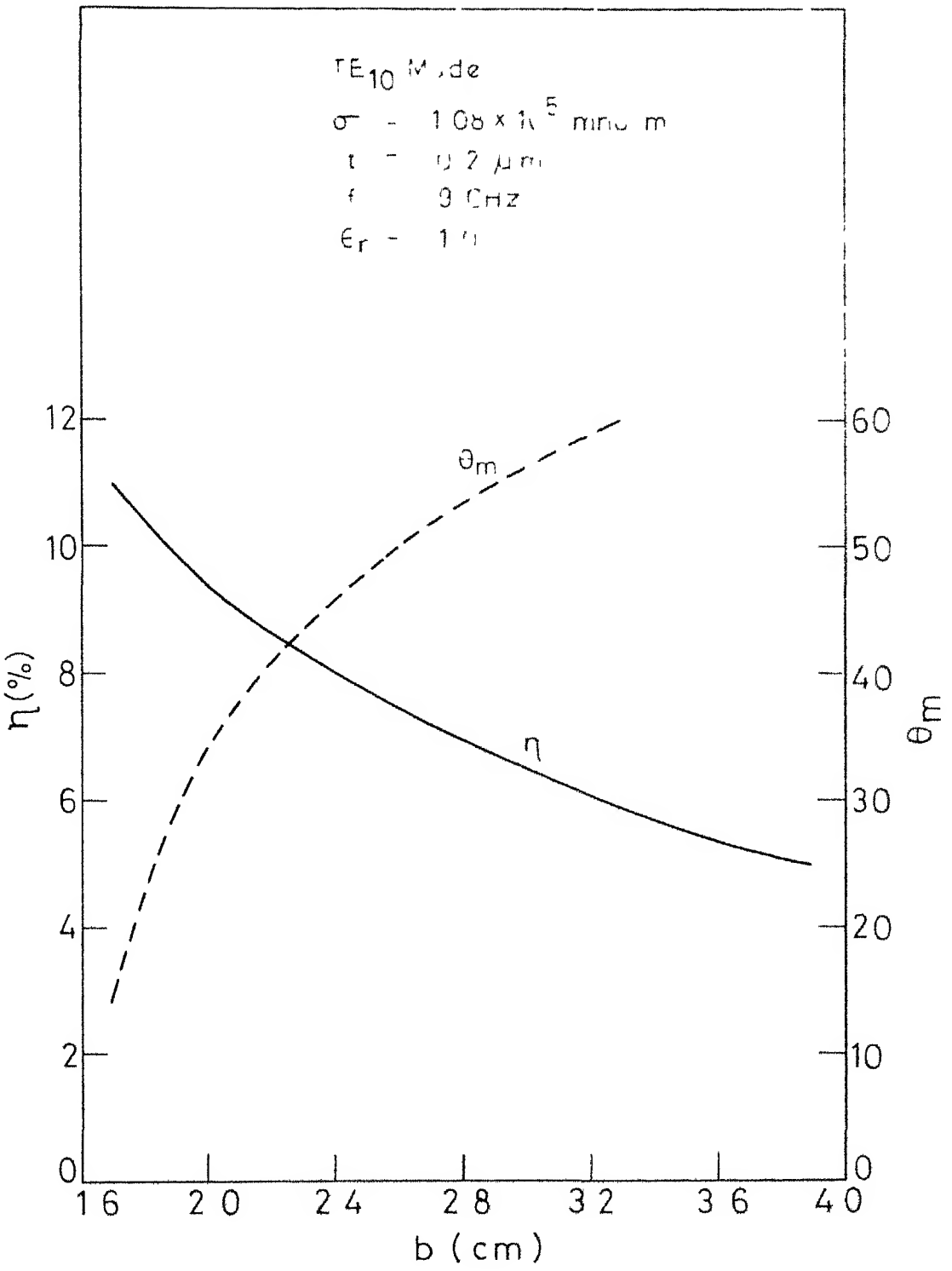

Fig.4.10 Variation of antenna efficiency with dielectric thickness b and beam position θ_m

For metal films which are not self supporting a thin sheet of dielectric is needed for support. The effect of this dielectric sheet has not been taken into account in calculating the antenna efficiency.

CHAPTER 5

EXPERIMENTAL MEASUREMENTS ON TLA

It has been pointed out in Chapter 4 that a thin wall leaky wave antenna can be designed by using TE_{10} mode in a rectangular waveguide. This Chapter deals with the experimental measurements on such an antenna. The experimental results for guide wavelength, attenuation and radiation pattern are compared with theoretical results. The agreement is found to be fairly good.

5.1 ANTENNA FABRICATION

The antenna is designed by replacing one of the narrow walls of a rectangular waveguide by a thin film of metal. It is shown in Figure 5.1. Thin film of metal acts as the imperfect wall. For metallic films which are not self-supporting, a thin sheet of dielectric is needed for support. The arrangement of the metal film deposited on a thin sheet of dielectric is shown in Figure 5.2. The supporting sheet protects the thin metallic film from outside environment also if it is held in contact with the waveguide in such a way that dielectric faces the outside environment. The dielectric support will give rise to some change in the propagation constant. Its thickness and dielectric constant should be such that the change in propagation constant introduced by it is negligible. The effect

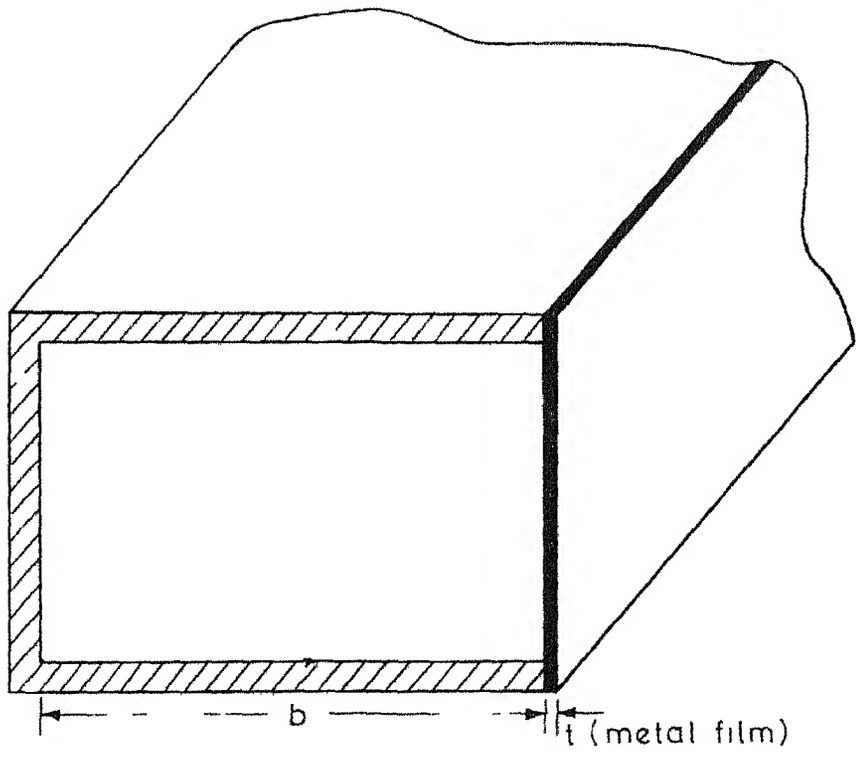

Fig.5.1 Thin wall Leaky waveguide Antenna (TLA) configuration

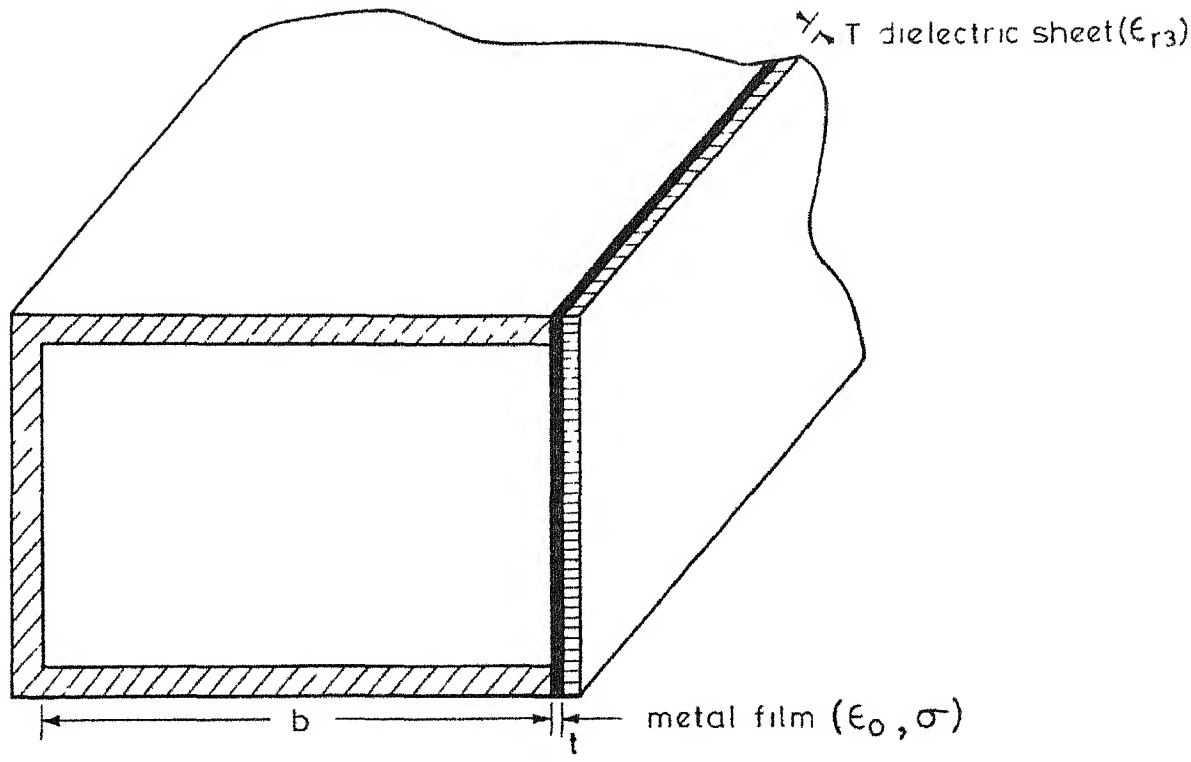

Fig.5.2 TLA configuration with the supporting dielectric sheet for the thin film of metal.

of supporting dielectric layer on the propagation constant is evaluated in Appendix C. It is shown there that the effect of the thin supporting dielectric layer on the propagation constant may be ignored.

5.1.1 Selection of metal for thin film

It has been shown in Section 4.4 that only a fraction of the power fed to TLA contributes to the radiation pattern. The amount of power leaking out depends on the thickness and conductivity of the thin film. This leakage increases with the decrease in thickness and conductivity of thin film. The thickness cannot be reduced below a certain minimum value beyond which the film becomes discontinuous. But a smaller value of conductivity can be used by choosing metals of lower conductivity. Keeping these considerations in mind, bismuth (Bi) has been chosen for the material of the film. Also, it is easier to deposit Bi than many other metals by means of vacuum evaporation. The boiling point of Bi is lower than that of most other metals.

5.1.2 Preparation of metal film and measurement of its parameters

Bismuth was deposited by means of vacuum evaporation on a Mylar sheet about 6 mil in thickness. Bismuth used was 99.9 percent pure. The parameters of the metal film

appear in the dispersion relation in the form of t/δ. Therefore, the parameters of interest of the film are thickness t and conductivity σ. The thickness of Bi film was measured using the method of α-ray absorption [16]. The maximum error in the measurement of thickness is estimated to be less than 10 percent. The conductivity of the film was measured using the method of 'Four-point probe' and the expression [17]

$$\rho = 4.53 \frac{V}{I} t \qquad (5.1)$$

where ρ is the resistivity of film

I is the current flowing in the film

V is the voltage difference between the inner probes. The measured values of t and σ for the vacuum deposited Bi film are 1300 AU and 1.08×10^5 mho/m respectively. The conductivity at microwave frequencies has been assumed to be equal to the measured d.c. value. The difference between the two values is negligible [18]. Thickness and conductivity of the film were checked by measuring the insertion loss of the film [19].

The geometry utilized for calculating the insertion loss is shown in Figure 5.3. The thin film is held between two flanges. Power transmitted through thin film is given by [19] .

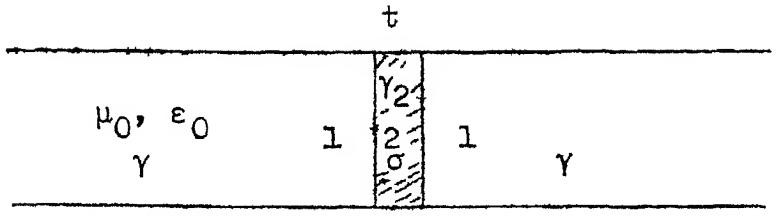

Fig. 5.3: Waveguide configuration for calculating the insertion loss of thin bismuth film

$$T = \left| \frac{4e^{\gamma_1 t}}{(1-\gamma_2/\gamma_1)(1-\gamma_1/\gamma_2)e^{-\gamma_2 t} + (1+\gamma_2/\gamma_1)(1+\gamma_1/\gamma_2)e^{\gamma_2 t}} \right|^2 \tag{5.2}$$

where $$\gamma_1 = \sqrt{(\pi/b)^2 - k_0^2} \tag{5.3}$$

and $$\gamma_2 = \sqrt{(\pi/b)^2 - k_0^2 + j\,\omega\mu_0\sigma} \tag{5.4}$$

For a metal film with $\sigma = 1.08 \times 10^5$ mho/m and t = 1300 AU theoretical value of insertion loss at 10GHz (b=0.9 in), obtained from eqn. (5.2), is 12.3dB. Measured value of insertion loss is 13dB.

5.2 MEASUREMENT OF PROPAGATION CONSTANT

In order to fabricate TLA using RG-52U waveguide (0.9'' x 0.4") one of the narrow walls of the waveguide was removed. Thin film of Bi deposited on Mylar sheet was used as a thin wall. The photographs of rectangular waveguide with one of the side walls removed and the Mylar sheet with the coating of thin film of Bi are shown in Figure 5.4(a).

Mylar sheet, with the metalised side making electrical contact with the waveguide, was held in place by using a cellophane tape over non-radiating portions. Care was taken to ensure that no air gaps were left. The photograph of TLA, so obtained, is shown in Figure 5.4(b).

5.2.1 Guide Wavelength

Guide wavelength λ_g was measured by holding the probe at a fixed position in the slotted section and moving the metallic plunger from one end of the antenna to the other end. Block diagram of the apparatus used is shown in Figure 5.5(a). The resulting standing wave pattern at 11 GHz is shown in Figure 5.5(b). Measured and calculated values of guide wavelength at three different frequencies are compared in Table 5.1.

TABLE 5.1

Measured and calculated values of guide wavelength

Frequency	Measured (cms)	Calculated (cms)
11 GHz	3.291	3.305
10 GHz	3.834	3.825
9 GHz	4.631	4.601

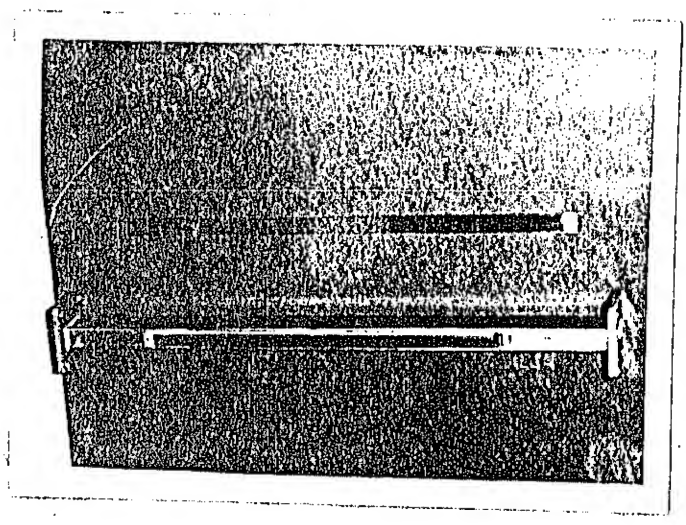

Fig.5.4(a) Photograph of a rectangular waveguide with a narrow wall removed, and metalised Mylar sheet

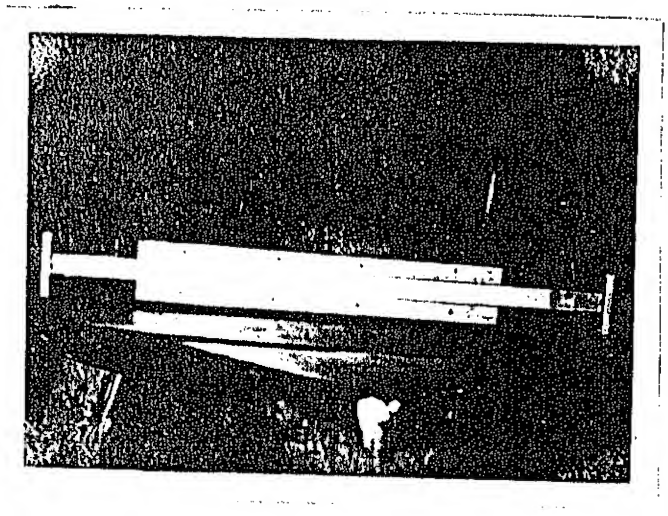

Fig.5.4(b) Photograph of TLA

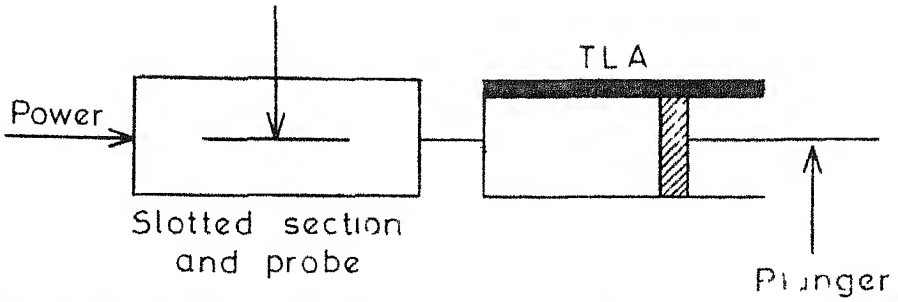

Fig.5.5(a) Block diagram of experimental set up for measurement of guide wavelength

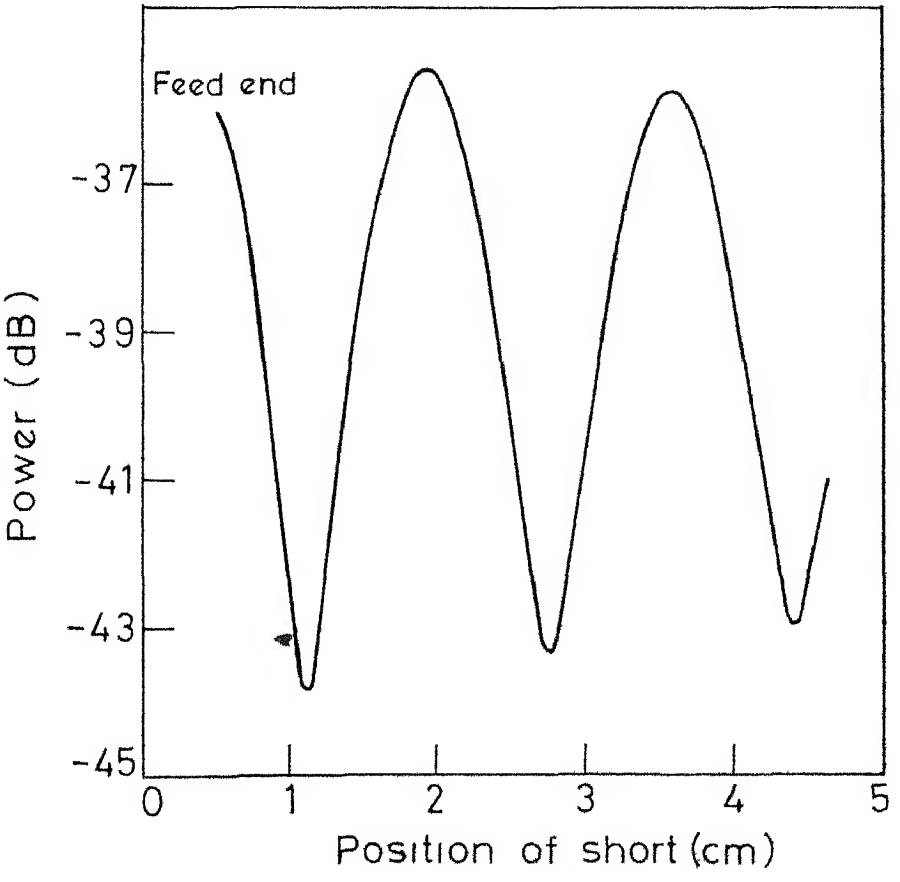

Fig.5.5(b) Standing wave pattern for measuring guide wavelength (f=11 GHz,b=0.95",σ=1.08x10^5 mho/m,t=0.13μm)

The agreement is seen to be very good. In calculating the theoretical value of guide wavelength use has been made of the phase constant obtained in Chapter 2.

5.2.2 Attenuation

Attenuation is measured by measuring the magnitude of the voltage standing-wave ratio (VSWR) of TLA terminated in a short circuit. The value of α is obtained from the relation

$$\tan h\ (\alpha L) = \frac{1}{VSWR} \qquad (5.5)$$

Equation (5.5) is valid for a perfect impedance match between the component to be measured and the standing wave device. Attenuation has also been calculated from the measurement of insertion loss. Measured values of attenuation are compared with the calculated values in Table 5.2.

TABLE 5.2

Measured and calculated values of attenuation

Frequency	Measured α(dB/cm)		Calculated α(dB/cm)
	From VSWR	From insertion loss	
11 GHz	0.31	0.37	0.25
10 GHz	0.41	0.44	0.30
9 GHz	0.48	0.55	0.39

It is seen that measured values are of the same order of magnitude as the calculated ones. Also, the former are higher than the latter. The discrepancy may be due to the following reasons:

(i) TLA is not perfectly matched to the slotted section. VSWR of TLA terminated in a matched load is given in Table 5.3.

(ii) Bismuth film has been pressed against the waveguide walls by means of cellophane tape. The area of contact of the film with the waveguide walls is small due to rounding off of the waveguide edges. The thickness of waveguide walls in contact with the film is of the order of 30 mil. Therefore, the film does not make a very good electrical contact with the rest of the waveguide. The contact resistance will increase the measured value of attenuation.

(iii) In spite of taking all the cares some gaps were left between the film and the waveguide through which there can be a leakage of power.

5.3 Measurement of radiation patterns

To measure the radiation pattern of TLA it was mounted on a turn-table. The feed end of the antenna coincided with the axis of the turn-table. A pyramidal horn was used as the receiving antenna. The separation

between TLA and the receiving antenna was adjusted so that the condition $R > 2L^2/\lambda$ for the far field is satisfied. Here, R is the separation between the receiving antenna and the transmitting antenna, L is the length of the radiating aperture and λ is the free space wavelength of operation. The length L of the antenna used is 20 cms. Block diagram of the apparatus used in measuring the radiation patterns is shown in Figure 5.6. Measured radiation patterns are shown in Figures 5.7, 5.8 and 5.9. The parameters selected are b=0.95 in, σ=1.08x10^5 mho/m, t = 1300 AU, L=20 cms and f = 11, 10 and 9 GHz respectively. The radiation pattern shown as dotted in these figures is the theoretical radiation pattern obtained by using eqn. (4.26).

5.4 Comparison with theoretical results

Some of the observations from Figures 5.7, 5.8 and 5.9 are summarised in Table 5.3. These include position of main beam, half-power beamwidth and level of highest sidelobe. It is seen from Table 5.3 that the agreement between the theoretical values and the measured values for these characteristics is fairly good. The measured beamwidths are slightly lower (about 1^0) than the calculated values.

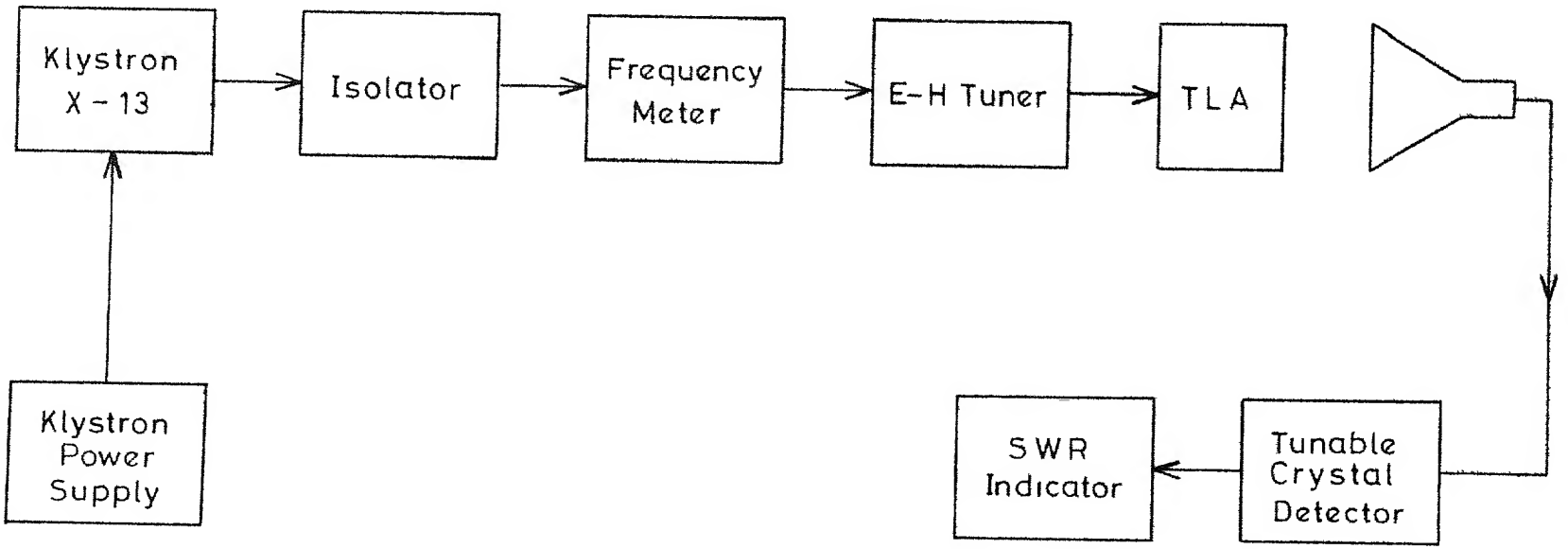

Fig. 5 Block diagram of experimental set up for measurement of radiation patterns

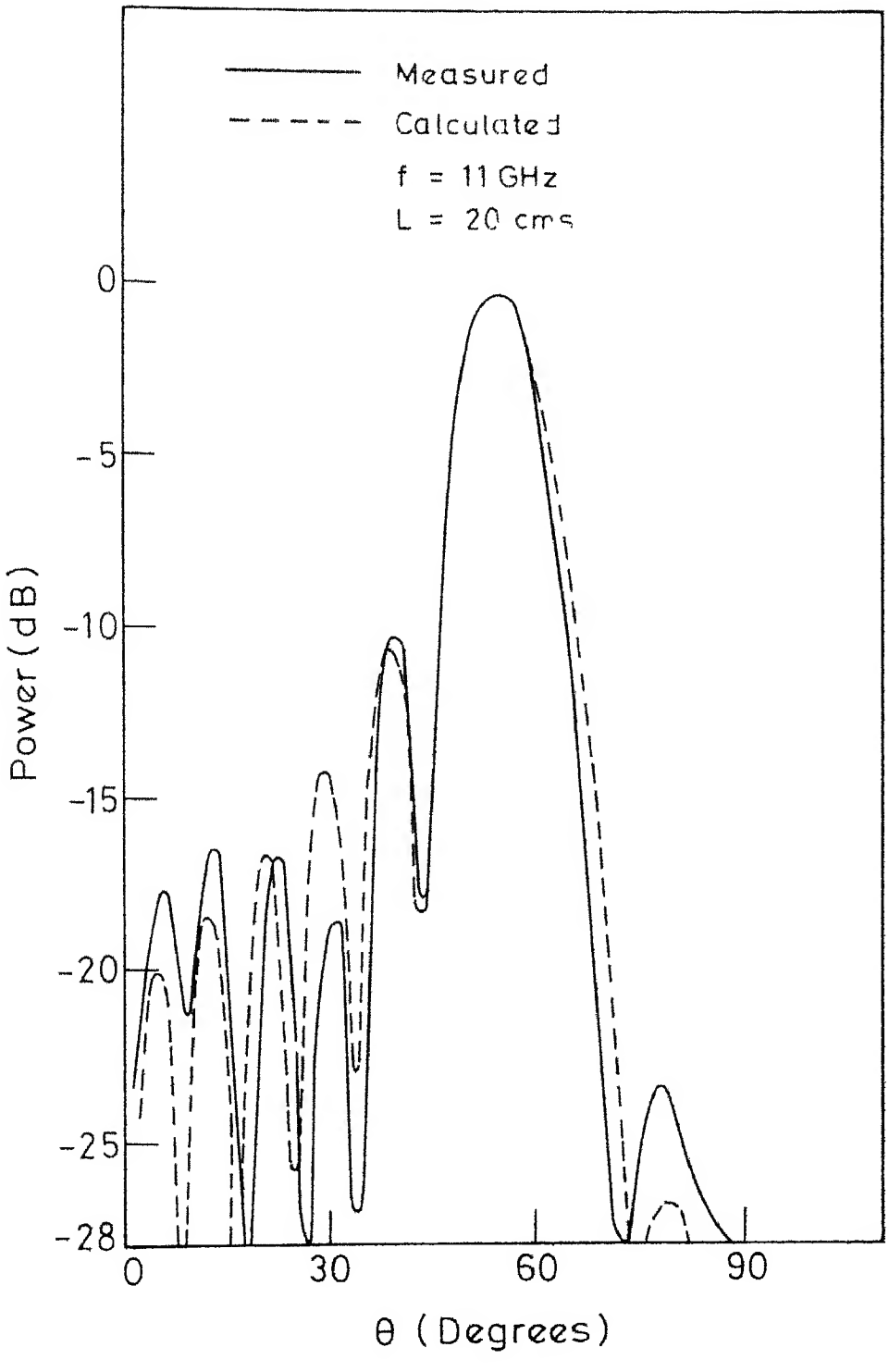

Fig. 5.7 Comparison of theoretical and experimental radiation patterns (b=0.95" σ=1.08x10^{5}mho/m, t=0.13μ m)

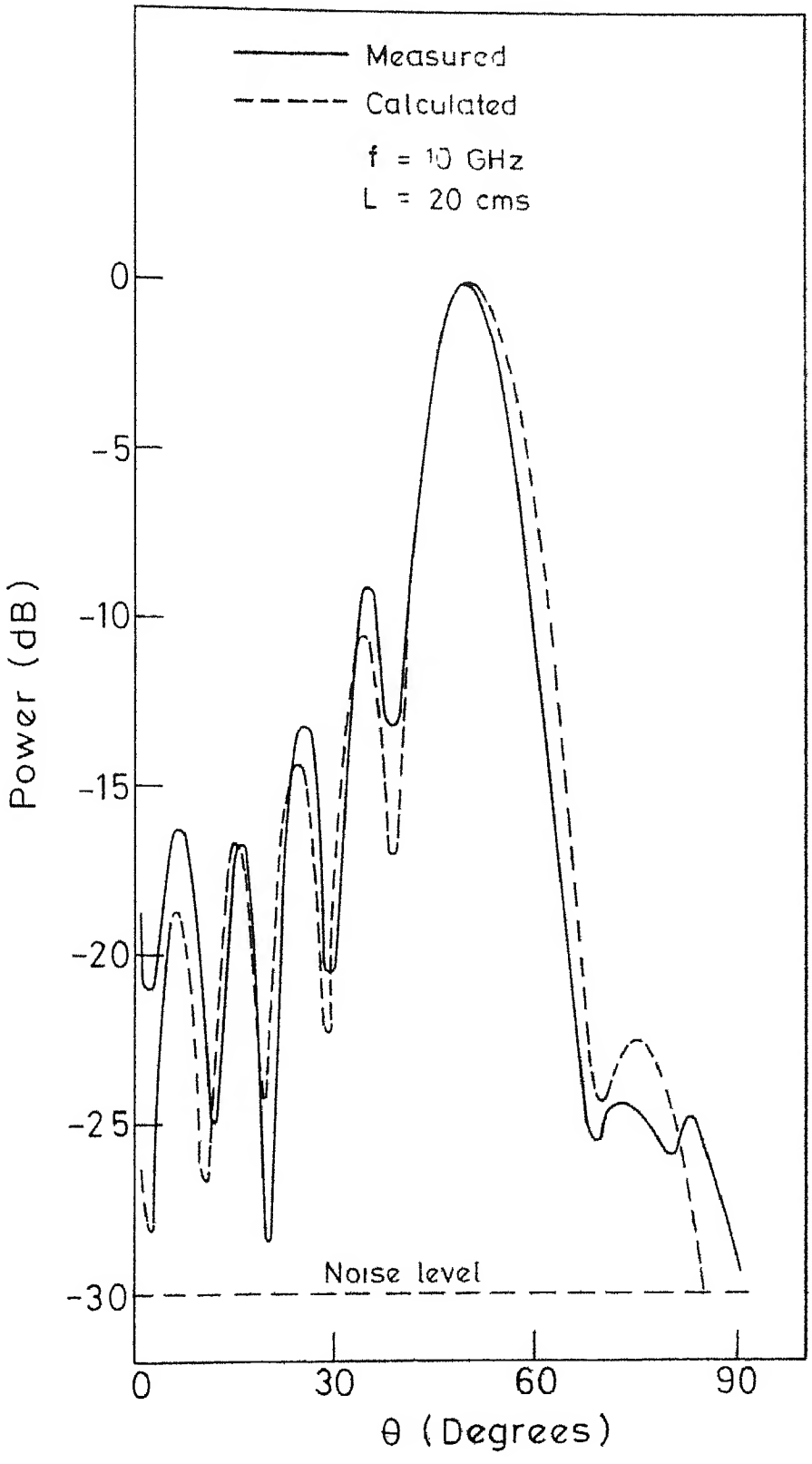

Fig. 5.8 Comparison of theoretical and experimental radiation patterns ($b=0.95^{"}$, $\sigma=1.08\times10^{5}$ mho/m, $t=0.13$ μm)

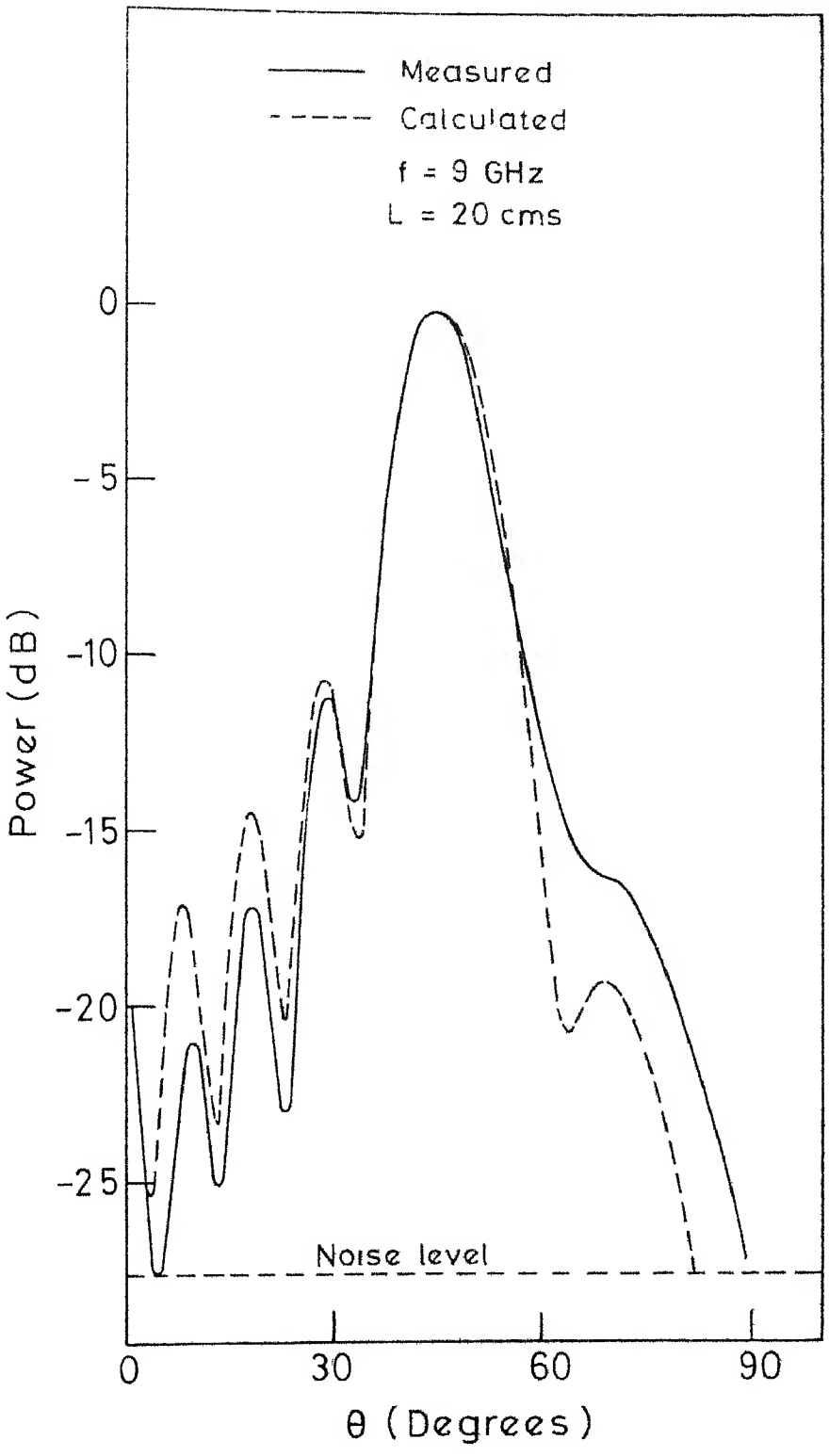

Fig. 5.9 Comparison of theoretical and experimental radiation patterns ($b=0.95^{\circ}$, $\sigma=1.08\times10^{5}$ mho/m, $t=0.13$ μm)

TABLE 5.3

Measured and calculated values for TLA

Conductivity of Bi film = 1.08×10^5 mho/m

Thickness of Bi film = 1300 AU

f	t/δ	VSWR	θ_m		-3dB beamwidth		Level of highest sidelobe (dB)	
			Meas.	Cal.	Meas.	Cal.	Meas.	Cal.
11 GHz	9.10×10^{-3}	1.03	55°	55°	10°	11.6°	-10.1	-10.4
10 GHz	9.05×10^{-3}	1.02	50°	50°	11°	11.7°	-9.0	-10.6
9 GHz	9.00×10^{-3}	1.10	45°	45°	11°	11.8°	-11.3	-10.7

CHAPTER 6

COMPARISON WITH OTHER LEAKY WAVE ANTENNAS

CHAPTER 6

COMPARISON WITH OTHER LEAKY WAVE ANTENNAS

The slotted waveguide and channel guide antennas are two most commonly discussed leaky wave rectangular waveguide antennas. These structures are obtained by interrupting the flow of microwave current by cutting slot in the wall of the waveguide, or by removing the wall completely. Therefore, the current distribution at the radiating aperture is difficult to determine accurately. However, in the case of TLA the current distribution at the radiating aperture (thin film wall) is a small perturbation of current distribution at the wall of rectangular waveguide and can be evaluated exactly by the analysis presented in Chapter 2.

6.1 EASE OF DESIGN

The design of TLA is simpler compared to other leaky wave antennas. The radiation properties of a leaky wave antenna are determined by the propagation constant γ. It has been shown in Chapter 2 that the propagation constant for TLA can be written in the form of a simple expression. c/v or β/k_0 variation of TLA is essentially that of a simple parallel plate waveguide. The expression for α/k_0, eqn. (3.24), is obtained by modifying the expression for α/k_0

for parallel plate waveguide for finite values of σ and t. In the range of parameters where change in phase constant is small (Figure 2.2) the difference between the value of α/k_0 given by the simplified expression and the exact numerical solution is less than 5 percent. As a result of the simplified expression for α/k_0 the beamwidth of TLA, eqns.(4.41) and (4.49), can be easily calculated. Another advantage of this simplification is that the position of the beam at which beamwidth is minimum, eqn.(4.55), can be obtained very easily.

6.2 NARROW BEAMS

For certain applications, it is needed to have small values of α/k_0 in order to obtain narrow beamwidths from long antennas. These small values of α/k_0 can be obtained either (i) by operation near endfire [6], or (ii) by using a very small slot width in a slotted waveguide antenna or very small channel width in a channel guide antenna (for operation away from endfire).

As an example, let us calculate the slot width or channel width required to obtain a propagation constant $\gamma/k_0=0.784+j0.0165$ at 10 GHz. For TLA to have this propagation constant the parameters are $h=2.41$ cms, $t/\delta=9.05\times10^{-3}$ and $\sigma=1.08\times10^5$ mho/m. Table 6.1 gives the dimensions of slotted waveguide and channel guide to have this propagation

TABLE 6.1

Comparison of dimensions of slotted waveguide antenna and channel guide antenna with TLA.

$\gamma/k_0 = 0.784+j0.0165$ at 10 GHz (for all the three cases)

Antenna Type	Slot width	Channel width or Height of W/G	Channel depth or width of W/G
TLA	-	-	2.41 cm
Slotted W/G	0.07 cm	1.02 cm	2.75 cm
Channel guide	-	0.07 cm	1.10 cm

constant. It is to be noted that the slot width or the channel width required is very small (0.07 cm.). These spacings decrease with the decrease in the value of α/k_0. The small spacings, however, may limit the power-handling capability of the antenna. In TLA, low values of α/k_0 can be easily obtained by increasing the thickness of imperfect wall (Figure 2.3). Thus, a long TLA can be used with a beam pointing away from endfire.

6.3 SIDELOBE CHARACTERISTICS

In this section the sidelobe characteristics of TLA has been compared with that of slotted waveguide antenna. Before the comparison, the sidelobe characteristics of slotted waveguide are discussed.

The slotted waveguide antenna supports an extra mode called the slot mode [20,21], over and above the perturbed waveguide mode. The propagation constant for the slot mode is approximately the same as that for the dominant mode in the corresponding double ridged waveguide [21]. The slot mode gives rise to an additional sidelobe in the radiation pattern of the slotted waveguide antenna. This additional sidelobe for two cases with different slot widths is shown in Figure 6.1 where measured radiation patterns have been plotted. The additional sidelobe is at

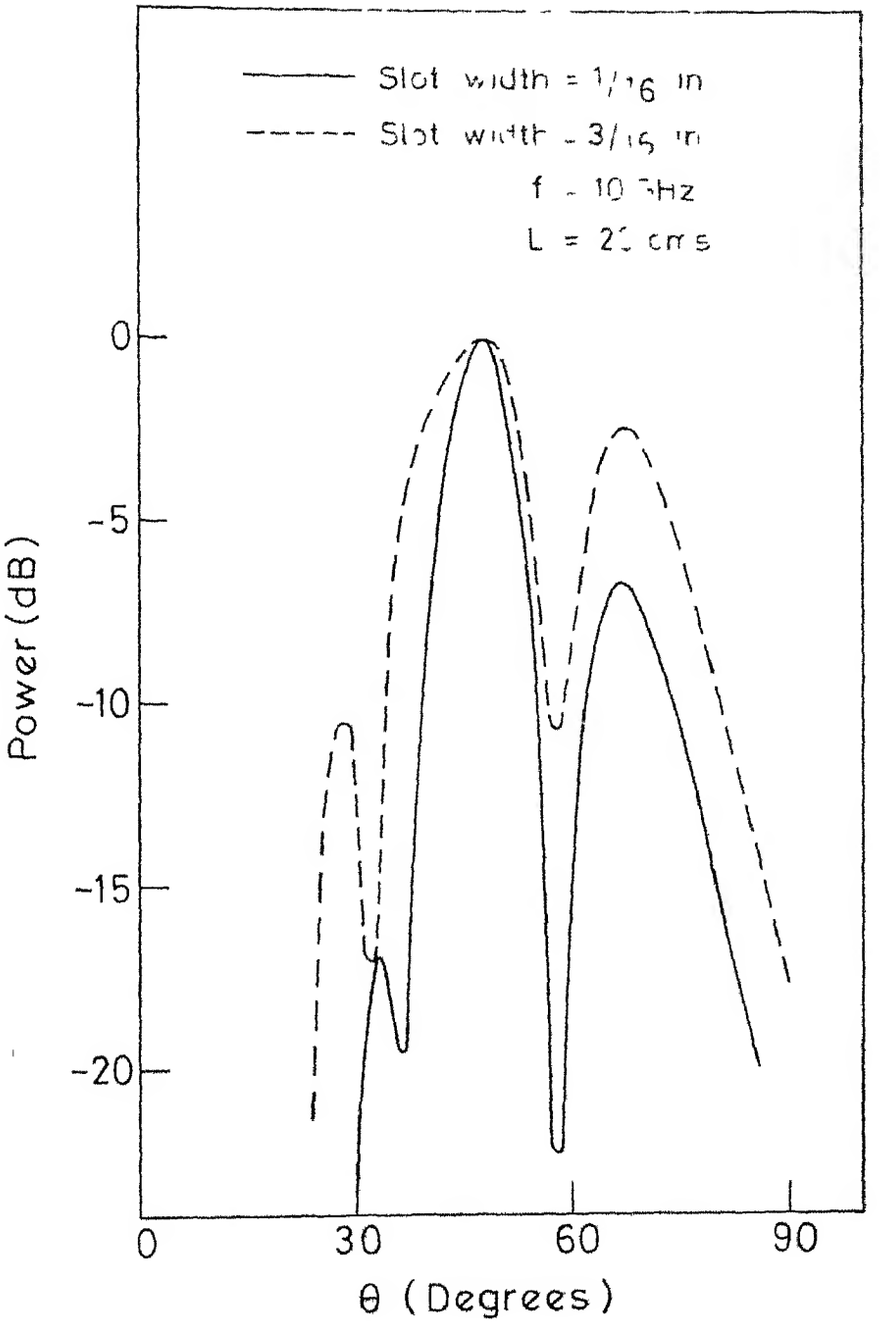

Fig.6.1 Measured radiation patterns of a slotted waveguide antenna for two different slot widths.

$\theta=68^{\circ}$ in both the cases. Furthermore, the efficiency of excitation of slot mode increases with the increase in slot width. This also is apparent from Figure 6.1. The power level of this additional sidelobe increases from -6.8dB to -2.4 dB when the slot width is increased from 1/16" to 3/16". Moreover, the level of the additional sidelobe at $\theta=68^{\circ}$ is higher than the highest sidelobe due to perturbed waveguide mode. It is shown below that TLA does not have this additional sidelobe.

Radiation patterns for slotted waveguide antenna and TLA are compared in Figure 6.2. For comparing the shape of the patterns, the peak levels have been adjusted to zero dB. Radiation pattern for slotted guide antenna (slot width 1/16 in.) is obtained by experimental measurements, whereas that for TLA is based on theoretical results. The theoretical radiation pattern for the slot width of 1/16 in. could not be obtained because the expression for the propagation constant of the perturbed waveguide mode given in [6], does not hold for this slot width. It is seen in Figure 6.2 that there is a sidelobe on the endfire side of the main beam in the radiation pattern for the slotted waveguide. As discussed earlier it is due to slot mode propagation. However, in the same figure one observes that there is no sidelobe towards the endfire side of the

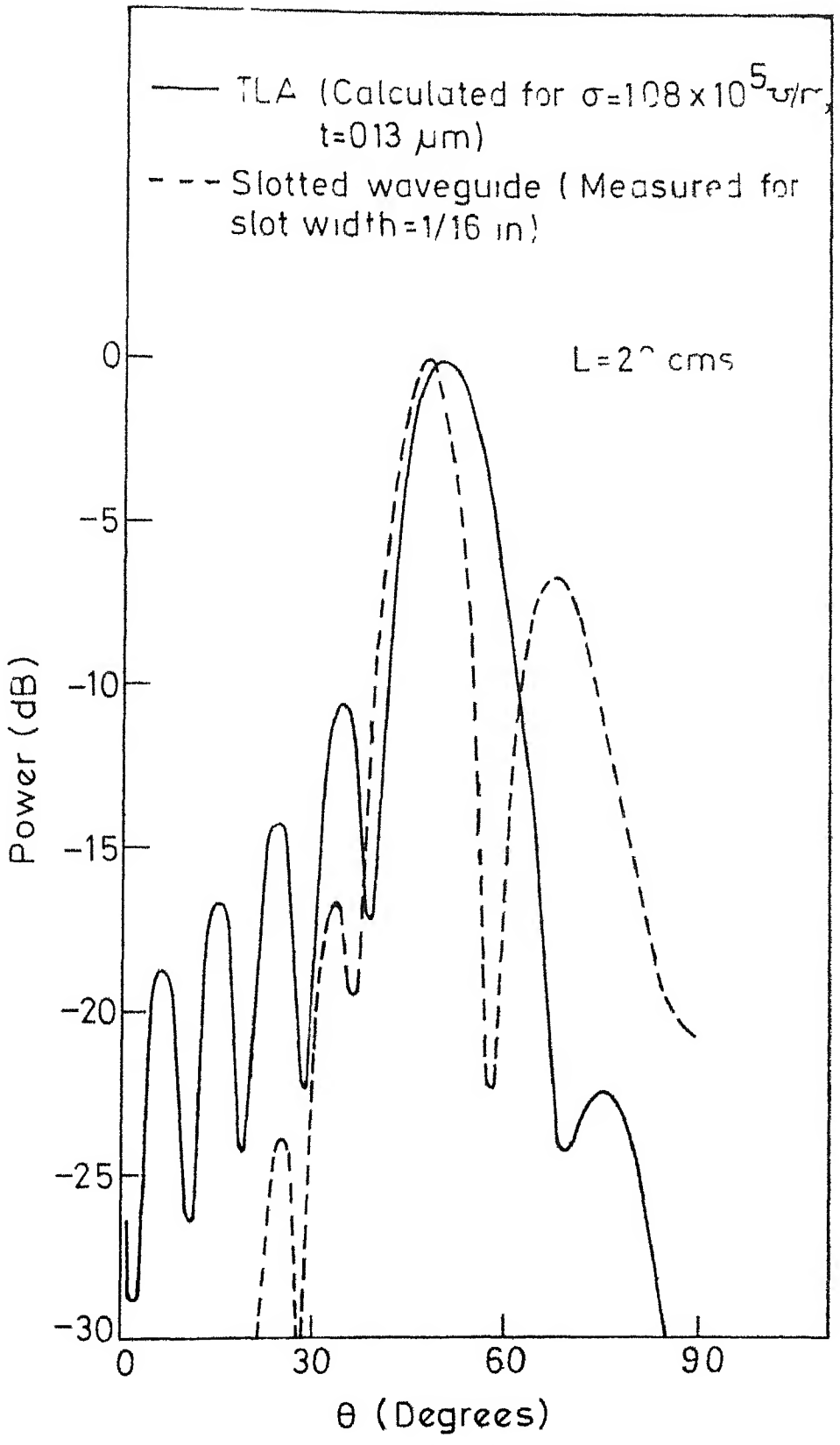

Fig.6.2 Comparison of radiation patterns for TLA and slotted waveguide antenna for f=10 GHz and using RG-52U (0.9"x0.4") waveguide.

main beam in the radiation pattern for TLA. Hence, the sidelobe characteristics of TLA are better than that of slotted waveguide antenna.

CHAPTER 7

CONCLUSION

CHAPTER 7

CONCLUSION

This chapter enlists the main results arrived at in this thesis and provides some suggestions for further work.

7.1 SUMMARY OF RESULTS

Waveguiding and radiation properties of a parallel plate waveguide with an imperfect plate ($\sigma \neq \infty$) has been studied. The effect of finite conductivity σ and thickness t of imperfect plate on the phase constant and attenuation constant for TEM-like, TM and TE-modes has been evaluated. It has been observed that for $t/\delta < \pi/2$ the value of phase constant and attenuation constant increases with the decrease in either or both σ and t for all the modes mentioned above. These constants also increase with increase in value of dielectric constant of medium separating the parallel plates.

Attenuation constant has been obtained by using the transverse resonance technique also. This approach shows that attenuation can be minimised by optimising the thickness of metal used. This optimum thickness is given by $t/\delta = \pi/2$.

A new type of leaky wave has been observed for $t/\delta < 10^{-4}$. This wave is associated with large values of attenuation. It is characterised by a phase velocity less than the velocity of light and its growth in transverse direction is similar to

that of leaky waves. This wave has been termed as slow leaky wave.

In addition to these slow leaky waves the structure can support fast leaky waves as well as slow surface waves. Based on the results of the radiation properties for fast leaky waves, a leaky wave antenna called TLA has been tested successfully at X-band frequencies. RG-52U waveguide (0.9" x0.4") has been used for fabricating TLA. A thin film of bismuth has been chosen for the imperfect wall. Thickness and conductivity of bismuth film used are 1300 AU and 1.08×10^5 mho/m respectively. Propagation constants and radiation patterns have been measured at 9,10 and 11 GHz. For an antenna length of 20 cm a beamwidth of 12° with main side lobe 11.3 dB down has been obtained at 11 GHz. The agreement between the theoretical and experimental values is fairly good.

TLA has been compared with other leaky wave antennas. It has been observed that designing a TLA is easier compared to other leaky wave antennas since c/v variation of TLA is essentially that of a simple rectangular waveguide and α/k_0 also can be evaluated easily. TLA can be designed to give narrow beams in directions other than endfire also. Moreover, TLA has better sidelobe characteristics than the slotted waveguide antenna. In the radiation pattern of

slotted waveguide antenna there is another sidelobe due to slot mode. This mode is not present in TLA.

7.2 CONCLUDING REMARKS

It was observed during this study that TLA can be designed to give narrow beams in directions other than end-fire also. This property of TLA may be utilized to construct a long antenna giving narrow beams. To obtain narrow beams the value of attenuation should be correspondingly low. Low values of attenuation can be obtained by depositing thicker metals. The method of electrodless deposition may be used for depositing metal on longer lengths of dielectric. The metal should be deposited directly on the dielectric. This will avoid the difficulty of electrical contact between the metal film and the rest of the waveguide experienced during this study.

The present study on TLA may also be extended to circular waveguide with thin imperfect wall.

The result obtained in this study about the optimum thickness for minimum attenuation can be utilized for reducing conductor losses in microstrips. Microstrips are obtained by depositing a strip of metal (usually $t > 4\delta$) on a slab of dielectric. For optimising the conductor losses, the thickness of strip line should be adjusted to an optimum

value, dependent upon the frequency of operation, during the fabrication of microstrip. The reduced thickness of strip, in addition to optimising the attenuation, will help in obtaining sharply etched patterns.

The optimisation of losses will also help in increasing the Q of the microstrip cavity. Here one should note that the attenuation is a function of frequency also.

It may be worthwhile to carry out further investigations on slow leaky waves observed during this study. It is not yet known what type of other structures could also support a wave of this type. Radiation characteristics of this type of wave deserve further study.

APPENDIX A

APPROXIMATIONS USED IN SOLVING THE DISPERSION RELATIONS AND THEIR PHYSICAL IMPLICATIONS

Equations (2.9) and (2.10) are the approximate solutions of the relations (2.5). In arriving at these equations some approximations were made for $\delta\gamma$, h_1, h_2, h_3 and $h_1 b$; p_1, p_2, p_3 and $p_1 b$. This Appendix lists these approximations. The implications of these assumptions in limiting the values of physical parameters of the structure for TE_{10} mode ($\varepsilon_r = 1$) have also been included.

Approximation for $\delta\gamma$: $|\delta\gamma/k_0| \ll \gamma_0/k_0$ for the perturbation approximation to hold good.

Approximation for h_2, p_2: since for a good conductor $|K| \gg (\gamma_0/k_0)^2$; $h_2/k_0, p_2/k_0 \simeq \sqrt{K}$.

Expression for h_1, p_1: (a) For TE, TM modes: Using eqn. (2.7) in eqn. (2.3a) or (2.3d) and assuming that

$$\left| 2 \frac{\delta\gamma}{k_0} \quad \frac{\gamma_0}{k_0} \right| \ll (n\pi/k_0 b)^2$$

the expression for h_1/k_0 or p_1/k_0 is obtained as

$$\frac{h_1}{k_0}, \frac{p_1}{k_0} \simeq \frac{n\pi}{k_0 b} - \frac{k_0 b}{n\pi} \frac{\gamma_0}{k_0} \frac{\delta\gamma}{k_0} \qquad \text{(1aA)}$$

(b) for TEM-like mode. $$\frac{p_1}{k_0} = j \left(2 \frac{\delta\gamma}{k_0} \quad \frac{\gamma_0}{k_0}\right)^{\frac{1}{2}} \qquad \text{(1bA)}$$

Approximation for $\tan(h_1 b)$, $\tan(p_1 b)$: For the parallel plate structure with perfectly conducting plates $p_1 b=0$ for TEM-mode, $p_1 b=n\pi$ for TM modes and $h_1 b=n\pi$ for TE modes. In case of imperfectly conducting plates, the following expressions for $\tan(h_1 b)$ and $\tan(p_1 b)$ have been assumed.

$$\tan(p_1 b) = p_1 b \quad \text{(TEM-like mode)} \tag{2aA}$$

$$\tan(p_1 b) = p_1 b - n\pi \text{ (TM modes)} \tag{2bA}$$

$$\tan(h_1 b) = h_1 b - n\pi \text{ (TE modes)} \tag{2cA}$$

Expressions for h_3, p_3: The expression used for h_3/k_0 or p_3/k_0, is different for $\varepsilon_r=1$ and $\varepsilon_r > 1$.

(a) $\varepsilon_r = 1$. Using eqns.(2.3) one finds

$$h_3/k_0 = h_1/k_0 \quad \text{(TE modes)} \tag{3aA}$$

$$p_3/k_0 = p_1/k_0 \quad \text{(TEM-like, TM modes)} \tag{3bA}$$

(b) $\varepsilon_r > 1$. (i) For TE, TM modes Using eqn. (2.7) in eqn. (2.3c) or (2.3f) and assuming that

$$\left| \left(\frac{\gamma_0 + \delta\gamma}{k_0} \right)^2 \right| \ll 1$$

one obtains,

$$\frac{h_3}{k_0}, \frac{p_3}{k_0} = 1 - \tfrac{1}{2} \left(\frac{\gamma_0}{k_0} \right)^2 - \frac{\gamma_0}{k_0} \frac{\delta\gamma}{k_0} \tag{4A}$$

(ii) For TEM-like mode: Here unperturbed value of p_3/k_0 has been assumed and is given by,

$$p_3/k_0 = j\,(\varepsilon_r-1)^{\frac{1}{2}} \qquad (5A)$$

The approximate expressions for h_1, h_2, h_3 and $\tan(h_1 b)$; p_1, p_2, p_3 and $\tan(p_1 b)$ have been listed above. These expressions were used in arriving at the closed form solutions of the dispersion relations (2.5). Because these approximations are valid under certain conditions only, they restrict the range of parameters f, b, σ and t for which solutions (2.9) and (2.10) are valid. The range of these parameters for which eqn. (2.9a) is valid is determined next.

Limitations on the values of parameters for the approximate solution (2.9a) to hold good

Limits on b and f: Equation (2.9a) is the leaky wave solution of eqn. (2.5a). Therefore, the range of γ/k_0 is $0 < \gamma/k_0 < 1$. The corresponding range of $\lambda/2b$ comes out to be

$$1 > \lambda/2b > 0$$

Limits on t and σ: It will be shown that when $t > 4\delta$ the perturbation $\delta\gamma/k_0$ is negligible. Therefore, there is no upper limit on the value of t. Hence, the lower limit on t is determined.

In order to arrive at eqn. (2.9a) the following approximations were made in eqn. (2.5a):

(i) $h_1 b = \pi + \Delta$, Δ is a small complex number.

(ii) $\tan(\Delta) = \Delta$ (The error will be less than 10 percent if $|\Delta| < 0.5$).

(iii) $h_2 = k_0 \sqrt{K}$

Since the lower limit on t is to be determined it may be further approximated that:

(iv) $\tan (h_2 t) = h_2 t$ (This is valid for $t/\delta < 0.4$), and

(v) $jh_3 t = jh_1 t = | j(\pi + \Delta) t/b | << 1$ (since t/b is very small)

Approximations (iv) and (v) are consistent with the end results as can be seen later from eqn. (12A).

Using the above approximations (2.5a) reduces to

$$\Delta = \frac{h_1}{jh_3 + k_0^2 t\, k} \tag{6A}$$

Approximation (ii) limits $|\Delta|$ to a value less than 0.5 for reasonable errors. Hence, the modulus of right hand side of eqn. (6A) should be less than 0.5. Therefore,

$$\left| \frac{h_1}{jh_3 + k_0^2 tK} \right| < 0.5 \tag{7A}$$

Note that $h_3 = h_1$ for $\varepsilon_r = 1$. Therefore, eqn. (7A) reduces to

$$\left| \frac{h_1}{jh_1 + k_0^2 tK} \right| < 0.5 \tag{8A}$$

For good conductors $\sigma / \omega \varepsilon_0 >> 1$, therefore $I_m(k_0^2 tK) >>$ Real $(k_0^2 tK)$. Also, h_1 may be replaced by its unperturbed value π/b. Under the above simplifications

eqn. (8A) reduces to

$$\frac{\pi}{\pi + k_0 t . k_0 b \ \sigma/\omega \varepsilon_0} < 0.5 \qquad (9A)$$

The above inequality is satisfied for

$$k_0 t \ k_0 b \ \sigma/\omega \varepsilon_0 > \pi \qquad (10A)$$

or $$\sigma t > \frac{1}{120\pi} \ \frac{\lambda}{2b} \qquad (11A)$$

or $$t/\delta > \frac{\pi}{2} \ \frac{\delta}{b} \qquad (12A)$$

with $$0 < \lambda/2b < 1$$

When a numerical computation for propagation constant is done for eqn. (2.5a), and is compared with eqn. (2.9a) it is found that eqn. (12A) is a good approximation for the range $0.1 \leqslant \lambda/2b \leqslant 0.95$. It is to be noted that for metal films the approximate solution (2.9a) is valid even for very small thicknesses e.g. for silver films (at 10 GHz, b=0.95") t/δ can be as low as 2×10^{-4}.

APPENDIX B

MULTIPLE REFLECTIONS

The power incident at the imperfect wall is distributed in the following ways:

(i) a portion of the incident power is reflected by the imperfect wall,

(ii) the rest of it is transmitted into the imperfect wall. The fraction of the power which is transmitted into the metal undergoes multiple reflections when the thickness t of metal is less than δ. A part of the power, incident in the thin film, gets absorbed in it, part of it gets transmitted into the feed region and the rest is transmitted into free space which is observed as a radiation.

In order to see how multiple reflections are built into the expression for T, write eqn. (4.62) in the form given below [14]

$$T = p(1-qe^{2jh_2t})^{-1} e^{jh_2t} e^{-jh_3t} \qquad (B1)$$

where

$$p = \frac{4}{(1+h_2/h_1)(1+h_3/h_2)} \qquad (B2)$$

and

$$q = \frac{(1-h_3/h_2)(h_2/h_1-1)}{(1+h_3/h_2)(h_2/h_1+1)} \qquad (B3)$$

APPENDIX C

EFFECT OF A SUPPORTING DIELECTRIC LAYER

Let the dielectric support has thickness T and relative dielectric constant ε_{r3}. Figure 1C shows the parallel plate configuration obtained by introducing this sheet between the metal film and outside space.

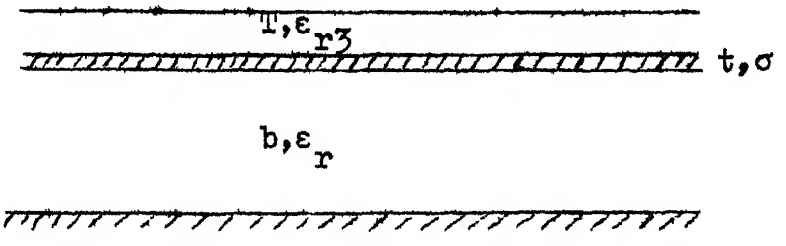

Fig. 1C . Parallel plate configuration with dielectric support for thin film

The dispersion relation for TE-mode for this configuration is obtained as,

$$h_3[jh_4+h_3 \tan(h_3T)][h_1\tan(h_2t)+h_2\tan(h_1b)]+$$
$$h_2[jh_4\tan(h_3T)-h_3][h_1-h_2\tan(h_2t)\tan(h_1b)] = 0 \qquad (1C)$$

where $h_3 = k_0\sqrt{\varepsilon_{r3}-(\gamma/k_0)^2}$

and $h_4 = k_0\sqrt{1-(\gamma/k_0)^2}$

h_1 and h_2 are the same as defined by eqns. (2.3). Note that eqn. (1C) reduces to eqn. (2.5a) when T=0 and $h_3=h_4$.

For b=0.95 in, ε_r=1, f=9 GHz, $\sigma=8.33\times10^5$ mho/m, and t/δ=0.002 the root γ/k_0 of the dispension relation

(2.5a) is (0.7259+j0.0334). When a thin layer of dielectric, with ε_{r3}=2.58 and T=5 mil, is introduced as a support for the metal film the root of the modified dispersion relation (10) is obtained as (0.7265+j0.0333). This shows that the introduction of a thin layer of dielectric gives rise to a very small change in the propagation constant. Therefore, the effect of the thin supporting dielectric layer on the propagation constant may be ignored.

APPENDIX D

DERIVATION OF RELATIONS BETWEEN β AND α FOR LEAKY WAVES AND SURFACE WAVES FOR A LOSSY STRUCTURE

Equations (2.24) are the relations between β and α for which leaky waves and surface waves are obtained. The detailed procedure for obtaining these equations is given in this Appendix.

Leaky waves and surface waves are characterised by the field configurations outside the structure. The field configurations are written in terms of conditions on real and imaginary parts of transverse wave number 'h'. Here, the conditions on 'h' are translated in the form of relation between the real and imaginary parts of more commonly used complex propagation constant $\gamma(=\beta+j\alpha)$ along the direction of propagation.

Since $h = \sqrt{h^2}$ is a double-valued function, the concept of Riemann surfaces is used to define it uniquely. In the case of a square root function, Riemann surface consists of two sheets. Here, proper (or top) sheet is chosen to be characterised by $\mathrm{Im}(h/k_o) > 0$, and improper (or bottom) sheet by $\mathrm{Im}(h/k_o) < 0$. The multi-valued functions are uniquely defined on Riemann sheets when plotted in polar-coordinate system. Therefore, we shall write h/k_o in polar coordinates.

Equation (2.16) for h/k_o gives (for $\varepsilon_r = 1$)

$$(h/k_o)^2 = X - j\,Y \tag{D1}$$

where
$$X = 1 - (\beta/k_o)^2 + (\alpha/k_o)^2 \tag{D2}$$

and
$$Y = 2[(\alpha/k_o)\,(\beta/k_o)] \tag{D3}$$

In order to define h/k_o in polar coordinates, let

$$(h/k_o)^2 = re^{j\phi} \tag{D4}$$

Equivalence of (D1) and (D4) gives

$$r = \sqrt{(X^2 + Y^2)} \tag{D5}$$

$$\text{and } \tan\phi = -\frac{Y}{X} = -\frac{2[(\alpha/k_o)(\beta/k_o)]}{1-(\beta/k_o)^2+(\alpha/k_o)^2} \tag{D6}$$

Equation (D4) is used to write h/k_o in terms of r and ϕ. It gives

$$h/k_o = \sqrt{r}\, e^{j\phi/2} \tag{D7}$$

Separating the real and imaginary parts of h/k_o yields

$$Re(h/k_o) = \sqrt{r}\cos(\phi/2) \tag{D8}$$

$$\text{and } Im(h/k_o) = \sqrt{r}\sin(\phi/2) \tag{D9}$$

Equation (D9) is used to characterise the two Riemann sheets, proper and improper, in terms of ϕ. It yields

$$\text{Proper-sheet (top)} \qquad 0 \le \phi < 2\pi \tag{D10}$$

$$\text{Improper-sheet (bottom)} \qquad 2\pi \le \phi < 4\pi \tag{D11}$$

The two Riemann sheets of h are shown in h^2-plane in Figure D1.

The conditions on $Im(h/k_o)$ have projected leaky waves ($Im(h/k_o) < 0$) and surface waves ($Im(h/k_o) > 0$) on the bottom and top sheets respectively of the two-sheeted Riemann surface. Now conditions on $Re(h/k_o)$ will be used to separate out regions of top or bottom sheet for the forward travelling waves.

(i) Leaky Waves. Leaky waves are characterised by $\mathrm{Im}(h/k_o) < 0$ i.e. $2\pi \leq \phi < 4\pi$. The condition $\mathrm{Re}(h/k_o) > 0$ restricts this range of values of ϕ to $3\pi < \phi < 4\pi$ (quadrants III_B and IV_B in Figure D1(b)). Further, the region corresponding to $3\pi < \phi < 7\pi/2$ (quadrant III_B) is not captured by the steepest descent path [8, p.175, Figure 19.24] and therefore, it does not contribute to the radiation pattern near the peak. Therefore, we are left with the region IV_B i.e.

$$7\pi/2 < \phi < 4\pi \qquad \text{(D12)}$$

i.e. $\tan\phi < 0$

Equation (D6) shows that $\tan\Phi < 0$ is obtained for $Y/X > 0$. Since $\alpha > 0$ and backward waves are unlikely to arise with the present structure, Y is greater than zero. Hence, $X > 0$ i.e.

$$1-(\beta/k_o)^2 + (\alpha/k_o)^2 > 0 \qquad \text{(D13)}$$

which is (2.24a).

(ii) Surface Waves: The structure considered does not support lossless surface waves because it is lossy in nature ($\alpha > 0$). The only possibility is lossy surface waves characterised by

$$\mathrm{Im}(h/k_o) > 0, \quad \mathrm{Re}(h/k_o) < 0 \qquad \text{(D14)}$$

Proceeding in the same manner as has been done for leaky waves it can be shown that lossy surface waves are obtained for $X < 0$ i.e.

$$1-(\beta/k_o)^2 + (\alpha/k_o)^2 < 0 \qquad \text{(D15)}$$

which is (2.24b).

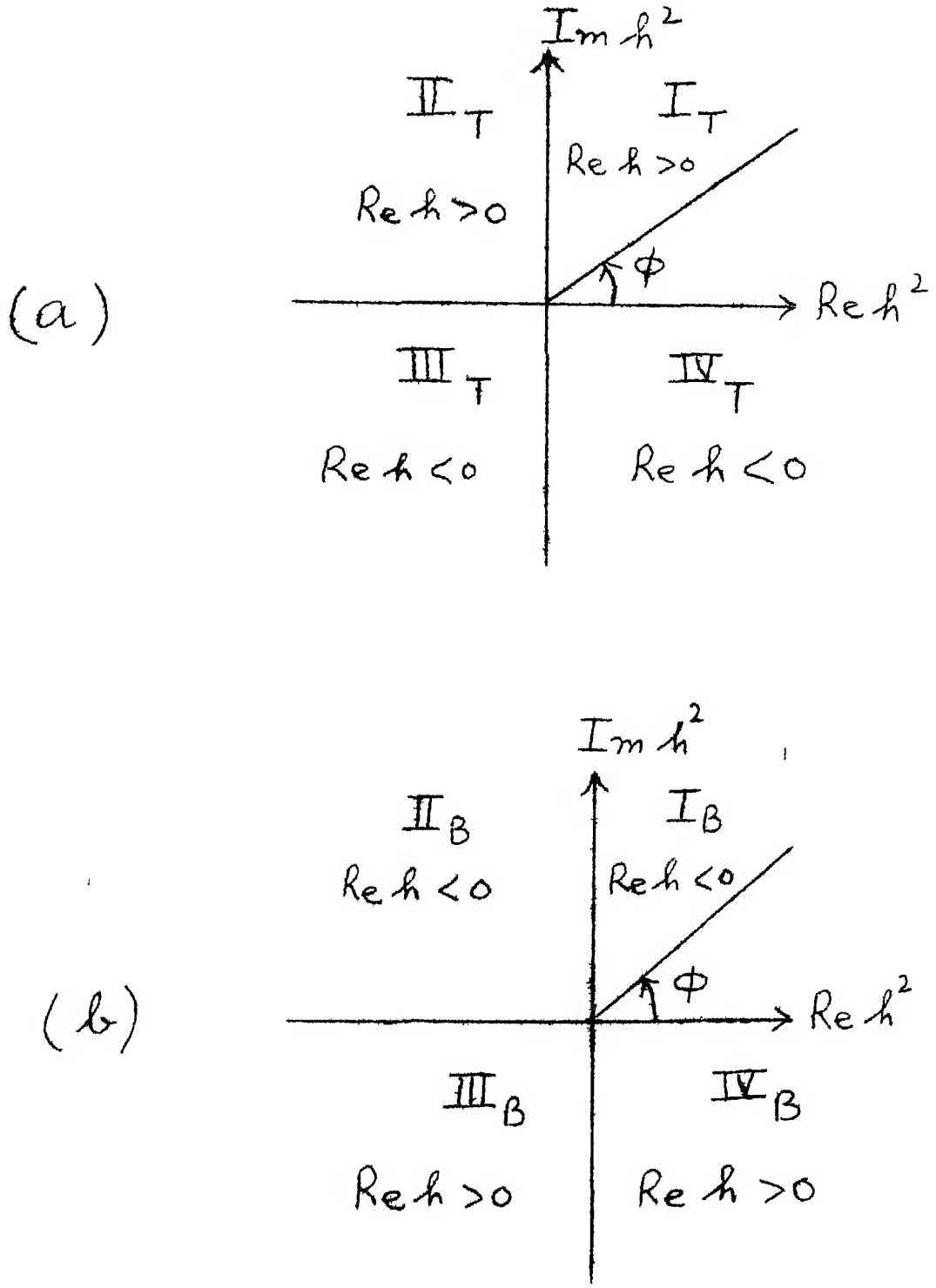

Fig. D1 : The Riemann sheet of h in h^2-plane

(a) Top sheet (Im h > 0)
(b) Bottom sheet (Im h < 0)

REFERENCES

[1] Ramo, S., Whinnery, J.R. and Van Duzer, T.,'Fields and Waves in Communication Electronics'. New Delhi: Wiley Eastern, 1970, Ch. 7.

[2] Adler, R.B., Chu, L.J. and Fano, R.M., 'Electromagnetic Energy Transmission and Radiation' New York: John Wiley, 1960, Ch.8.

[3] Jordan, E.C. and Balmain, K.G., 'Electromagnetic Waves and Radiating systems.' New Delhi: Prentice-Hall of India, 1969, Ch.7

[4] Larrabee, R.D., 'Characteristics of waveguides with a semiconductor side wall', IEEE Trans. Microwave Theory Tech., Vol. MTT-14, p.306, 1966.

[5] Gunn, M.W. and Sheikh, R.H., 'Wave propagation in a rectangular waveguide with a semiconducting wall', Proc. IEE (London), Vol.115, p.32, 1968.

[6] Walter, C.H., 'Traveling Wave Antennas' New York: McGraw-Hill, 1965, Ch.5.

[7] Zucker, F.J., 'Surface and Leaky-wave Antennas', in Antenna Engineering Handbook, H. Jasik, Ed. New York: McGraw-Hill, 1961, Ch.16.

[8] Oliner, A.A., 'Leaky-wave Antennas', in Antenna Theory, Part 2, R.E. Collin, and F.J. Zucker, Ed. New York: McGraw-Hill, 1969, Ch.20.

[9] Karbowiak, A.E., 'Theory of imperfect waveguide: The effect of wall impedance', Proc. IEE (London), Vol.120B, p.698, 1955.

[10] Collin, R.E., 'Field theory of guided waves'. New York: McGraw-Hill, 1960, Ch.11.

[11] Tamir, T. and Oliner, A.A., 'Guided complex waves Part 1 (Fields at an interface)', Proc. IEE (London), Vol.110, p. 310, 1963.

[12] _____,'The influence of complex waves on the radiation field of a slot-excited plasma layer', IRE Trans. Antennas Propag., Vol.AP-10, p. 55, 1962.

[13] Gupta, K.C., Garg, R.K. and Singh, Amarjeet, 'Narrow beam antennas using cylindrical columns of isotropic plasma', Int. J. Electronics, Vol. 35, p. 198, 1973.

[14] Schelkunoff, S.A., 'The impedance concept and its application to problems of reflection, refraction, shielding and power absorption,' Bell System Tech. J., Vol. 17, p.17, 1938.

[15] Bahl, I.J. and Gupta, K.C., 'A leaky-wave antenna using an artificial dielectric medium', IEEE Trans. Antenna Propag., Vol.22, p. 119, 1974.

[16] 'Tables of Range and Rate of Energy loss of charged particles of Energy 0.5 MeV to 150 MeV,' Service de Physique Nucleaire a Basse Energie. Rapport C.E.A. No.2180

[17] Chopra, K.L.,'Thin Film Phenomena'. New York: McGraw-Hill, 1969, Ch.3.

[18] Chaurasia, H.K.,'Resistivity of thin metal films,' IEEE Trans. Microwave Theory Tech., Vol. MTT-21, p.51, 1973.

[19] Ramey, R.L. and Lewis, T.S.,'Properties of thin metal films at microwave frequencies,' J. of Applied Phys, Vol.39, p. 1746, 1968.

[20] Green, R.E. and Richardson, J.R.,'Aperture field of a leaky wave antenna of finite length,' Electron.Letters, Vol.2, p. 68, 1966.

[21] Clarricoats, P.J.B., Green, P.E. and Oliner, A.A., 'Slot-mode propagation in rectangular waveguide ,' Electron . Letters, Vol.2, p. 307, 1966.

[22] Oliner, A.A.,'Leaky waves in electromagnetic phenomena,' in Electromagnetic Theory and Antennas, Part 2, E.C. Jordan, Ed. New York: Pergamon Press, p.837, 1962.

[23] Horton, R., Easter, B. and Gopinath, A., 'Variation of microstrip losses with thickness of strip,' Electron. Lett., Vol.7, p.490, 1971.

[24] Southworth, G.C.,'Principles and Applications of Waveguide Transmission'. New York: D. Van Nostrand Company, 1950, Ch.5.

[25] Linder, E.G.,'Attenuation of electromagnetic fields in pipes smaller than the critical size', Proc. I.R.E., Vol.30, p.554, 1942.

PHY-1974-D-GAR-WAV